Surface Properties of Kuiper Belt Objects and Centaurs

Thesis by

Kristina M. Barkume

In Partial Fulfillment of the Requirements

for the Degree of

Doctor of Philosophy

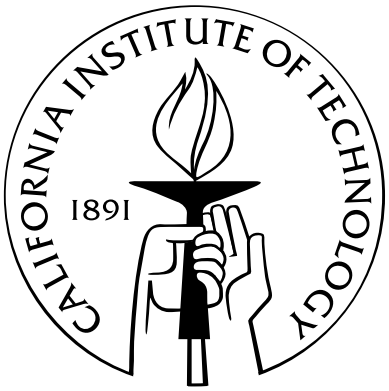

California Institute of Technology

Pasadena, California

2008

(Submitted January 14, 2008)

To Jon, who has supported me through every step of this endeavor, to my father, who introduced me to the night sky, and to my mother, who endowed me with a great love of learning

Acknowledgements

One person has stood by me through all the wonderful and disastrous moments of my adult life. I could not have done this without the love and support from my husband, Jon Young.

I thank my many advisors, professors, and teachers who have shared their wisdom with me and encouraged me to become the individual I am today. I am particularly grateful to Mike Brown, Oded Aharonson, and Geoff Blake at Caltech who have seen me through this endeavor. Laura Woodney pointed me in the right direction and inspired me in so many ways. David Griffith taught me the elegance of physics.

I'm thankful for the mentorship I have received along the way from friends and faculty. I'm particularly grateful to Chris Lee, whose many years of guidance brought me to Caltech. At Caltech, I could not have asked for a better friend or mentor than Emily Schaller. Her endless encouragement has helped me grow as an academic and as a person. I will always be grateful for the inspiration Emily has given.

I am in debt to the many people who have helped me observe over the years. I can only hope that all my observing partners are as talented and helpful as Emily Schaller. My Palomar observations would not be possible without Henry Roe, who taught me a new appreciation for the man in black. Antonin Bouchez and Chad Trujillo shared many words of observing wisdom with me, particularly in regards to ice cream. Darin Ragozzine gave me new, interesting targets to pursue. Megan Schwamb, Terry Suer, and Greg Knoke have assisted me during many long, often iffy, nights at Palomar. Finally, I'd like to express my thanks for all the staff who make observing possible at Keck and Palomar Observatories, particularly Jean Mueller, Karl Dunscombe, and Marc Kassis.

My friends and family have supported me throughout graduate school. Many of them don't know

what I do, but they love me anyway. My parents always encouraged my academic tendencies, even when they involved staying out late. If my twin, Kate, hadn't been so artsy, I probably wouldn't have been so sciencey. Thanks also to my adopted family, Neal and Ashley Young, the Boettchers, and Pam Shields for the much needed support. I will always treasure my memories of the many hours I've spent with the graduate students in Planetary Science, especially with Emily Schaller, Kevin Lewis, Colette Salyk, Xin Guo, and Sloane Wiktorowicz.

Abstract

The outer solar system is inhabited by a population of small solar system bodies called Kuiper belt Objects (KBOs) and Centaurs. I present a survey of visible and near infrared (NIR) spectra of the brightest KBOs and Centaurs. The visible spectra of 19 KBOs were obtained at Palomar Observatory. At the W.M. Keck Observatory, NIR spectra were obtained for 33 KBOs and 12 Centaurs. This data marks a significant leap in the available spectra, allowing for the population to be studied as whole.

The spectra reveal that most KBOs are covered with a material with characteristics similar to irradiate ices rich in complex organic compounds. Water ice is also observed on some KBOs and Centaurs, though its abundance is variable across the samples. A two end member mixing model is found to describe the NIR spectral properties well, but poorly fits the visible-NIR data. This suggests that the non-water ice component is heterogeneous across the KBO and Centuar populations. To characterize the non-ice component better, the visible spectra are analyzed for signatures of both organic and mineralogical features. No evidence is found for the presence of minerals, but the spectra suggest complex organics are a dominant spectral component. The abundance of water is shown to directly correlate with diameter for KBOs, but not Centaurs, suggesting it is controlled by geophysical processes on KBOs.

The analysis of these spectra has revealed an unusual population of KBOs that are now identified as mantle fragments from the large KBO 2003 EL61. The collision that spun-up 2003 EL61, formed its satellite system, and ejected the mantle fragments into the Kuiper belt is discussed. The unusual spectral properties of 2003 EL61, its brightest satellite, and the fragments are examined. Analysis suggests that the surfaces of all these objects can be composed of nearly pure water ice,

suggesting that their volatile organic inventory has been lost. The discovery of crystalline water ice on these small KBOs suggests that crystallization is not an indication of recent surface activity as was previously suggested.

Contents

Chapter 1

Introduction

> We live in a changing universe, and few things are changing faster than our conception of it. - Timothy Ferris, "The Whole Shebang"

The region beyond Neptune was long thought to harbor a population of small solar system bodies left over from the formation of the planets. Edgeworth (1943), Kuiper (1951), and others argued that Pluto was unlikely to represent the "edge" of our solar system and that additional planetary bodies in the trans-Neptunian region could be the source population for short-period comets. In 1992, Jewitt & Luu found a slow moving object in orbit beyond Neptune now dubbed (15760) 1992 QB1[1]. Currently, over a thousand objects have now been found orbiting the sun in the outer solar system. Their discovery confirmed the speculations by Edgeworth (1943), Kuiper (1951), and others. These objects also offer a new, unexpected understanding of our solar system and how it formed.

It is now evident that Kuiper belt objects (KBOs)[2] can be divided into three major dynamical classes based on their orbital characteristics; the classical, resonant, and scattered populations. Additionally, a population of small bodies with orbits crossing the outer planets have been called the Centaurs. The classical KBOs, so named because they have orbits similar to those originally envisioned by Kuiper and others, can be further divided into two populations. The cold classical population, so named because they are dynamically "cold," is comprised of objects with low ec-

[1]Small Solar System bodies are given provisional designation based on their day of discovery. The first four numbers give the year of discovery. The first letter essentially corresponds to the fortnight in which the object was discovered and the second letter and subsequent numbers are uniquely designated badsed on the number of objects previously discovered in that fortnight. After the orbit of an object is sufficiently determined (usually several oppositions for KBOs) the object is given a permanent number and may receive a name.

[2]Also referred to as Trans-Neptunian Objects (TNOs) in the literature

centricities and inclinations $< 4°$, while the hot classical population has higher eccentricities and inclinations, with some objects having inclinations above 20°(Brown, 2001). The resonant population includes any object that shows mean motion resonance with Neptune, with a majority of these objects inhabiting the 3:2 resonance (called Plutinos after Pluto). The scattered population also has high eccentricities and inclinations, but these objects also have weak scattering interactions with Neptune. Finally, many designate the objects with orbits that bring them into the region of the giant planets as the Centaur population, though it can be argued that they are the low perihelia tail of the scattered population. These objects are quickly on their way to being ejected out of the solar system or caught as a short period comet by Jupiter (Duncan and Levison, 1997).

The diverse dynamical characteristics of KBOs retain the fingerprints of the giant planets' migration at the final stages of planet formation in our solar system. A full review of this topic is beyond the scope of this introduction, but is thoughtfully discussed in Morbidelli et al. (2007) and is only summarized here. Even before the discovery of 1992 QB1, it was realized by Fernandez and Ip (1984) that interactions with small bodies after the formation of the giant planets would cause the planets to migrate, and the distribution of any remaining small bodies would record this migration. Later, Malhotra (1993) showed that the migration of Neptune could lead to the capture of Pluto and other KBOs into mean motion resonances. Currently, the "Nice Model," first proposed by Tsiganis et al. (2005), is a favored model for the formation of the Kuiper belt, as it provides a unified explanation for many of the dynamical characteristics of KBOs, the occurrence of the Late Heavy Bombardment, and the capture of the Jupiter Trojan population (Tsiganis et al., 2005; Gomes et al., 2005; Morbidelli et al., 2005). In this model, the original circumstellar disk was truncated at 35-38 AU. Neptune migrates outward, briefly achieving high eccentricities due to Saturn and Jupiter interacting in a 2:1 mean motion resonance. As Neptune migrates, it creates the various Kuiper belt populations, including the separate cold and hot classical populations. In this model, the cold population originates near the outer edge, while the remaining populations form closer to the giant planets (Levison and Morbidelli, 2007). Other models have been presented to explain the various populations in the KBO, including ones that involve crossing orbits of the ice giants (Gomes,

2003) and an ultra-large KBO scattering the KBO populations before ejection by the giant planets (Lykawka and Mukai, 2007).

As planetary leftovers from the formation of the gas and ice giants, KBOs are of particular interest in understanding the initial chemistry and physical states of the material that formed the planets in our solar system. Regardless of the details of the migration model used, it is possible that some of the dynamical populations originated in different regions of the circumstellar disk. As such, they may provide an additional constraint on the mixing and processing of materials through the disk. Tegler and Romanishin (2000) found that the cold classical KBOs have a different color distribution than the other populations, which can be reproduced qualitatively by the Nice Model. As such, understanding the chemical and physical state of KBOs will provide invaluable clues to the nature of the materials that built the planets and how they varied throughout the disk.

Based on cosmochemical models of the Solar Nebula, KBOs are thought to be roughly half rock and half ices -mostly in the form of water ice. The very smallest KBOs, those a few tens of kilometers or less in diameter, are the most likely to retain the initial composition of the solar nebula, and their physical characteristics likely resemble comet nuclei. However, a small fraction of the KBO population is much larger in size, with objects like Pluto and Eris having diameters over 2000 km. These "dwarf planets," or planetoids, probably appear very different from their smaller brethren. KBOs with diameters $\gtrsim$ 500 km have sufficient gravitational energy to have melted their ice component, though whether they fully differentiate is unclear. These giant KBOs may also have or had other planetary processes occurring on them, including out-gassing, convection, "cryovolcanism," and atmospheric cycling. This highlights two issues in studying the KBO population. First, the features of largest, most easily studied KBOs may not provide easily deciphered information about the primordial materials from which they were originally formed. Second, while some KBOs may not be "primordial," the considerable size range of KBOs does offers a unique opportunity to study the geophysics of icy planetary bodies.

However, as some of the most distant denizens of our Solar System, the study of these objects is difficult. Unlike other small bodies, asteroids in particular, we have no direct sample of KBOs and

the first mission to a KBO, *New Horizons*, will not arrive until 2015. We may gain some ground by studying those solar system bodies that are thought to originate in the Kuiper belt– namely Phoebe, Triton, and the short period comets. Studies of the population as a whole are reserved to large telescopes using both photometric and spectroscopic techniques. Even with the largest telescopes, the majority of the population is too small, distant, and dark to study in detail. Therefore, we are left to study the smaller subset of large KBOs, the "dwarf planets" of the population, and must make careful extrapolations down to smaller sizes. Telescopes give us the ability to understand the bulk properties of these objects, including their size, mass, and density in certain cases, as well as their surface composition. The bulk of the work presented here is concerned with the latter, and the following is a brief discussion of the various processes that may be acting on KBOs that could be expressed in observable surface characteristics. This discussion is presented for the benefit of the reader who is unfamiliar with the current speculations on formation and subsequent evolution of KBO surfaces. For the various processes, I highlight how each process might be observed geochemically and/or morphologically. This discussion will lead to the development of a model of surface characteristics of the general Kuiper Belt population. This model, or hypothesis, will then be tested in subsequent chapters.

Space Weathering

Space weathering occurs on all KBOs and appears to be an important chemical process acting on the surfaces of these objects. It is assumed that KBOs have, roughly, cometary abundances of water ice, organics, and inorganic carbon ices. Laboratory studies of these ices show that irradiation from UV light and cosmic rays leads to the overall loss of hydrogen from the system, and subsequent combination of the remaining material leads to an organic-rich mantle on the surface (e.g.,, Strazzulla et al. (1991); Johnson (1991)). Analysis of this material reveals that it is generally made from complex carbon ring structures joined together by carbon chains, though it can take a variety of forms based on the original materials present. This refractory material has a low albedo with increasing absorption at wavelengths shortward than 1.0 μm, giving it a "red" color (Khare et al.,

1993; Cloutis et al., 1994). It has absorptions in the mid IR, notably at 3.0, 8.0, and 12 μm , due to various C-X, O-X, and N-X stretching modes (see Cloutis et al. (1994) for specific details.) This irradiated, organic-rich material is called by various names, but Sagan and Khare (1979) propose the model - independent name "tholin," though some authors distinguish between "ice tholins" formed on icy surfaces, "Titan tholins" formed in Titan's atmosphere, and "Trition tholins" formed in a Nitrogen-rich environment.

Carbon-rich compounds likely make up a large portion of the dark material on comet mantles (Sagan and Khare, 1979) and the surface of Phoebe (Clark et al., 2005). Many KBOs have surface properties similar to the observed properties of tholin material. Typically, KBOs have low albedos, (Stansberry et al., 2007) find the average to be ∼10-20% [3] for KBOs and ∼ 4% for Centaurs (Stansberry et al., 2007). Visible photometry show that most KBOs have red sloping reflectance for wavelengths shortward of 1.0 μm. However, KBOs are extremely faint in the mid-IR, and therefore there is little data on the spectral characteristics of KBOs longwards of 3 μm that could confirm the presence absorption bands due to complex organic materials. From both cosmochemical and observational evidence, though, it is assumed that complex carbon substances contribute significantly to the observed surface properties of KBOs.

Space weathering also alters the structure of water ice at temperatures relevant to the Kuiper Belt in ways that are detectable in the near and mid IR. The low temperature, slow deposition of water should form amorphous ice, but if the ice is heated to temperatures much above ∼100 K, it will spontaneously and rapidly form (hexagonal) crystalline water ice, which has an additional absorption feature at 1.65 μm and a fresnel peak at 3.0 μm. The crystal structure of water, though, is expected to be destroyed on timescales of ∼10 Myr due to solar radiation and high energy particle bombardment (Strazzulla et al., 1991). The early discovery of crystalline water ice on the surface of some KBOs (e.g.,, Charon and Quaoar) has led some investigators to suggest that recent (geologically speaking) resurfacing of warm water ice had occurred and invoked such processes as cryovolcanism (Brown and Calvin, 2000; Jewitt and Luu, 2004; Cook et al., 2007). Subsequently, we have found

[3]This is notably higher though than comet nuclei which have ∼ 4% albedos. As a result, the KBOs appear to be generally smaller in size than originally thought.

crystalline water ice on every KBO where water is detected with sufficient signal-to-noise, and in particular, objects that are likely not to be geologically active (see chapters 2 and 3). We discuss in greater detail in chapter 3 how these results argue for a ubiquitous, non-thermal mechanism to crystallize the surface water ice on KBOs.

Geothermal Processes

The geophysical state of KBOs is poorly understood. What we know is applied either from the study of ice satellites or comet nuclei. Icy satellites likely formed under very different thermal and chemical conditions than KBOs because they form in warm, circumplanetary disks. Therefore, direct comparisons between icy satellites and KBOs may be problematic (Stevenson et al., 1986). Conversely, comets are small compared to many of the known KBOs, and scaling up comet models (e.g.,, Choi et al. (2002)) may miss important processes in the geophysics due to the different size regimes in question. KBOs that are $\sim$ 500 km in diameter have sufficient gravitational energy to melt their ice component, which could lead to chemical and structural changes to the KBO. Simple calculations show that the thermal length scale, that is the distance which heat can conduct, is a few hundred kilometers for icy bodies over the age of the Solar System. Thermal modeling of KBOs by McKinnon (2006) suggests that that KBOs $\sim$ 400 km or larger can reach internal temperatures from radiogenic heating alone approaching the water/ammonia melting temperature or higher as long as convection does not set in. Recent modeling by Merk and Prialnik (2006) that includes both accretional and internal heating suggests that even $\sim$ 100 km-sized bodies can become sufficiently hot to melt a substantial fraction of their water ice. These models suggest that large scale melting may occur on many KBOs, but it remains unclear whether this process actually occurs.

Differentiation could be suggested by the surface characteristics of KBOs. If the differentiation event is sufficiently hot, it could drive off the volatile organic materials that create the dark radiation mantle. The KBO surface may resemble an icy satellite's surface, with strong signatures of water ice in its spectrum and high reflectances. If this is indeed the case, then we could expect to see different spectral properties for KBOs of different sizes. The small KBOs would be dark, spectrally

dominated by tholin material. Larger KBOs may have stronger signatures of water ice. Looking for such a pattern in the distrubution of icy surfaces in the KBO population will allow for this hypothesis to be tested.

Several authors have found that their models of the largest KBOs, which are assumed to be differentiated in these studies, suggest they may be able to form interior oceans and retain them to the present day (McKinnon, 2006). In these cases it is unclear if this melt can reach the surface of the KBO via cryovolcanism or some other extrusive mechanism, though several authors have invoked this to explain their detections of crystalline water (and occasionally ammonia hydrate) ice on the surfaces of KBOs (Jewitt and Luu, 2004; Cook et al., 2007). Cryovolcanoes could be expected to leave signatures of salts or possibly patchy regions of water ice on the surface. To date, cryovolcanic activity has not been directly detected on any KBO, and their activity in the modern era is questionable.

Impacts

The collisional history of the Kuiper Belt remains an outstanding question in the field. Collisions were an important process in the early Kuiper belt. However, the primordial size and velocity distribution KBOs and the degree to which mass has been lost due to collisional grinding remains poorly understood. A break in the size distribution at 70 km and below suggests that nearly all small KBOs have experienced a disrupting collision in their past (Bernstein et al., 2004; Pan and Sari, 2005). For KBOs, Luu and Jewitt (1996b) proposed that impacts dredge up fresh, icy material and emplace it on the surface overlaying the dark radiation mantle. The fresh material then darkens over time as it becomes further irradiated. This process of impact gardening was offered by Luu and Jewitt (1996b) to explain the color variation seen in the Centaur and KBO populations. The authors argued that this scenario would cause smaller KBOs to be statistically bluer than large KBOs since the small KBOs experience impacts that resurface a proportionally larger fraction of their surface more often than large KBOs. It was also suggested in Luu and Jewitt (1996b) that this would typically cause azimuthal variations in color and brightness as the bright, blue ejecta rotated in and

out of view. Later analysis of larger samples of objects failed to find a correlation between the size (or rather the absolute magnitude) and color of either population and Luu and Jewitt (1996a) reject the impact gardening hypothesis as the major explanation for the varied surfaces characteristics of KBOs and Centaurs.

However, it is clear that impacts have played an important role in the history of some KBOs. A large impact likely formed the Pluto-Charon system (Canup, 2005), though the role of this impact in altering the surfaces of these objects is unclear. Another dwarf planet, 2003 EL61, also experienced a giant impact, with important implications for the Kuiper Belt. I will return to this singular object in more detail below to discuss how it has led us to understand an important, anomalous set of KBOs. Overall though, the findings of Luu and Jewitt (1996a) have not substantially changed, as many more KBOs and Centaurs have been subsequently observed.

Atmospheric Interactions

The only molecules of cosmochemical importance that are volatiles at temperatures in the Kuiper belt are N_2, CO, and CH_4, which are some of the molecules identified on surfaces of large KBOs like Pluto (Schaller and Brown, 2007a). Water has a vapor pressure of essentially zero at temperatures in the Kuiper belt. Pluto's tenuous N_2-CH_4 atmosphere was first detected using stellar occultations near its perihelion passage (Hubbard et al., 1988), but the atmosphere is expected to freeze out onto the surface as Pluto moves further from the sun. It is expected that the CH_4 and N_2 frosts preferentially evaporate from the darker, warmer regions of Pluto and refreeze on the brighter, colder spots, causing an atmospheric transport of these constituents and contributing to the patchy appearance of Pluto. The CH_4 and N_2 frosts dominate the surface spectral characteristics on Pluto and obscure any water ice that may be present near the surface.

CH_4 ice has been detected on other giant KBOs, namely Eris, 2005 FY9, and now Quaoar (Brown et al., 2005b, 2007a; Schaller and Brown, 2007b), but not on any small KBOs (see Chapter 3). It was suggested by Stevenson (1993) that cold, large icy objects may be able to retain their volatiles in an atmosphere that is in vapor pressure balance with the ice surface. This idea was modeled in

detail by Schaller and Brown (2007a), and they find a size-temperature dependence that determines whether a KBO is sufficiently large and cold to retain its inventory of volatiles. Thus far, the Schaller and Brown (2007a) model has successfully explained the presence of various volatile species on the surfaces of large KBOs and was even used to predict the discovery of methane on Quaoar.

Grand Unified Theories of KBOs Surfaces

The aim of the work presented here is to find an elegant, encompassing hypothesis that explains the observed surface properties of KBOs, which in turn will provide insight into their formation and subsequent evolution. Already, I have discussed major processes that may be observable on KBOs. Below I detail the observations as they stood at the beginning of this endeavor that must be explained by this hypothesis. It should be noted that only a few years ago, only a few dozen objects had photometric color measurements, and the total number of KBOs with spectra could be counted on two hands. Much effort put forth to collect spectral data on many more objects now allows for these questions to be examined with a significant sample. The three major observations that require explanation are:

1. The color variation of KBOs and Centaurs. As mentioned earlier, these objects exhibit a wide variety of colors from neutral (or blue, depending on your nomenclature) to extremely red. Indeed, some KBOs are among the reddest objects in our solar system. Additionally, the color distribution of the cold classical KBOs appears to be uniformly red compared to the other populations (Tegler and Romanishin, 2000). While the colors seem to be quite scattered, Barucci et al. (2005) argue that they can divide the KBOs into four different color groups. This taxonomy was meant to lend the KBOs the same organizational structure that exists for the asteroids with the hope that it would also prove to be of similar scientific value. In Chapter 3, I discuss how this taxonomy appears to not reflect the overall spectral characteristics of our enlarged data set.

2. The variable degree of water ice detected on KBOs. While most KBOs in the early studies appeared to have radiation mantles similar to comets, a small set of objects had detectable

amounts of water ice on their surfaces. In some cases, the surfaces could be modeled entirely with water ice, while others appeared to require the presence of some tholin materials. Determining what factors, if any, regulate the degree of water ice on the surfaces of KBOs stands as an essential question in the work presented here.

3. The presence of CH_4 on the surfaces of the largest KBOs. As mentioned above, this piece of the puzzle appears to be well solved by the Schaller and Brown (2007a) model, and it is left to the reader to read to fuller details about this work in E. L. Schaller's thesis.

Several theories were put forth in Luu and Jewitt (1996b) to explain observation #1. While their favored explanation, impact gardening, has been dismissed, the remaining theories remain influential today in the community's conceptual understanding of both observations #1 and #2. The first hypothesis proposed by Luu and Jewitt (1996b) is that inherent inhomogeneities in the solar nebula lead to a variety of compositions and surface properties. This hypothesis was rejected by Luu and Jewitt (1996b) since the outer regions of the solar nebula are not expected to be so heterogeneous. However, most of the KBO community now feel that the red characteristics of the cold classical population is a result of their formation in a colder, more distant region of the solar nebula.

Another hypothesis discussed by Luu and Jewitt (1996b) is a modification of their impact gardening scenario. Rather than impacts dredging up fresh material to cover the radiation mantle, they suggest that out gassing may create the same effect. Later, various authors have also suggested that extrusion of warm water from the interior (e.g., cryovolcanism) can also produce this effect and explain observation #2 as well. The unifying principle here is that these all constitute variation of a hypothesis that the surfaces can be described using a two-component system in various mixing ratios. The first component or end member, is a tholin-rich, irradiated material. The second end member is water ice mixed with small amounts of organic ices. Over time, radiation may alter the water mixture back into carbon-rich materials. Even if the extruded water is devolatilized, preventing further formation of a radiation crust, the resulting *population* should follow a compositional mixing line between the two end members. To date, all the spectra published have either been published

individually or in small sets, which do not provide an understanding of whether the population fits into the two-component mixing hypothesis. Examining spectra in this way only gives vignettes of the surface properties. In Chapter 3, we present a collection of spectra and systematically parameterize their spectral properties. With this data, we can finally examine whether the two-component conceptual model for KBO surfaces reflects reality by searching for the mixing line.

Early indications from KBO spectra suggested that two-component mixing was a promising conceptual model for KBO surfaces, though the process that emplaces water on the surfaces was not understood. In the absence of impact gardening, authors were apt to invoke geophysical processes like those outlined above, especially given the detections of crystalline water ice. However, some of the KBOs that appear to have the iciest surfaces were proving to be rather small, especially when a more physical albedos were assumed (that is, an albedo more similar to icy satellites than comets) These objects appeared far too small to have significant geothermal heating (particularly in the present era) to generate cryovolcanism. Furthermore, it was unclear why only a small fraction of the modest-sized KBOs had icy surfaces, while much of the remaining population did not. The issue posed a major problem for understanding KBO geophysical properties that seemed irreconcilable and required contortions of reasonable geophysical models. This issue was solved by the realization that this small set of KBOs had an unusual connection to the dwarf planet, 2003 EL61. I offer the following brief discussion of 2003 EL61 and these unusual KBOs below. The story of 2003 EL61 is essential for understanding the work presented here, as it motivates the work in Chapter 2 and colors the work in Chapters 3 and 4. This story is important to the understanding of KBO surfaces because it, in some sense, restored order to our understanding of the KBO population while also revealing a novel and unique event in the history of the outer solar system. It is discussed in greater detail in Brown et al. (2007b)

2003 EL61 and its collisional family

The large KBO 2003 EL61 is perhaps the most unusual body in the Kuiper belt. With a mass of 4×10^{21} kg, it is about 30% as massive as Pluto, making it one of the largest bodies currently

known in the Kuiper Belt. Shortly after its discovery, Rabinowitz et al. (2006) found that 2003 EL61 rotated with a period of 4 hours, making it the fastest rotating body over 100 km in size in the solar system. The rapid rotation causes 2003 EL61 to elongate into a Jacobi ellipsoid (assuming hydrostatic equilibrium), with one axis about twice as long as the others, producing the significant variation in light curve. Rabinowitz et al. (2006) used the shape and rotational period of 2003 EL61 to determine it is density of 2.6 g/cc. This density is significantly higher than the density of Pluto and Triton ($\rho \sim 2$ g/cc). If 2003 EL61 started with a rock-ice fraction like Pluto, which is closer to the rock-ice fraction predicted by cosmochemical models of our solar system, then its current density suggests that 2003 EL61 has at least 40% of its original mass in the form of water ice. While 2003 EL61's bulk properties suggest its a rock-rich body, its surface reflectance spectrum shows that it is covered in a relatively pristine layer of water ice. The spectral data then suggest that 2003 EL61 may be a differentiated body with a large rock core and thin icy shell. 2003 EL61 also has two small satellites, and Chapter 1 is devoted to discussing the unusual surface of the brighter of the two satellites. A spectrum of this object also reveals signatures of water ice, but the absorptions are even stronger than those observed on 2003 EL61. The unique surface of the satellite along with its small size argue that the satellites of 2003 EL61 did not form through a capture event, the mechanism thought to form many of the satellites in the Kuiper belt.

All of the features listed above are unique to 2003 EL61 and suggest that it has experienced an unusual history. Specifically, all of these features can be explained by a single large impact occurring on a proto-2003 EL61 at some point in its past. Simulations of giant impacts (e.g., Canup (2005); Asphaug et al. (2006); Canup and Asphaug (2001)) suggest that a significant fraction of material can be lost from the target body, mostly from its mantle if the body is differentiated, if the impact speed is a few times the target's escape speed, and if the impactor is sufficiently large. Such impact speeds can be reasonably achieved for 2003 EL61, as its moderate eccentricity and inclination gives it significant crossing velocity. These impacts also tend to spin-up the target body. Finally, models of the moon forming impact suggest that satellites formed from impacts are enriched in the lower-mass mantle materials (Canup, 2005). It was proposed in (Brown et al., 2005a; Barucci et al., 2006)

that all the unusual features of 2003 EL61 can be explained by a shattering impact occurred on a differentiated proto-2003 EL61. To date, though, the models used to study impacts on asteroids and large bodies have not been developed to study the case of 2003 EL61 and, particularly, whether small moons can form from collisions that eject such a large degree of material.

As the evidence for a giant impact on 2003 EL61 emerged, further studies of other KBOs were revealing a peculiar subset of KBOs. From our large, uniform survey of the spectral properties of KBOs (discussed in more detail in Chapter 3), we found that a small number of KBOs had very strong signatures of water ice and unusually blue (neutral) colors compared to the rest of the KBO population (see figure 1.1). However, using a plausible albedo expected for icy bodies, these KBOs are likely only a few hundred kilometers in diameter and too small to have active geothermal processes like cryovolcanism bring water ice to the surface. Differentiation also seemed unlikely, particularly since most KBOs of similar size do not have icy signatures. In addition to the unexpected spectral properties, it was found that all these especially icy KBOs has similar orbits to 2003 EL61(figure 1.2). This suggested a viable genesis for these unique objects, as remnant fragments ejected from 2003 EL61's icy mantle during the giant impact. Shattering models suggested that dozens of large fragments ($\sim$ 1% the mass of the parent body) could be produced, which is the likely mass ratio of the fragments to 2003 EL61, assuming they have similar albedos (Brown et al., 2007b). The spread in orbital parameters can be easily achieved for objects ejected at $\sim$ 100 m/s above the escape speed of 2003 EL61 ($\sim$ 1 km/s). However, 2003 EL61 is not at the "center" of the collision- it has a greater eccentricity than all the other objects. While this could be explained by the fact that 2003 EL61 is near a dynamically unstable region in the Kuiper belt, which could cause some fragments to be lost, further studies done by Darin Ragozzine and discussed in (Brown et al., 2007b) show that 2003 EL61 is in a weak 12:7 mean motion with Neptune. This resonance causes 2003 EL61 to diffuse in eccentricity out of the center of the collision. Further work on this issue has shown that the timescale for 2003 EL61 to diffuse to its current position is at least a billion years (Ragozzine and Brown, 2007).

The collision is actually more likely to occur in the early solar system when the density of KBOs

is much higher than it is currently. Detractors of this collisional model argue that the probability of such an encounter is still very low, perhaps as low as $\times 10^{-4}$ given the current understanding of the size distrubution of KBOs (Brown et al., 2007b). Also, if the collision occurred in the early solar system, it still must happen after the migration of Neptune for all the fragments to remain in orbits close to 2003 EL61. This poses an issue, as the collision must occur late enough that Neptune has cleared much of the disk, but not so late that impactors become scarce. Despite these complications, the collisional hypothesis has proved to have powerful predicting capabilities, with at least two new fragments confirmed after the discovery. To date, no KBO with spectra similar to the fragments has been found far from 2003 EL61. The current list of fragments is 1995 SM55, 1996 TO66, 2003 TX300, 2003 OP32, 2005 RR43, and 2003 UZ117. 1993 OY3 and 2005 CB79 are also likely member based on their colors. These objects, along with 2003 EL61 and it satellites, provide a unique glimpse into the dynamics of a collision as they are the only known bodies in the solar system in which the target body, satellites and fragments have been preserved. As more fragments are discovered and further details emerge, these objects are poised to offer a singular opportunity to test the various models of the formation of the solar system.

The Rest of the Story The remaining chapters of this work are devoted to finding resolution to the problems posed in this introduction. Chapter 2 is devoted to the spectral characteristics of 2003 EL61 and its satellite. Other than a spectrum of Charon, this is the only other satellite in the Kuiper belt for which spectral data has been obtained. The satellite's unique spectral properties are discussed along with its implications for the giant impact scenario.

In Chapter 3, the NIR spectral properties of a large sample of KBOs and Centaurs are discussed. The focus of the work is to examine the characteristics of the KBOs as a population rather than provide a simple catalog of surface properties. It is through this large study that the anomaly of the family members became evident and their spectral properties are discussed in greater detail there than in Brown et al. (2007b). Much of Chapter 3, though, is devoted to understanding whether the two-component surface hypothesis discussed in §1 provides a good physical model for the spectral properties of KBOs. I also examine how these surface components relate to other physical properties

such as orbital parameters and diameter in an effort to understand the physical processes acting on KBO surfaces.

Finally, in Chapter 4, I examine the visible spectral properties of a large sample of KBOs. The visible spectra are examined to find evidence for both mineralogical and organic surface components. The visible spectra complement the information available in the NIR data and provide further insight into the overall surface composition of KBOs. The major goal of this work is to further understand the heteorogeneous appearance of KBOs surfaces, particularly in their visible color gradients. Both the methane giants and the collisional family members are also examined to understand the nature of ices on their surfaces and whether additional constituents are present.

This work provides a significant increase in the available spectra of KBOs and Centaurs. For the benefit of the community, the spectra will be made available through the following website:

`http://web.gps.caltech.edu/~pa/data.html`

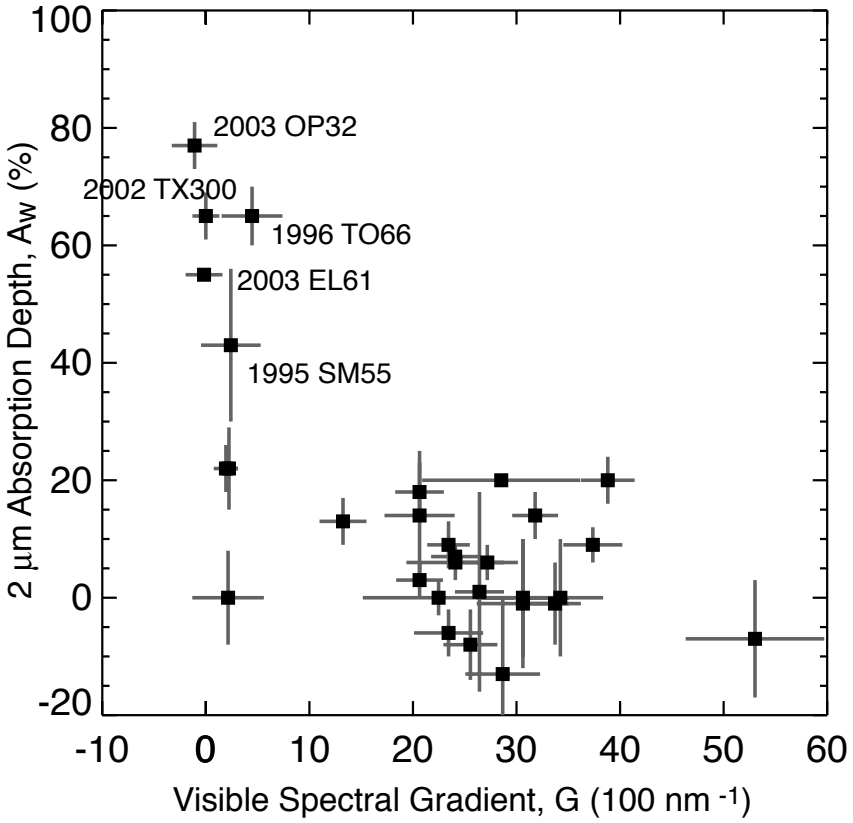

Figure 1.1: The absorption depth, Aw, versus visible color gradient, G, plot for KBOs in our survey and all KBOs with published spectra. G is defined as the fractional change in reflectance per 100 nm. A single gradient can generally characterize the reflectance spectra of KBOs between .5 and .8 μm , where few absorption features have been observed24. The V-R and V-I color measurements used to calculate G are available in Chapter 3. For objects with both V-R and V-I measurements, the error in the gradient is from linear regression and errors in the measured colors. In the case that only one color measurement was available (usually V-R), the error in the gradient is the error in the color plus a factor to account for the error due to using a single color measurement. This factor was determined by finding G for objects with both V-R and V-I colors using a single color measurement and comparing it to the G found by the linear regression. The median difference in the two G was then added to the error of objects with only a single color measurement. The four objects, 1999 TO66, 2002 TX300, 2003 OP32, and 2003 EL61, are different in both the magnitude of Aw and their variation in G. The G of these four objects is uniformly grey and consistent with a surface of pure water ice, though other materials may be present. We calculated using the Kuiper variant of the Kolmogorov-Smirnov test that the likelihood that the four objects with strong water ice absorption are from the same color distribution, as the remaining population is less than 4%.

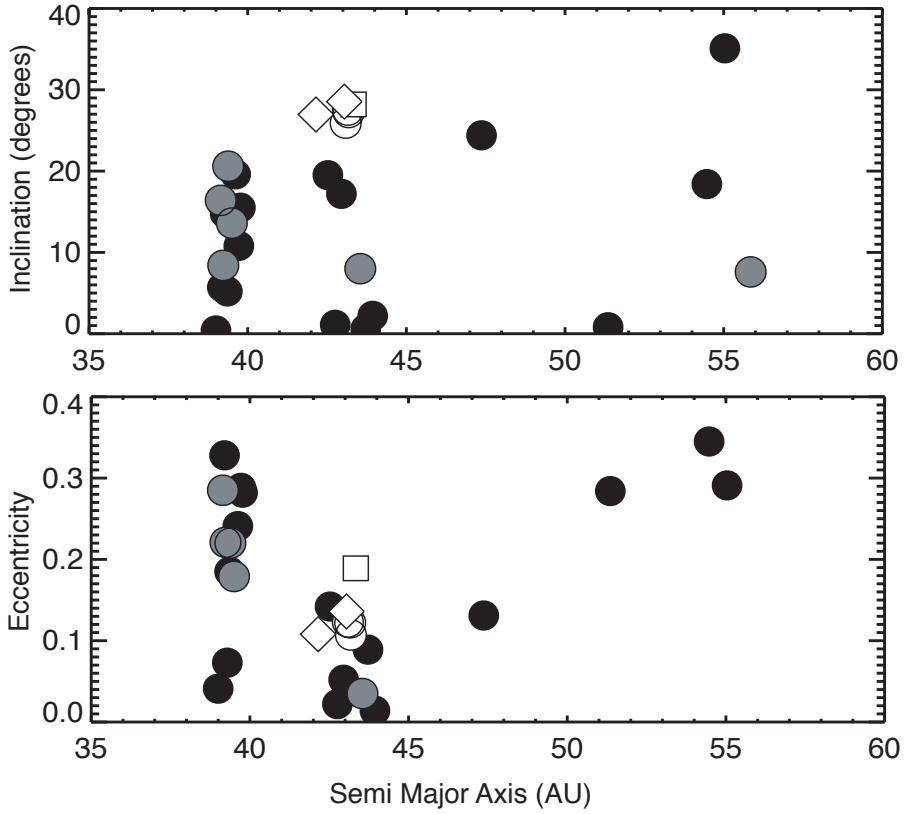

Figure 1.2: The osculating eccentricity and inclination of KBOs in our sample as a function of semi-major axis. The distributions in eccentricity and inclination of our population reflect the general distribution seen in Kuiper belt. The black dots indicate objects with absorption depth, Aw, less than 10%; the grey dots represent objects with Aw less than 30%. The white dots represent objects with Aw greater than 30%, and 2003 EL61 is shown by the white box. The white diamonds represent KBOs that have colors similar to the family. Four scattered objects with semi-major axes between 95 AU and 103 AU have been excluded so that the general distribution is clearly illustrated. We find that the objects with the strongest water ice absorption have clustered orbital parameters.

Chapter 2

Water Ice on the Satellite of Kuiper Belt Object 2003 EL6

2.1 Introduction[1]

Satellites in the Kuiper Belt provide unique insights into the internal properties of icy bodies as well as the early dynamical history of the trans-Neptunian region. To date, over a dozen satellites have been found around Kuiper Belt Objects (KBOs) and the overall satellite fraction is estimated to be $11\pm^{5}_{2}\%$ (Stephens et al. 2005). The first KBO satellites discovered (excluding the Pluto-Charon system) were found to have high eccentricities, large orbital separations, and have similar brightness to the primary, indicating that the satellites are nearly as large as their parent. Various capture mechanisms were proposed to account for the high specific angular momentum of these systems (Goldreich et al. 2002). Recently, Brown et al. (in press) have found several satellites around the largest known KBOs, and these satellites appear to be different than those discussed above. The satellite fraction appears to be higher around large KBOs and, like the Pluto-Charon system, the satellites have lower fractional brightness compared to the primary. The orbit of the brightest satellite around 2003 EL61 is nearly circular and Brown et al. (in press) suggest that these systems likely formed by a different mechanism and may be the result of giant impacts (McKinnon 1989, Canup 2005). The density, albedo, and surface composition of these satellite systems may help to clarify the origins of satellites in the Kuiper belt.

[1]This chapter has been published in its entirety under the same title with authors K.M. Barkume, M.E. Brown, E.L. Schaller, in *The Astrophysical Journal Letters*, Volume 640, Issue 1, pp. L87-L89

Near infrared spectroscopy is a particularly well suited method for remotely studying the surface composition of KBOs. Many of the abundant species in the outer solar system, including CH_4, CO_2, and H_2O ices, have absorption features in the near IR. Pluto and other large KBOs have spectra that are dominated by CH_4 (Cruikshank et al. 1976, Brown et al. 2005, Licandro et al. 2006). A small amount of water ice has been observed on a number of KBOs and some show evidence for the presence of other ices (Fornasier et al. 2004 and references therein). Charon, the only other KBO satellite for which a spectrum has been published, has strong features due to crystalline water ice absorptions (Brown & Calvin 2000). The spectra of satellites may shed light on their origin. Specifically, captured objects are likely to have spectra similar to other KBOs, but satellites formed from other mechanisms could show unusual or altered surface compositions.

2003 EL61 is currently the third brightest known KBO and is elliptical in shape with axes of 1960 and 2500 km (Rabinowitz et al. in press). The near IR spectrum of 2003 EL61 is similar to Charon's and shows strong water ice absorption features (Trujillo et al. in press). Its satellites offer an excellent opportunity to study the formation and dynamics of KBO binaries. The brighter satellite, S/2005 (2003 EL61) 1, has a period 49.12 $\pm$ 0.03 days and a maximum separation of 1.4 arcseconds (Brown et al. 2005). The orbit is nearly circular, with an eccentricity of 0.05. The inner satellite, S/2005 (2003 EL61) 2, appears to have an orbit of 34.7 $\pm$ 0.1 days, though there are currently insufficient data to reliably fit a non-circular orbit. The inner satellite has a fractional brightness of 1.5% compared to 2003 EL61, making it difficult to study with spectroscopic techniques. The outer, brighter satellite has a fractional brightness of 5% and is a viable target for low resolution infrared spectroscopy. We report here on the near-IR (J through K band) spectrum of 2003 EL61's brighter satellite. We compare the spectrum of the outer satellite to 2003 EL61's as well as to other KBOs. We discuss possible formation scenarios for the satellite and find that the surface composition is consistent with formation by giant impact.

2.2 Observations

Observations of 2003 EL61 were obtained on the Keck Telescopes on UT 2005 April 26 and 27 using NIRC, the facility infrared camera (Matthews & Soifer 1994). J band images revealed that the brighter satellite was near its maximum separation on these nights, with an average distance of 1.4 arcseconds from the primary. The average seeing was 0.5 arcseconds on both nights. Signal from the satellite was easily separated from the primary in the raw imaging and spectral data. Figure 1 shows the J band image of 2003 EL61 and the outer satellite. The dimmer satellite was not detected.

Spectra of 2003 EL61 and the brighter satellite were taken simultaneously by placing them in a .52 $\times$ 38 arcsecond slit. We obtained a spectrum in first order from 1.0 to 1.5 μm by placing a 150 lines mm^{-1} grism and a J through H sorting filter in the light path. A 1.4-2.5 μm spectrum was obtained using a 150 lines mm^{-1} grism and an H through K band sorting filter. Our spectral resolution in J-H is approximately $\lambda/\Delta\lambda \approx 132$ and in H-K the resolution is ≈ 162. The spectra were acquired by taking 200 second exposures at five set dithered locations with a 5 arcsecond separation between offset positions. The telescope guided at the predicted rate of motion for 2003 EL61. The total integration time over both nights was 8000 seconds in H-K and 2000 seconds in J-H. Nearby calibration stars were also observed each night at a range of air masses similar to those of 2003 EL61.

2.3 Data Reduction

The satellite's spectrum was marginally detected in the 200-second exposures. We hand selected data in which the satellite spectrum was most clearly separated from the primary in the raw data for further analysis. In the H-K band, a total of 8 spectra from the first night and 10 from the second night were selected, reducing the total integration time to 3600 seconds. In the J-H band, 3 spectra from first night and 4 from the second were used, for a total integration 1400 seconds. Data reduction was performed on the individual spectra similarly to the procedures described in Brown (2000). After dividing each spectrum by a flat field, a majority of the sky background was removed by differencing adjacent pairs of spectra. The residual sky background was measured in

20-pixel wide swaths above and below both 2003 EL61 and the satellite. The average of the residual sky backgrounds was subtracted from every row of the spectrum. The spectra were then shifted to place 2003 EL61 in the center of the array and the individual spectra at similar air mass were added together to increase the signal from the satellite.

2003 EL61 contributes a few percent of the flux detected at the location of satellite. To remove this contamination, a median profile of 2003 EL61 was created in the spatial direction for each night. The profile of the data was then reflected across the point of maximum flux. At each column, the profile was then scaled by the flux from 2003 EL61 in that column and subtracted from the coadded data. The spectrum of the satellite was extracted by summing over 5 rows centered at the location of the satellite. The final spectra were then divided by a calibration star spectrum to remove the solar spectrum and the resulting reflectance spectra were averaged. The spectra were smoothed to increase signal-to-noise. The spectral data were averaged at every fourth pixel using a Gaussian weighting function with a full width half maximum of 8 pixels in both the J-H and H-K band data, resulting in an oversampled spectrum with a resolution of $\lambda/\Delta\lambda \approx 33$ in the J-H band data and 41 in the H-K band data.

For comparison, the spectrum of 2003 EL61 was extracted in an identical manner to that of the outer satellite. The H-K band data for both objects were normalized by the flux at 1.7 μm. The J-H band overlaps with the H-K band and a scaling factor for the J-H data was determined by fitting 2003 EL61's J-H and H-K band data, which have higher signal-to-noise. This scaling factor was then used to scale the J-H band spectrum for the satellite.

2.4 Discussion

The satellite spectrum shows strong absorption features at 1.5 and 2 microns, which are consistent with absorption due to water ice (Fig 2.2). However, the resolution is too poor to detect the 1.65 μm crystalline water ice absorption feature seen on 2003 EL61 (Trujillo et al., in press). The depth of the water lines suggests that much of the satellite's surface is covered with smooth water ice. We calculated a model water ice spectrum using laboratory optical constants from Grundy & Schmitt

(1998), assuming a temperature of 50 K. Our model uses Hapke theory (Hapke 1981) to transform the optical constants to a reflectance spectrum. We vary the grain size of ice in our models and find that the grain size of 250 microns provides a good fit to the absorption lines at 1.5 and 2 microns. A better fit may be achieved with the addition of a second blue component or a multiple grain size water ice model. The poor fit of the water ice model shortward 1.2 μm is likely due to the uncertainties in the model in this region (Grundy & Schmitt 1998). A deviation is also seen at 2.2 μm, where spectral features are sometimes reported (Cruikshank et al. 2005). However, the signal-to-noise of the spectrum is insufficient to identify an additional component with confidence.

The absorption features in the spectrum of the satellite are significantly deeper than water ice features typically observed on KBOs. The ratio of flux at 1.7 μm to the flux at 2.0 μm is $\sim$ 80%. Most KBOs with water ice features have depths of less than $\sim$20% and the deepest absorptions ($\sim$60 %) are found on 2003 EL61, Charon and 1996 TO66 (Brown et al. 2000, Fornasier et al 2004, Dotto et al 2003 and references therein). As such, the brighter satellite of 2003 EL61 appears to be an unusual object in the Kuiper belt. Captured objects are likely to resemble the parent population where they are formed, thus the satellite's spectrum suggests that formation through capture is unlikely.

An alternative to capture is that the satellite could have formed via impact. Models of the Charon-forming impact by Canup (2005) are consistent with many of the features of the 2003 EL61 system. In these models, Charon is likely formed from a grazing impact where the impactor remains mostly intact and creates a large satellite. However, the models also show that a more direct impact creates a disk around the target body and smaller satellites can eventually coalesce from the disk material. The small satellites around 2003 EL61 are more likely to be formed by the latter kind of impact than by the Charon-type grazing impacts. In models where a disk was created, the satellite preferentially forms from the less dense disk material. In the outer solar system, this trend will lead to water-enriched satellites around KBOs, which may account for the strong water ice features seen in the satellite's spectrum. Direct impacts can also spin up the target body, which is consistent with the high rotation rate observed for 2003 EL61 (Rabinowitz et al., 2005). 2003 EL61 has a mean

density of 2.6-3.4 g/cm^3, indicating that it has lost most of its volatiles (Rabinowitz et al. 2005). Further modeling is needed to show if a high energy impact can eject a substantial amount of ice off of 2003 EL61 to account for its high rock-to-ice ratio. In sum, 2003 EL61 and its brighter satellite exhibit many of the features predicted by Kuiper belt impact models. Further analysis of other satellites may provide a greater understanding of the dynamical history of the early Kuiper belt.

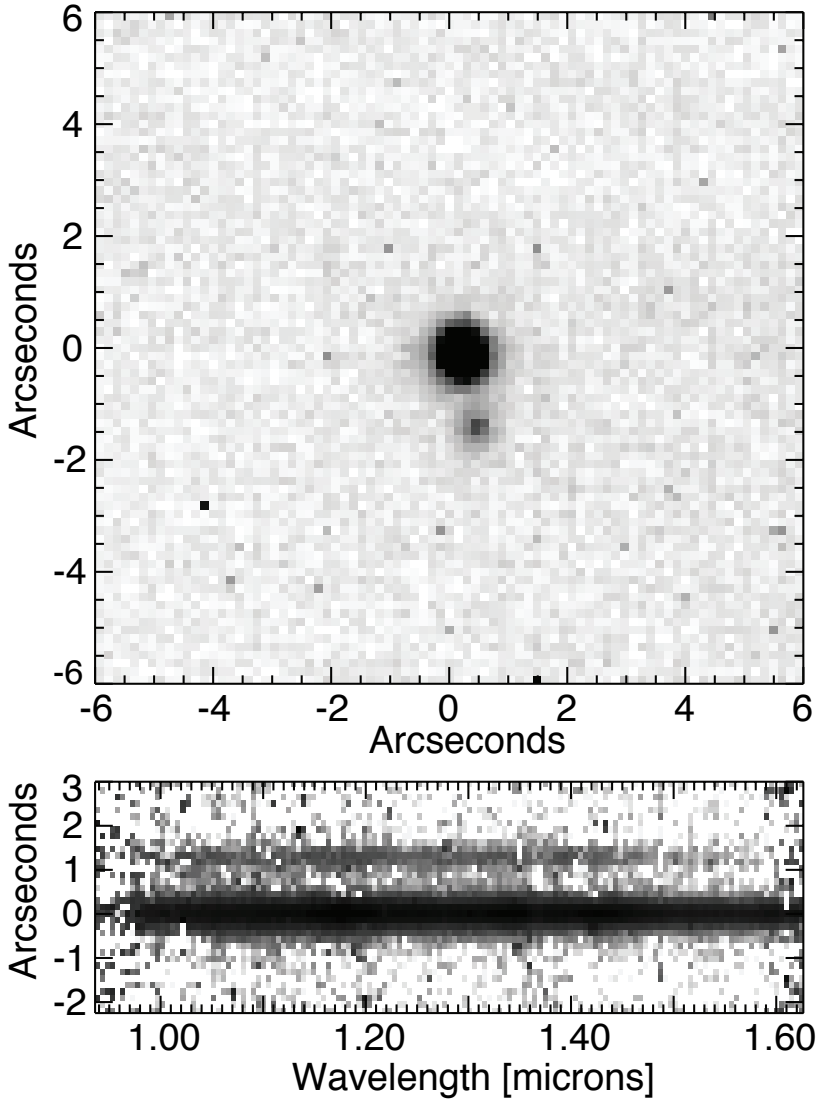

Figure 2.1: The J-band band image and raw spectral data of 2003 EL61 and its outer satellite from UT 2005 April 27. The satellite was near its maximum separation of 1.4 arcseconds. The spectral data show that the satellite's spectrum is separated from 2003 EL61.

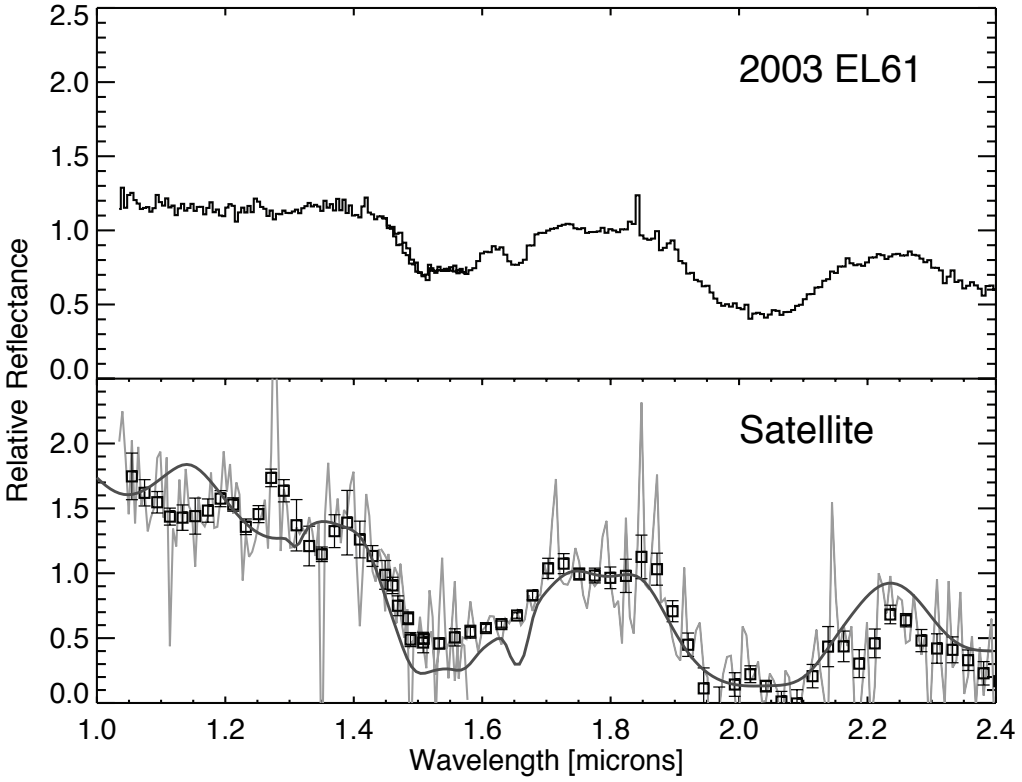

Figure 2.2: The 1.0-2.4 μm spectrum of 2003 EL61 (top) and its outer satellite (bottom). Both spectra are scaled to the flux at 1.7 μm. The light grey line is the full resolution spectrum of the satellite and the boxes are the Gaussian smoothed data with error bars. The dark grey line shows our best fit water ice model with a grain size of 250 μm. The resolution is insufficient to detect the 1.65 μm crystalline water ice feature on the satellite. A slight blue component improves the model fit, but there is no evidence for other common ice species.

Chapter 3

Near Infrared Spectra of Centaurs and Kuiper Belt Objects

3.1 Introduction[1]

The Kuiper belt poses a unique opportunity for astronomers to peer back into the formation of our solar system. Composed of the debris left after planet formation, Kuiper belt objects (KBOs) are thought to be among the most pristine bodies in the solar system. However, KBOs have likely undergone some alteration since their formation from geophysical, collisional, and space weathering processes. Centaurs may have undergone even more alteration as their temperatures are increased by closer perihelion passages. KBOs span several orders of magnitude in diameter, and at small sizes they are thought to resemble comets and be composed largely of primordial materials that remained at relatively low temperatures. The largest members of the Kuiper belt, like Eris and Pluto, resemble planets with tenuous atmospheres, active resurfacing and possibly differentiated interiors. While this size spectrum provides a singular opportunity to study a variety of planetary processes, the largest objects may be very different than their smaller brethren. This complicates the task of understanding the small bodies by extrapolating results from the more easily studied large objects. Furthermore, the surfaces of all these objects are also likely to be altered by cosmic rays, impacts, and interstellar dust, thereby obscuring the materials from which they are made. Despite these complications, the study of KBOs will provide important clues to the formation of our solar

[1]This chapter will be published in its entirety under the same title with authors K.M. Barkume, M.E. Brown, E.L. Schaller, in *The Astronomical Journal*, January 2008

system and the processes that continue to shape it.

Much effort has been put forth in the past decade to understand the physical and chemical state of KBOs and Centaurs and is well summarized by Barucci et al. (2008, Barucci et al. chap). To date, over a hundred objects have measured photometric colors in visible wavelengths, but far fewer objects have spectra due to the faintness of KBOs. Spectra in the visible wavelengths are often characterized by a red continuum component typically identified as carbon-rich material and some objects may have subtle silicate spectal features. Near infrared (NIR) spectra taken over the past decade have revealed a variety of ices on the surfaces of KBOs including methane, water, methanol, and nitrogen. Previous studies have shown that the largest KBOs, Eris, Pluto and 2005 FY9, have spectra dominated by methane (see Barucci et al. chapter in Barucci et al. (2008) and references therein). In the case of Pluto, N_2 and CO have also been detected. The presence of these species on the largest objects is likely due to their large masses which allow for volatiles to be retained (Schaller and Brown, 2007a). It has been noted that moderately sized KBOs, like Quaoar and Orcus, often have surfaces dominated by water ice. Finally, the smallest KBOs and Centaurs for which we have spectra typically appear to be largely featureless in the NIR. The exception is a handful of smaller KBOs that have among the deepest water ice absorption features ever detected in the Kuiper Belt. These objects have been shown to be dynamically associated with the large KBO 2003 EL61 and are thought to be fragments from its mantle that were ejected during a catastrophic impact (Brown et al., 2007b).

To date, there is no widely accepted standard model of KBO surface processes that accounts for the varying presence of water ice on the moderate to smaller KBOs. One commonly proposed model describes essentially a two component surface made of dark, carbon-rich deposits and exposed, fresh water ice (Luu and Jewitt, 1996a). The dark surfaces are thought to be similar to those observed on comets or Saturn's moon, Phoebe, and are likely a mixture of materials (Clark et al., 2005). The spectral properties of the crusts are often characterized by amorphous silicate material, and irradiated, polymerized hydrocarbons called tholins (Moore et al., 1983), producing the red visible colors observed and nearly featureless spectra on most KBOs. In this model, fresh ice initially

exposed by erosion, impact gardening, out gassing, or cryovolcanism creates a surface with strong water ice signatures. Over time, the surface eventually darkens and reddens as it becomes irradiated and a new crust forms, obscuring the water ice signatures.

Thus far most spectra have been analyzed individually offering only vignettes of KBO surface characteristics. A comparative study using the visible and NIR photometric colors of KBOs by Barucci et al. (2005) found four different color groups, though it remains unclear how these color groups relate to specific spectroscopic features or surface characteristics. Here we present a survey of low-resoultion NIR spectra of bright KBOs and Centaurs taken with the Near Infrared Camera (NIRC) on the Keck I Telescope (Matthews and Soifer, 1994). The uniformity of this survey allows us to study these objects comparatively as well as individually. Several of the objects in our survey that showed evidence of particularly interesting or unique surfaces have already been published previously (e.g. 2005 FY9 and 2003 EL61). Thus, we concentrate here on a comparative study with the aim of understanding the surface processes that may be generally acting on the Centaur and KBO populations. We begin by describing our sample of observed objects in section 3.2. We discuss the observations and data reduction in section 3.3, and the analysis of the spectra, including the spectral fitting, in section 3.4. We find that the properties of the collisional family members of 2003 EL61 differ from the general population of KBOs and therefore we describe our results for these two populations separately in sections 3.5.1 and 3.5.2. Finally, we discuss impact that the results of this work have on our general understanding of the physical processes that are occurring in the outer solar system in section 3.6.

3.2 The Sample

For our survey we preferentially selected KBOs with an absolute magnitude less than 5.0, corresponding to objects with a diameter greater than about ∼400 km, assuming a 10 percent albedo (Stansberry et al., 2007), though six KBOs have absolute magnitudes greater than 5.0. We excluded any KBOs and Centaurs with visual magnitudes greater than ∼21, which we found was our effective magnitude limit with NIRC. Targets located near the galactic plane were also abandoned due to

contamination from field stars. Of the possible targets, the KBOs were evenly distributed between hot classical and resonant population, with a few objects belonging to the scattered disk. For the purpose of our survey, Centaurs are defined to be objects with perihelia less than 25 AU. No cold classical objects were observed due to the lack of bright targets in this population. In total, we observed 33 bright KBOs and 12 Centaurs with NIRC from March 1998 to April 2007.

3.3 Observations & Data Reduction

Low resolution ($\lambda/\Delta\lambda \sim 160$) spectra from 1.4 to 2.5 μm were obtained with NIRC for each object using a 150 lines mm^{-1} grism and an H-through-K order sorting filter. A complete list of observations is provided in Table 3.6. Targets were identified in fields by their motion and tracked during observations by the telescope. The exposure times for the spectra were between 150 s and 300 s, but were typically 200 s. Dithering between subsequent images by 5 arcseconds was used to subtract most of the background sky emission. Solar-type stars were observed for calibration purposes at similar air masses and times to target observations, with the typical differences in air mass being less than 0.1.

The raw image processing and spectral extraction were done using standard procedures. We first subtracted sequential images to remove most of the sky background emission and divided by a flat-field image constructed from a median dome flat. We then measured and removed any curvatures in the sky lines in individual images. Residual sky emission was measured on either side of the target spectrum and subtracted from the image. The spectrum was then extracted by summing in the spatial direction, typically a 7 to 10 pixels swath, centered on the target at each spectral position. Bad pixels were identified by visual inspection and removed. Spectra of calibration stars were extracted similarly with the exception of removing the curvature. Since exposures were too short for calibration sources to measure the skyline curvature accurately the curvature measurements were used from target observations. Target spectra were then divided by a calibration star spectra taken at a similar air mass and time to remove atmospheric absorptions and produce a reflectance spectrum. A more detailed discussion of our data reduction methods is described in Brown (2000).

The signal to noise was low in individual spectra and therefore multiple spectra were added together to obtain higher signal-to-noise. In many cases, spectra were added over multiple nights (see Table 3.6). Multiple spectra of a single target were then summed together weighted by their noise to produce a final spectrum. We examined individual spectra to for look for substantial variability with time or rotational phase. We did not detect any significant variation in the spectra of any object, though small changes are undetectable due to noise. As such, the spectra we show here represent an average spectrum. High signal-to-noise spectra were obtained for most objects with an average of 6000 seconds of total integration time.

3.4 Analysis

The reflectance spectrum for each object is shown in Figures 3.1 through 3.6. We broadly find that our results fit with the spectral trends seen previously for KBOs (see Barucci et al. chapter in Barucci et al. (2008) for a review). The largest object in our survey, 2005 FY9, has spectral features dominated by methane ice, which has previously been explained by the low escape rate of volatiles on large KBOs (Schaller and Brown, 2007a). The lack of observed methane on the remaining objects in the sample supports the models of Schaller and Brown (2007a), which suggest that differential loss rates of volatiles can provide a first order explanation for the surfaces of KBOs and Centaurs. 2005 FY9 has been discussed in previous studies (e.g. Licandro et al. (2006c); Brown et al. (2007a)) and therefore will not be considered for further analysis.

With few exceptions, the remaining objects have either spectral signatures of water ice at 1.5 μm and 2.0 μm with varying line strengths or show no identifiable spectral features. Ideally, these spectra can provide information about the abundance of surface constituents. Approximations to the equations of radiative transfer for particulate surfaces have been developed by Hapke and others. They allow for the abundances and relative grain sizes of particles to be determined quantitatively using the reflectance spectra (Hapke, 1993). However, in practice, it is difficult to obtain accurate abundances because of the uncertainties in a number of parameters. To begin, the true geometric albedo, not the relative reflectance, is needed to estimate abundances accurately and few objects in

our survey have albedo measurements. For those with albedo measurements, uncertainties remain due to the limited knowledge of the particle scattering properties, degeneracies between intimate and geographic mixtures of the constituents, and poor constraints on the optical constants of the materials. With these difficulties in mind, we do not attempt to make precise surface models of the KBO in our survey. Still much can be learned by parameterizing the spectra of the whole population and comparing the relative strengths of the spectral signatures of water ice on the surface using Hapke models. In particular, we can determine if the data is consistent with the simple two component surface hypothesis of water ice and dark, carbon-rich material for the population as whole. Furthermore, we can relate the fitted parameters of the spectra to other physical and chemical properties of the sample with the aim of determining the processes that control surface characteristics.

Previously, the spectra obtained in our survey were parameterized by finding the flux ratio between 1.7 μm region where water ice produces little absorption and the 2.0 μm region, which is at the bottom of the water ice absorption feature (Brown et al., 2007b). This method introduces large errors into the parameterization as only small portions of the spectrum are utilized. To use the full information available in our spectra, we create spectral models of the surface reflectance between 1.4 and 2.4 μm using the equations of radiative transfer developed by Hapke (1993). To allow for comparison between objects, each spectrum was normalized to 1.0 by finding the median reflectance between 1.4 and 2.5 μm . The region near the 1.8 μm telluric water lines was excluded due to the large errors in this wavelength region. After each spectrum was normalized, it was fit with a spectral model using a least-squares minimization scheme that utilizes the Powell method for finding minima. A linear reflectance model of water ice and a continuum component was fit to each spectrum and solved for f, the fraction of water in the spectrum, and m, the slope of the continuum component. The model can be written as

$$R(f, m, \lambda) = f\mathcal{R}_w(T, g, \lambda) + (1 - f)\Big(m(\lambda - 2.0\,\mu m) + 1.0)\Big). \tag{3.1}$$

$\mathcal{R}_w$ is reflectance spectrum of water ice calculated using the optical constants from Grundy & Schmitt(1998) at a temperature, T, and for grain size, g. The spectral features of water ice show only slight changes with temperatures in range expected for the Kuiper belt, and therefore the temperature was set to 50 K (Grundy and Schmitt, 1998). The grain size, which parameterizes the optical path length through the ice, affects both the line shape and depth of water ice absorption features but has been found to be between $\sim$ 20 and $\sim$100 μm on KBOs. To allow f to be compared across all objects, we set the grain size to 50 μm , though different grains may exist on some objects. The slope of the continuum component, m, is allowed to vary but the reflectance of the continuum is constrained to be 1.0 at 2.0 μm . To match the model to the data, we normalize the model using the same method of dividing by the median that was used to normalize the data. The error in the reflectance at each wavelength used to calculate χ^2 was found by first subtracting a smoothed spectrum from the data and finding the standard deviation of the surrounding pixels. The smoothed spectrum was created using a boxcar average of a 9 pixel wide region centered at each wavelength and the standard deviation was calculated over the same 9-pixel swath.

Formal statistical 1-σ errors in the fit parameters were found by determining the values of f and m that produced χ^2 values equal to $\chi^2_{min} + 1$, where χ^2_{min} is the minimum χ^2 value (Bevington, 1969). However, the formal statistical errors do not take into account systematic errors and we find that they likely underestimate the true errors in our data. To obtain better estimates of the true errors, we selected objects in our survey whose spectra appeared to be consistent with no water ice by visual inspection. For these objects, we determined the actual error required to have an f consistent with 0 within 3-σ errors. We found that the formal statistical errors underestimated the true errors by a factor of $\sim$2 for these objects and therefore we take the actual 1-σ errors to be twice what was found by the formal statistics for all objects. The fit parameters for each object are listed in Table 3.6.

In addition to the spectral parameters we measured from the NIR spectra, we considered the visible color gradients of the objects, which are thought to be diagnostic of the carbon-rich materials on KBOs. It has been shown that the visible spectrum of KBOs between 0.5 μm and 0.8 μm is

well described by a single color gradient, G_v, measured using broadband photometery (Hainaut & Delsanti, 2002). We obtained visible color measurements for 35 of the 45 objects in our survey from published sources (see Table 3.6 for the full list) and calculated the color gradient and its uncertainty using the V, R, and I colors and the method described in Hainaut and Delsanti (2002). Five objects had no I-band measurements and one object had no R-band measurement. The spectral gradients were calculated for these objects using only the two available measurements. We find that the average difference in the gradient calculated using two versus three reflectance measurements is small compared to the errors in the color measurements. We also consider the sizes, albedos, and orbital characteristics of those objects in our survey for which measurements are available to gain a comprehensive understanding of these objects. The sizes and albedos are take from Stansberry et al. (2007) and are reproduced in Table 3.6 along with the orbital elements of the objects in our survey.

3.5 Results

We find that most of the spectra are well fit by our two component model and that the spectra had a final reduced χ^2_{min} of $\sim$1. See Figures 3.1 through 3.6 for the spectra and the best-fit model. Other than 2005 FY9, we find no compelling detections of additional ices such has NH_3, CH_4, CO, or CO_2, which are observed on some outer solar system bodies, though these species may be present in low abundances. Detections of NH_3 has been reported for Charon and Quaoar (Brown and Calvin, 2000; Jewitt and Luu, 2004). Our spectrum of Quaoar shows a similar flattening at 2.2 microns that was observed by Jewitt and Luu (2004) but the χ^2_{min} is not significantly decreased by the inclusion of NH_3 or its hydrate. CH_3OH has been previously detected on Pholus and 2002 VE95 (Cruikshank et al., 1998; Barucci et al., 2006). We find that our two component model works poorly for Pholus unless the region near the 2.3 CH_3OH absorption line is excluded. A three component model that included CH_3OH was constructed to determine if a better fit could be made by including this ice. We find that Pholus had a significant decrease in the χ^2_{min} value by including CH_3OH. For 2002 VE95, we find that the inclusion of CH_3OH did not produce a significantly better fit to our spectrum

and that our measured fraction of CH_3OH in the spectrum is consistent with 0. However, CH_3OH can contribute up to 25 percent reflectance of the spectrum without being detected because this region of our spectrum has lower signal to noise. Consequently, our spectrum may have insufficient signal-to-noise to detect the feature seen by Barucci et al. (2006). We find that 1996 GQ21, which has similar spectral features to Pholus, also does not have a significant detection of CH_3OH, but the signal-to-noise is similar to 2002 VE95. In summary, we find that Pholus is the only object in our survey for which the inclusion of a third component, CH_3OH, significantly improved the fit.

We detected water ice, that is f greater than 0, on 4 out of the 12 Centaurs and 12 of the 33 KBOs at the 3-σ level or greater. An additional 2 Centaurs and 4 KBOs have 1-σ detections of water ice on their surfaces. In our modeling, we find the family members of 2003 EL61 are distinguished from the general KBO population by significantly higher fractions of water ice in their spectra, f and the negative (blue) values for the slope of the NIR continuum, m. The four members of the 2003 EL61 collisional family in our survey, 1995 SM55, 2002 TX300, 2003 OP32, and 2005 RR43, as well as 2003 EL61 itself have a mean f of 0.93 and a standard deviation of 0.07. In contrast, the rest of the sample has values of f less than 0.55. Given that the family members are likely not representative of the general KBO population, we will treat these objects separately below and then return to the discussion of the spectral properties of the general population.

To best characterize the spectra, we allow the fraction of water ice in the spectrum to take on negative values in our modeling, effectively creating the inverse of the water ice spectral features. The aim was to discover if additional spectral characteristics could be identified. We find that five objects, Chaos, 1999 RZ253, 2002 KX14, 2005 RN43, and 2005 QU182 have negative f values to within 1-σ, but not within the 3-σ errors. These objects appear to have broad dips in their reflectance between 1.7 and 2.0 μm . This region straddles the telluric 1.8 μm water line and the dip may be due to poor correction of the telluric line as at least three of the objects, 2002 KX14, 2005 RN43, and 2005 QU182, were observed under variable weather conditions and their spectra are likely to have systematic errors. Phyllosilicates and other silicate materials have spectral features at 1.9 μm , but these minerals do not reproduce the broad dip thats extends to the region of 1.7 μm

in the spectrum. We also note that our model produces negative f values for spectra dominated by methane bands like that of 2005 FY9, though there is no indication that methane exists on the five objects listed above.

3.5.1 The 2003 EL61 Collisional Family

All the objects in our survey with the strongest signatures of water ice, that is f greater than 0.55, have previously been shown to be dynamically related to 2003 EL61 and are likely 100 to 300 km-sized fragments ejected from its mantle during a massive collision. The evidence for the giant impact and the formation of the fragments as well as their general spectral characteristics are discussed in Brown et al. (2007b). Ragozzine & Brown (2007, in press) discuss the dynamical nature of this family and find that the collision is over one billion years old and likely primordial. Here we discuss in greater detail their spectroscopic features.

In addition to the deep water ice absorption features, the family members have uniformly neutral color in the visible. This contrasts with the general KBO population, which shows a diversity of colors but are generally red (Figure 3.8), typically attributed to the presence of irradiated organics (Strazzulla et al., 1991; Hansen and McCord, 2004). The neutral visible colors are consistent with a relatively pure water ice surface but may also indicate a low abundance of the simple ices and organic materials from which tholins are formed. The model fits of the family members revealed that a second, blue continuum component significantly decreased the minimum χ^2 value with the exception of 2003 OP32. The blue component could be an artifact of modeling with a fixed grain size that is too small. Larger grain sizes would produce a slightly bluer water ice spectra. To determine if the blue component is required by the data, we created more complex models involving both intimate and geographically mixed water ices of varying grain sizes but were unable to reproduce the observed spectra. As such, the blue continuum component appears to be a real feature in the spectra of most of the family members. The slope of the component is varied, which may reflect the normalization rather than intrinsic differences between the objects. In an attempt to identify the blue component, we examined the spectra for additional features, but we find no evidence for additional absorptions

in the spectra. A similar blue component was reported by Trujillo et al. (2007) for 2003 EL61 and by Pinilla-Alonso et al. (2007) for 2005 RR43. In the case of 2003 EL61, HCN and phyllosilicate clays were both proposed as possible sources of the blue continuum component, but no positive identification was possible.

While difficult to determine much physical information for the blue continuum component without better data, the spectra do provide a few clues about the physical state of water ice on the surface. The 1.65 μm crystalline water ice feature is evident in all the spectra of family members. The crystal structure of water ice is expected to be destroyed by high energy particles and solar radiation on time scales short compared to the age of the family (Strazzulla et al., 1991; Hansen and McCord, 2004; Kouchi and Kuroda, 1990), causing the 1.65 μm feature to disappear. However, crystalline water ice is reported on surfaces of icy satellites as well as icy KBOs when spectra of sufficient signal-to-noise are available, suggesting a general process is likely acting to maintain the crystallinity of the water ice surfaces. Both thermal and non-thermal mechanisms have been proposed as a means to reform crystalline ice on these bodies. Cryovolcanism and out gassing, where surface materials are heated well above the crystallization temperatures of $\sim$100K have been proposed for bodies like Quaoar (Jewitt and Luu, 2004). Grundy et al. (2006) and Brown and Calvin (2000) have proposed maintaining crystalline ice through non-thermal processes such as slow vapor deposition from micrometeorite bombardment and non-thermal energy input from radiation. The presence of crystalline water ice on the family members appears to preclude thermal processes as the primary crystallization mechanism. KBOs with diameters less than 300 km are not expected to have sufficient geothermal energy to produce crystalline water ice near or at their surfaces. As such we argue that the processes of crystallizing water ice on these objects is non-thermal in nature. In the future we expect that any water ice detected on the surface of a KBO will be in the crystalline form regardless of size of the KBO.

In addition to the crystalline feature, the large depths of the 1.5 and 2.0 μm overtone features suggests that the grain size is higher for some of the members of the family than is often measured on KBOs. Though the grain size may not represent the true crystal grain size of the ice, it can be

used to judge the relative grain structures and impurities between objects. Using the models for a water ice surface that include scattering developed for Orcus and 2003 EL61 (Trujillo et al., 2005, 2007), we find that the grain sizes are between 100-125 μm on 2002 1995 SM55, 2002 TX300 and 2005 RR43- larger than is typically found for KBOs ((Barucci et al., 2008, Barucci et al. chap)). The water ice on 2003 OP32 was found to have a grain size of 60 μm , similar to grain size that Trujillo et al. (2007) found for 2003 EL61. The larger grain sizes on the family members may be consistent with water ice surfaces where the crystals have grown due to fewer impurities (Brown et al., 2007a).

From the spectra alone, it is difficult to infer specific details about the giant impact on proto-2003 EL61 as many of the parameters are poorly constrained or ambiguous. The large fraction of water ice detected on the family members could indicate that the proto 2003 EL61 was differentiated with material ejected largely from an icy mantle. Additionally, the spectral evidence is consistent with heating of the fragments during the impact, leading to devolatilization of carbon-bearing species, but the spectral signatures could be explained by other processes. With this in mind, the spectral characteristics may be best interpreted as identifying markers for the family members.

3.5.2 KBOs and Centaurs

A two component surface, with water ice as one end member and a dark, red, carbon-rich material at the other, could explain the variety of visible colors and variable presence of water ice seen on KBOs (e.g. Barucci et al. (2005)). In such a model, the measured f should correlate with the visible colors. In Figure 3.8 we see that there is little correlation between these parameters for either the KBO or the Centaur population. The colors of KBOs and Centaurs show no clear trend with f and are often variable amongst objects with similar f values. For example, 2003 AZ84 and Quaoar show similar degrees of water ice on their surfaces but 2003 AZ84 is neutral while Quaoar is moderately red. Barucci et al. (2005) argue that KBOs and Centaurs can be organized into four separate color groups (BB, BR, IR, RR). We find that all the 2003 EL61 collisional family members fall in to the bluest group (BB) as well as 2003 AZ84, suggesting that this group strongly correlates with the presence of water ice on the surface (Figure 3.9). The remaining objects in our survey

are distributed between the three other taxonomic groups, BR, IR, and RR. We find no correlation between the remaining three taxonomic groups and any NIR spectral characteristics we measured for our spectra. Specifically, we find that the fraction of water ice in the spectrum can vary widely amongst the objects in a particular group and that the groups have similar distributions of f with the exception of the BB group. As such, we do not anticipate that these taxonomic groups will yield specific information about the surface characteristics above predicting the likelihood of the presence of ices for objects in the BB group.

Though we do not physically model the surfaces of the KBOs and Centaurs in our survey, we can use models of simulated surfaces to predict trends that could be detected in the parameterization of a population of spectra. We created artificial spectra of idealized, two-component surfaces with varying ratios of water ice and a featureless component that represents carbon-rich material. We assume properties of the water ice and the featureless component based on those observed on icy bodies. The water ice reflectance was modeled in the NIR using the optical constants from Grundy and Schmitt (1998) and assuming isotropic scattering. We assumed a 60% albedo for the visible portion of the water ice reflectance and a grain size of 50 μm was used. The carbon-rich component is far less characterized though, so we created a family of models assuming different properties for the carbon-rich end member. We assumed that the visible gradient varied between 10% per 100 nm and 50% per 100 nm, which are typical values of the gradients measured on KBOs (Hainaut and Delsanti, 2002). The average NIR gradient, m, that we measured in our own data was much smaller than the visible gradient and therefore we set m to 0 for our synthetic carbon-rich component. The carbon-rich component was given an albedo of 10% at 550 nm, which is the average albedo of the ice-free objects in our survey (Stansberry et al., 2007). Since the surfaces of KBOs could be mixed either intimately or geographically, we consider both cases. In these simulations, we tacitly assume that while the carbon-rich component may be a mixture of materials, it is the same for all objects and that this material does not alter over time. For intimate mixtures we use our assumed reflectance for the carbon-rich component to calculate its single scattering albedos. The intimate mixture models were created by linearly mixing the single scatter albedos of water ice and the carbon-rich material

and calculating the resulting reflectance using the equations of radiative transfer from Hapke (1993). The synthetic NIR spectrum is then analyzed to determine f and m using the same methods used for the real spectra and the visible color gradient is calculated using the methods described in Hainaut and Delsanti (2002). Figure 3.8 shows the measured G_v and f for the synthetic surfaces.

We see that our results for the KBOs do not follow any of the models produced above, indicating that the surface of these KBOs is not well described by our synthetic two component surface model. While the exact f and m measured for our synthetic data depend on poorly known parameters like the albedo, the overall trends that our simple surface modeling predict should be similar regardless of the parameters of the modeling. Even a model in which the carbon-rich material reddens or the grain size is altered over time cannot explain the data if this material increasingly obscures the water ice.

The relationship between the albedo of the objects and f further suggest that a simple mixing of two components does not describe the surface of KBOs well. The albedos of KBOs are diverse, ranging from greater than 4% to 80% (Stansberry et al., 2007). The dwarf planet-sized KBOs have the highest albedos likely due to resurfacing of CH_4 or N_2 through atmospheric deposition (Stansberry et al., 2007; Brown et al., 2005b). In our sample, 17 KBOs and 10 Centaurs have measured albedos. If we exclude the methane giants and the KBOs in the collisional family of 2003 EL61, we find that there is no significant correlation between f and albedo of either KBOs or Centaurs using a Kendall rank-correlation test(see figure 3.10). In some cases, we see that objects like 1999 TC36 have significant detections of water ice on their surfaces had low albedos- 7%. Again, using the same two component synthetic surface models described above, we calculated the expected visual albedo as a function of f (Figure 3.10). It is apparent that our two component description of the surface fails to describe the data and that any new formulation of the surface characteristics must allow for a variety of albedos for a given abundance of water ice.

While there appears to be no clear trends in the colors or the albedos of KBOs and Centaurs and fraction of water ice in their spectra, we do find that there may be a correlation in the KBO population between f and the diameter. A Kendall rank-correlation test gives a correlation coef-

ficient of 0.5 with a probability of obtaining this correlation coefficient for a random data set of 1%. Barucci et al. in Barucci et al. (2008) noted this trend for the largest KBOs, but Figure 3.11 shows that this trend nominally extends down to moderate-sized KBOs in our survey and is not the result of observational bias against detecting water ice on smaller objects with lower signal-to-noise spectra. This trend may indicate that the formation of water ice on the surface is geophysically controlled as larger objects have greater heat from accretional energy and radiogenic materials than smaller objects. The higher heat available would make it more likely for these objects to experience geothermal processes, though there is no indication of recent geological activity.

However, we do not detect a correlation between size and the fraction of water ice in our sample of Centaurs. In contrast to the KBO population, we find that Centaurs of similar sizes can have a wide range in water ice abundances on their surfaces. This suggests that the processes that control the presence of water ice on the surface of Centaurs could be different than those on KBOs. We investigated if a mechanism relating to the far warmer temperatures on Centaurs may be responsible by examining the relation of f with perihelion distance. There too, a Kendall rank correlation test gives no significant correlation between the perihelion distance and f as well.

In general, we find no correlation between the NIR surface characteristics and the orbital elements of the KBOs or Centaurs in our population other than what has been previously noted for the collisional family of 2003 EL61 (Brown et al., 2007b). Figure 3.12 shows that the orbital elements of our sample with both icy and non-icy objects are evenly distributed thought the Kuiper belt's hot classical and scattered populations. As such, we conclude that no correlation seems to exist amongst the KBO orbital parameters for these dynamical populations and f above what has been previously been noted for the 2003 EL61 family.

Finally, the coincidence between icy surfaces and moon-forming collisions on 2003 EL61 and Pluto prompted us to examine if this trend extends to the other icy KBOs. We note that a number of objects in our survey with significant water ice absorptions including 2003 AZ84, Quaoar, 2003 TC36, and Ceto have satellites or are binary (Barucci et al., 2008, Noll et al. chap). Orcus, while not in our survey, also fits with this trend. It may be that collisions emplaced water ice on the

surfaces of these objects, but the spectra offer no definitive indications of a particular mechanism. Alternatively, 2002 UX25 has a satellite but shows no signatures of water ice. With this limited data it is unclear what trend, if any, exists between collisions, the abundance of water ice on the surface, and the presences of satellites in the KBO population.

3.6 Discussion

The lack of obvious trends in color, albedo and spectral characteristics suggests that multiple coloring agents are present in a variety of mixing ratios on KBOs. Differing grain sizes of the carbon-rich materials may account for some of the observed variation in the visible gradients and albedos, but it cannot fully account for the diversity of surface properties seen in the Kuiper belt. This may be indicating inherent heterogeneity in the surface properties of the general KBO population. With the exception of very blue, icy objects, the results presented here for the NIR data do not support clear ties between the photometric colors, specific spectral types, and surface characteristics.

The modest trend in size and water ice abundance that we detected indicates that water ice may be geothermally controlled on the surfaces of KBOs. With these mechanism though, we find no evidence that suggests that these surfaces are a result of recent activity. From the minimum dynamical lifetime of the 2003 EL61 family members of approximately 1 Gyr (Ragozzine & Brown, 2007, submitted), it is possible that the water ice surfaces we observe in the Kuiper belt are ancient surfaces formed when the KBOs had hotter interiors and the impact rates were higher.

At the moment though, trends seen in our data are sufficiently tenuous that it is difficult to make any strong conclusions about the relative importance of size and collisions in determining surface properties. Our survey included nearly all the KBOs that are bright enough to easily obtain NIR spectra from large telescopes, but future spectral studies of newly-discovery, bright objects and additional albedo measurements should clarify trends seen in our data. While much remains to be learned about the overall mechanisms shaping the outer solar system bodies, we find that a comparative approach to examining spectra provides a powerful additional tool for understanding these processes.

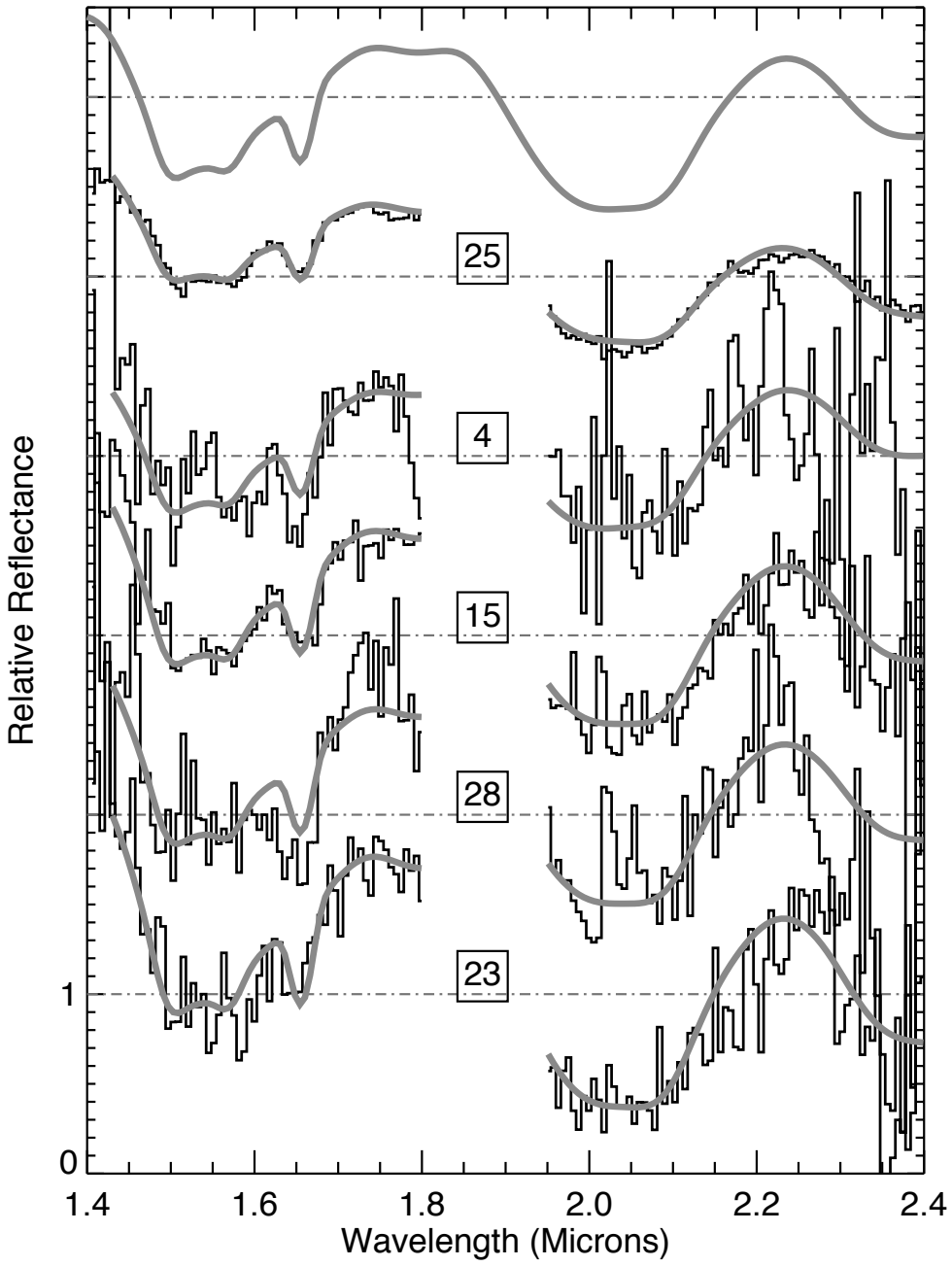

Figure 3.1: The relative reflectance spectra of 2003 EL61 and its collisional family. The KBOs shown above are 25– 2003 EL61, 4–1995 SM55,15–2003 TX300, 28–2005 RR43, and 23–2003 OP32. Each spectrum is normalized to 1.0 (the dashed grey lines) and offset to allow for comparison. A model spectrum of pure water ice is also shown at the top (thick dark grey line). The region between 1.8-1.9 μm is masked due to the high errors introducted by H_2O telluric lines. The thick grey line represents the best fit model to each spectrum and is a combination of water ice and a sloped continuum component. See Section 3.4 for more information on the modeling and Table 3.6 for the fit results.

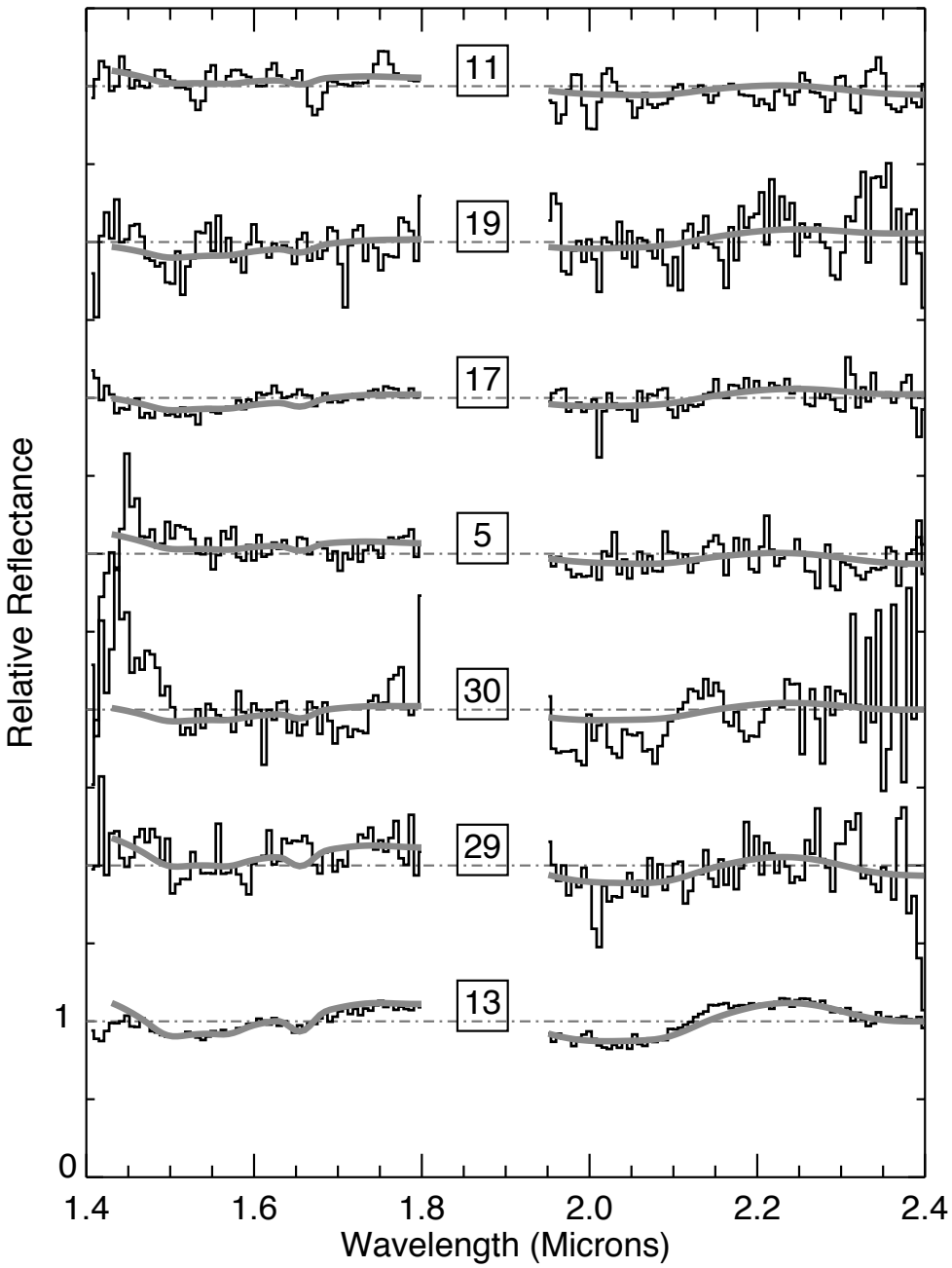

Figure 3.2: The relative reflectance spectra for the following KBOs: 13– Quaoar, 29– 2003 AZ84, 30– 2004 NT33, 5– 1996 GQ21, 17– 2002 VE95, 19– 2002 TC302, 11– 1999 TC36. The spectra are shown in decreasing fraction of water ice from bottom to top. See Table 3.6 fraction of water ice detected in the spectrum and the other fit results for the spectral models. Water ice is detected on Quaoar, 2003 AZ84, 1996 GQ21, 2002 VE95 and 1999 TC36 at the 3-σ level or greater. 2003. 2002 TC302 has a 2-σ detection of water ice. We do not detect additional ice species in the spectra of these KBOs.

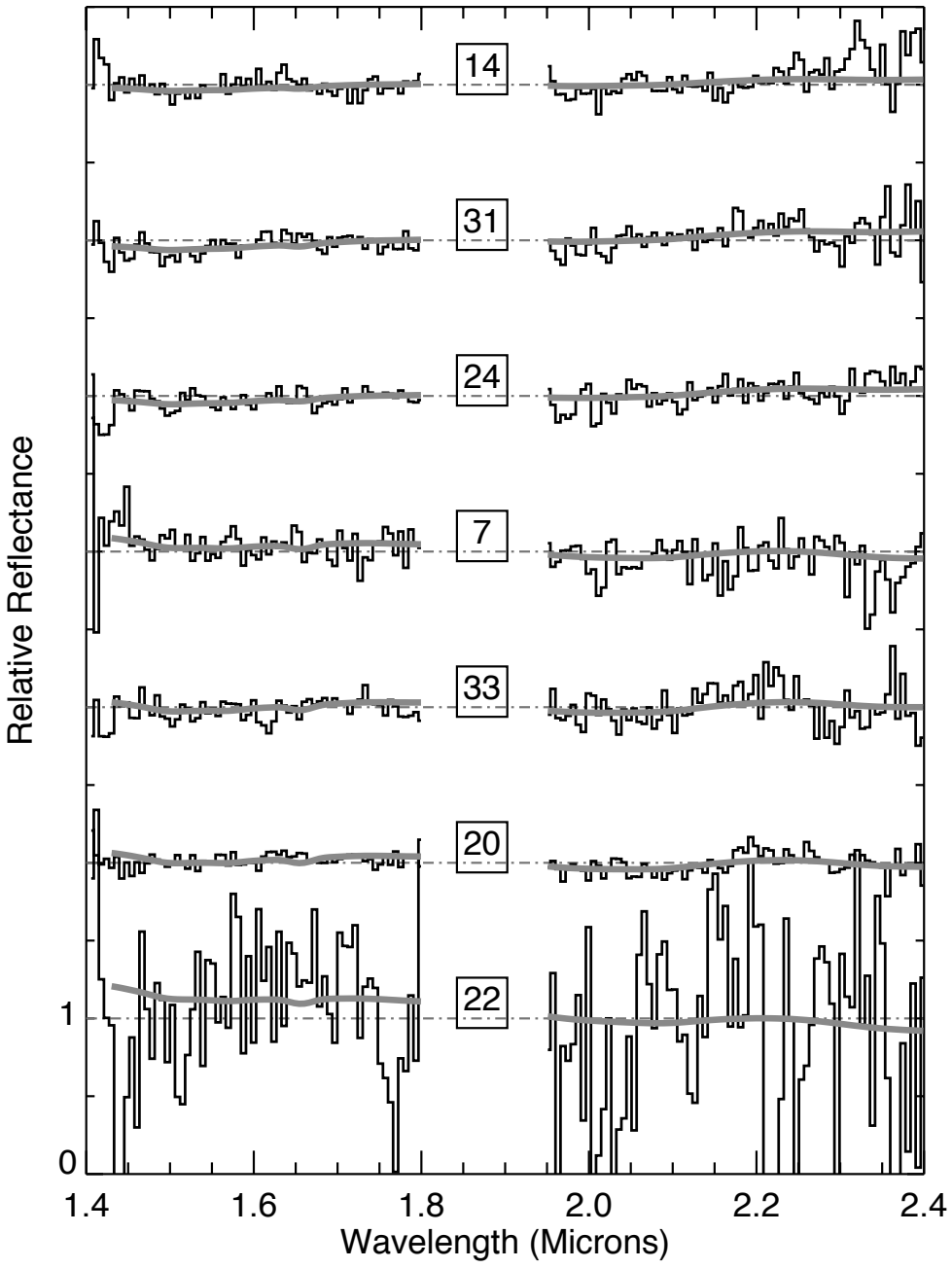

Figure 3.3: The relative reflectance spectra for the following KBOs: 22– 2003 FY128, 20– 2003 VS2, 33– 2005 UQ513, 7– Ixion, 24– 2004 TY364, 31–2004 PG115, and 14– 2002 AW97. The spectra are shown in decreasing fraction of water ice from bottom to top. See Table 3.6 fraction of water ice detected in the spectrum and the other fit results for the spectral models. Water ice is detected on 2003 VS2 at greater than the 3-σ level. It is marginally detected on 2005 UQ513, Ixion, 2004 TY364, and 2004 PG115 at at least the 1-σ level.

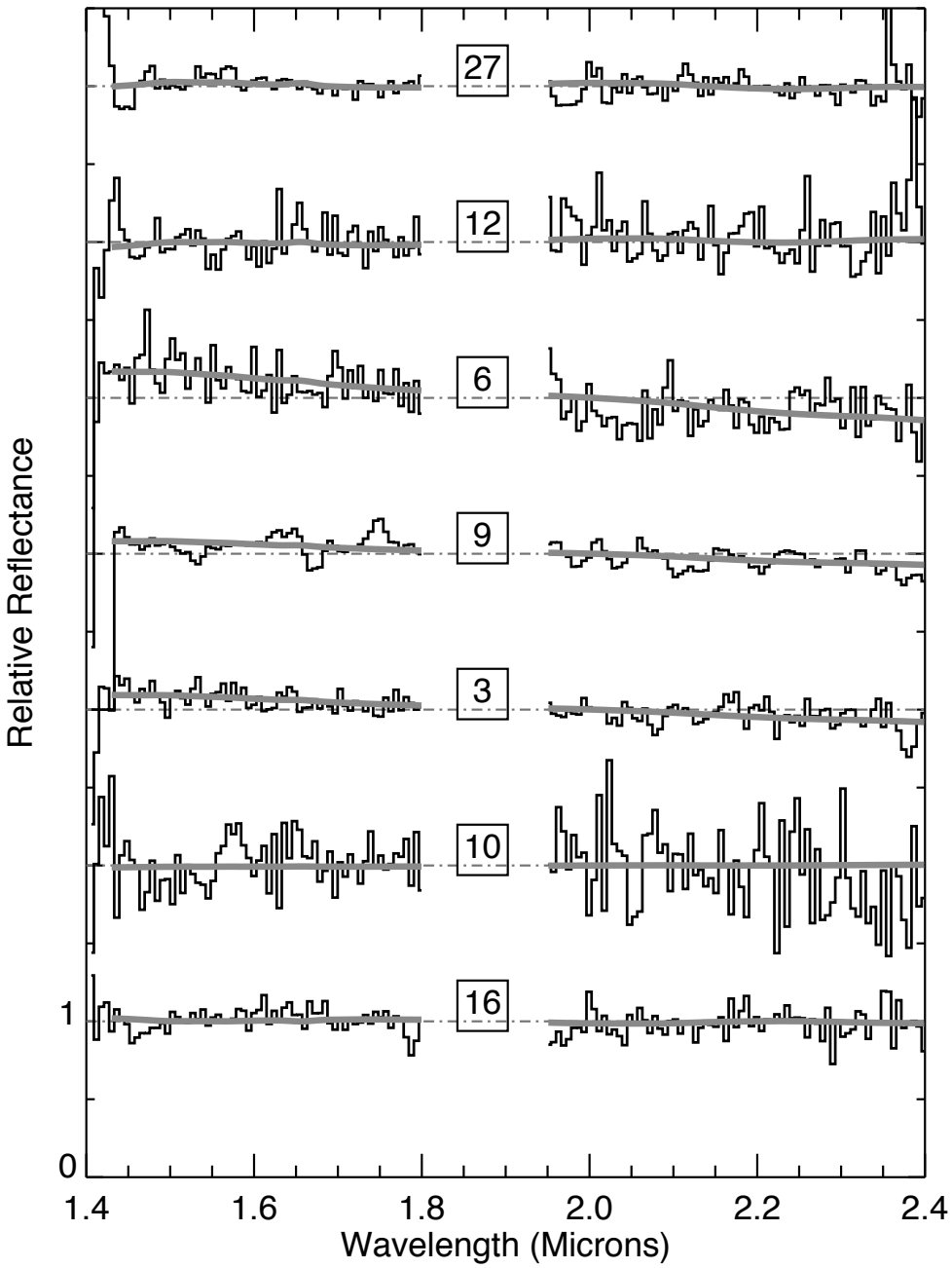

Figure 3.4: The relative reflectance spectra for the following KBOs: 16– 2002 UX25, 10– 2001 UR163, 3– Varuna, 9– Huya, 6– 1999 DE9, 12– 2000 GN171, 27– 2005RN43. The spectra are shown in decreasing fraction of water ice from bottom to top. See Table 3.6 fraction of water ice detected in the spectrum and the other fit results for the spectral models. No ices are detected on these KBOs.

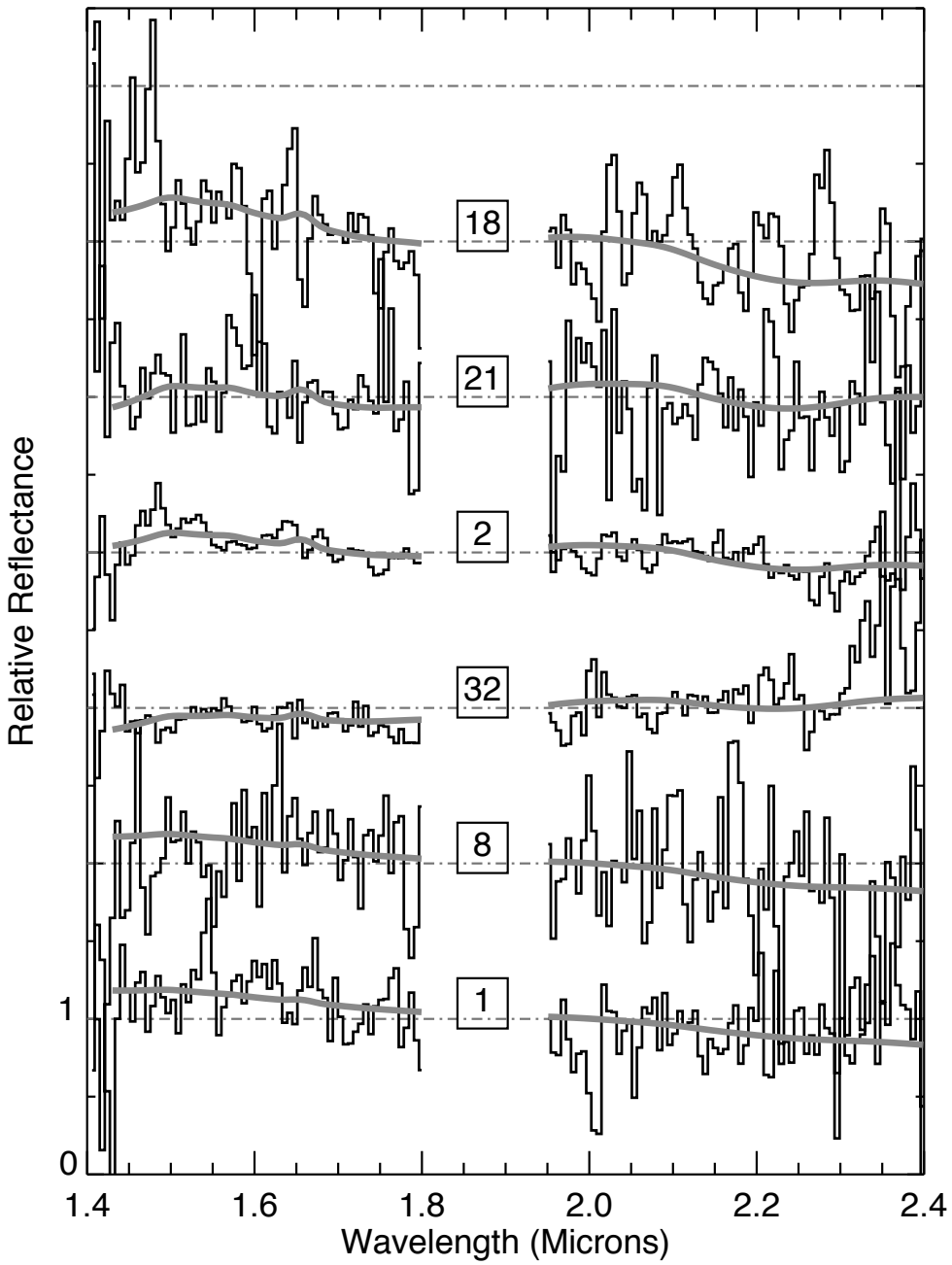

Figure 3.5: The relative reflectance spectra for the following KBOs: 1– 1996 TP66, 8– 1998 VG44, 33– 2005 QU182, 2– Chaos, 21– 2002 KX14, 18– 1999 RZ256. The spectra are shown in decreasing fraction of water ice from bottom to top. See Table 3.6 fraction of water ice detected in the spectrum and the other fit results for the spectral models. Best-fit models produce negative f values for these KBOs which may be related to variable weather conditions during observing. See Section 3.5 for more details.

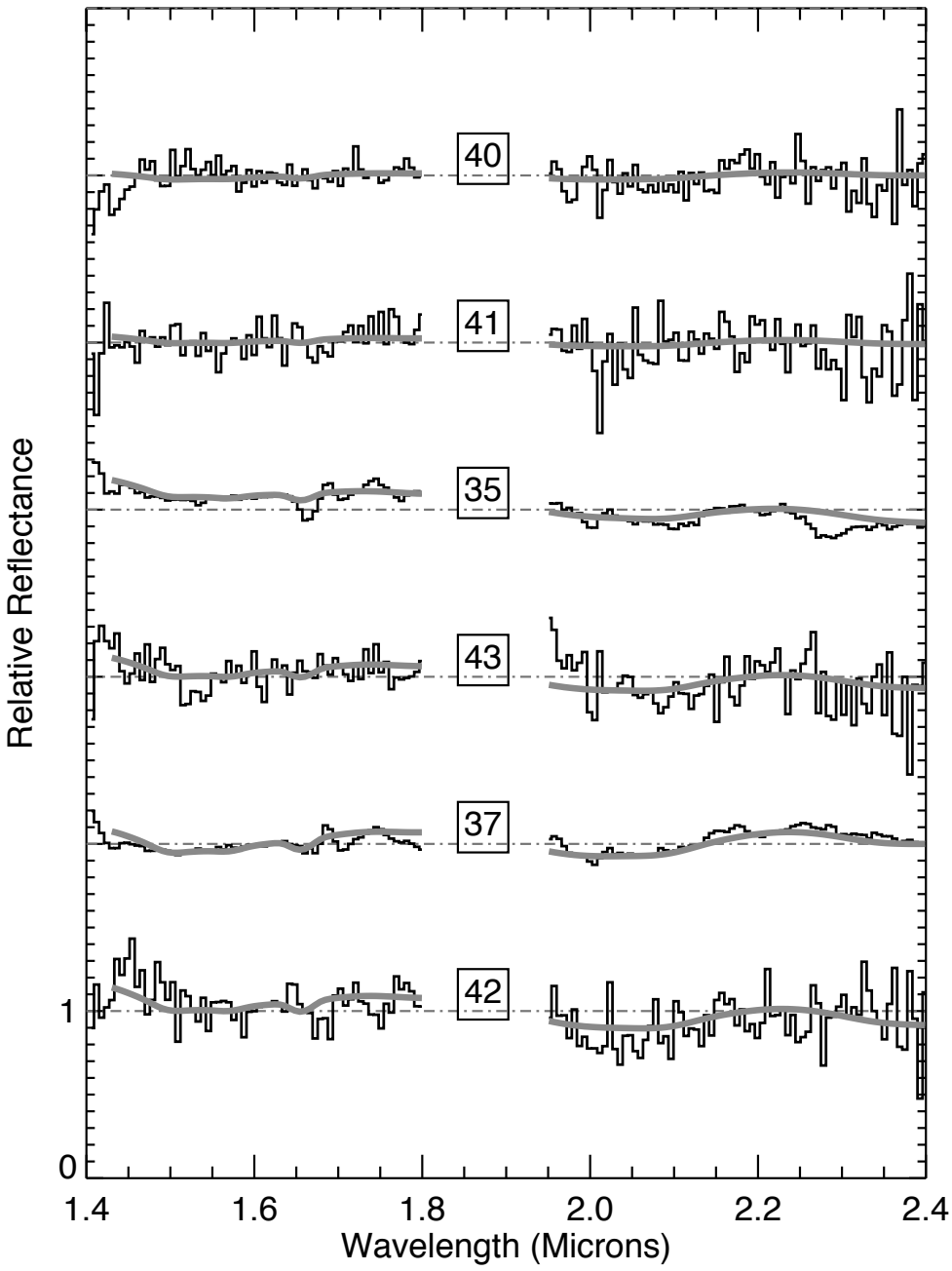

Figure 3.6: The relative reflectance spectra for the following Centaurs: 42– Crantor, 37– Chariklo, 35– Pholus, 43– Ceto, , 41– Bienor, 40– Okyrhoe. The spectra are shown in decreasing fraction of water ice from bottom to top. Water ice is detected on Crantor, Chariklo, Pholus, and Ceto at the 3-σ level or greater. Bienor and Okyrhoe have detections of water ice at a level between 1-σ and 3-σ. See Table 3.6 fraction of water ice detected in the spectrum and the other fit results for the spectral models.

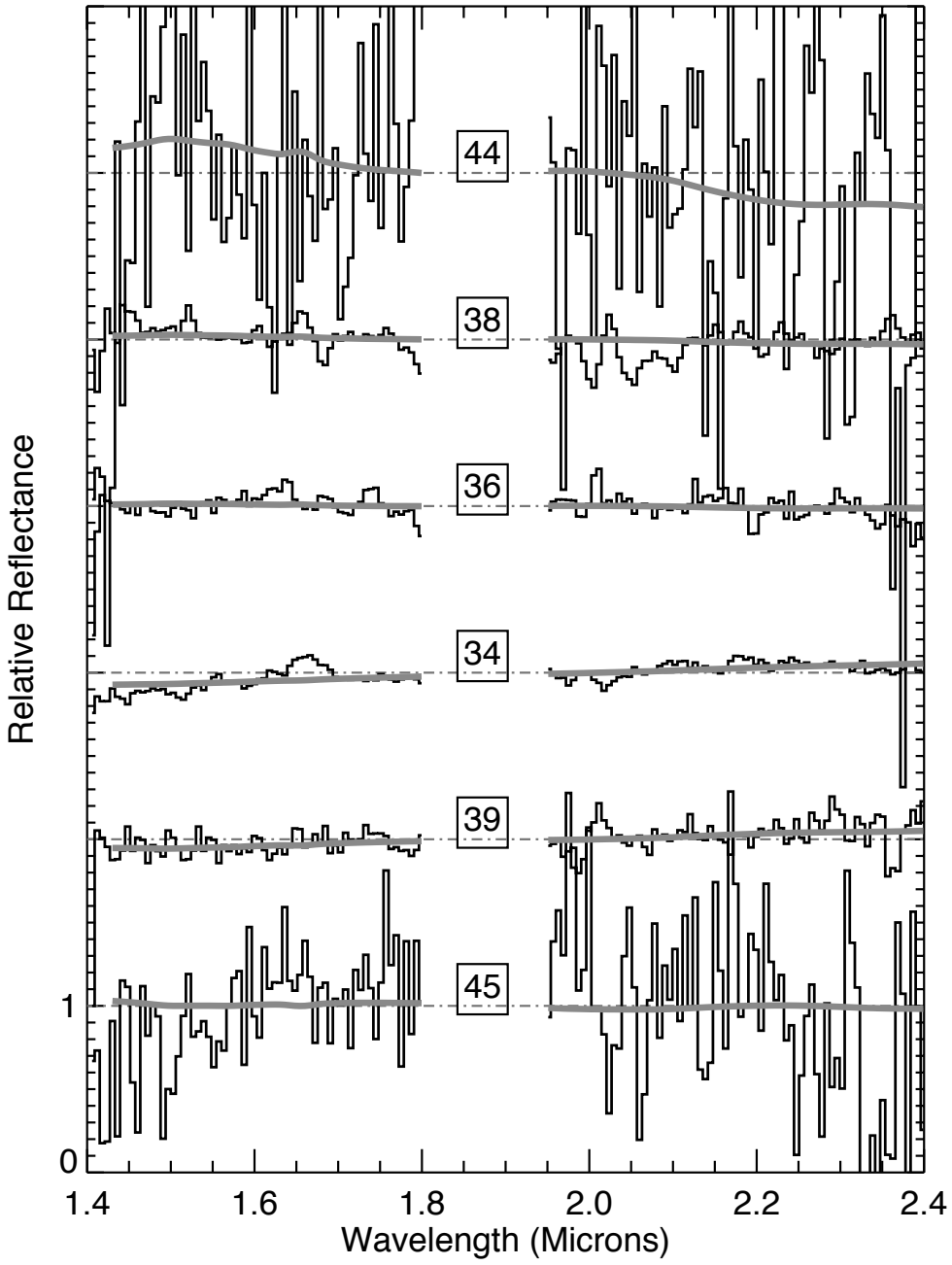

Figure 3.7: The relative reflectance spectra for the following Centaurs: 45– 2002 XU93, 39– Elatus, 34– Chiron, 36– Asbolus, 38– 1999TD10, 44– 2002GZ32. The spectra are shown in decreasing fraction of water ice from bottom to top. No water ice is detected on these Centaurs in our data.

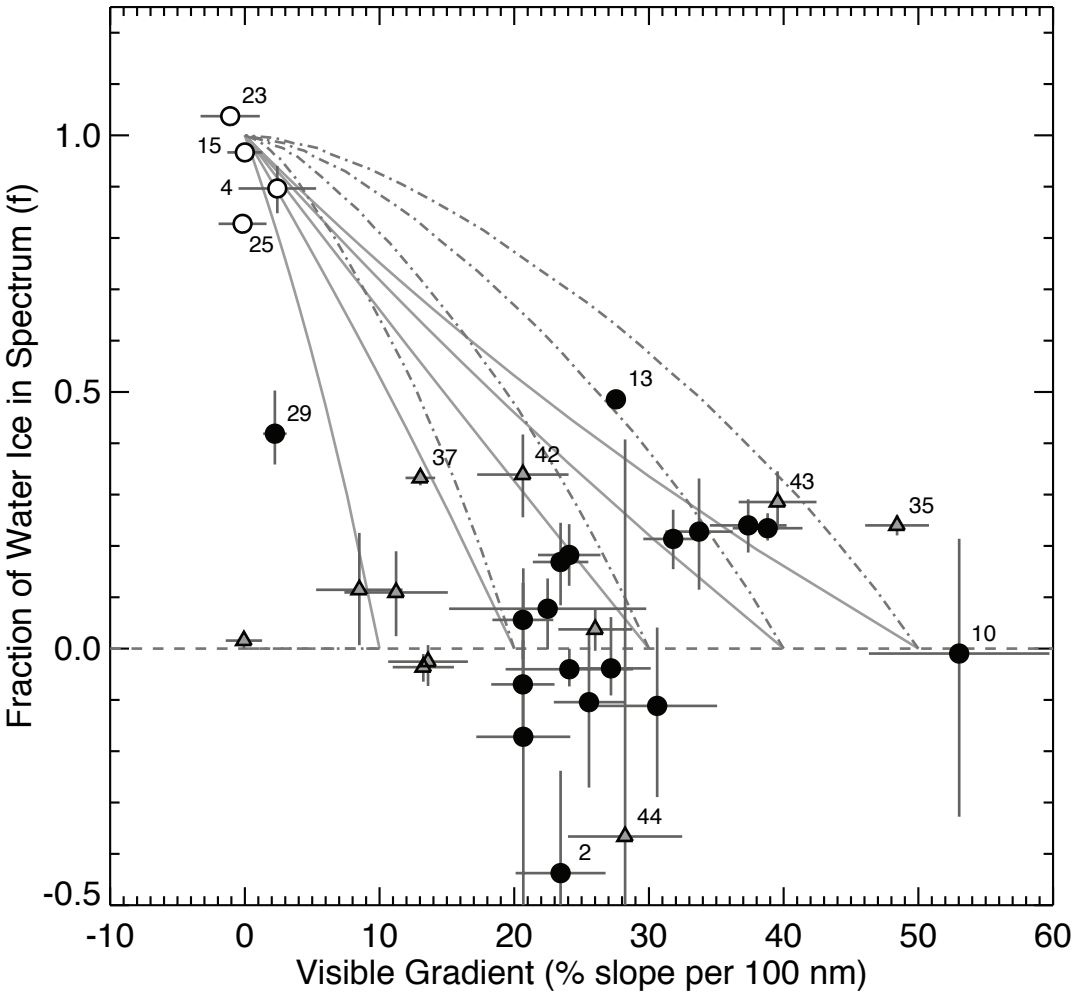

Figure 3.8: The fraction of water ice detected in the spectrum versus the visible color gradient for KBOs (black circles) and Centaurs (grey triangles). 2003 EL61 and its collisional family are represented by white circles. The errors are the 3-σ error bars. Objects of interest are labeled with numbers as they appear in tables. The thick grey lines represent the expected distribution for a two component system where water ice and a featureless continuum are the end members and are mixed geographically (see Section 3.5.2). The different lines represent different color gradients for the featureless component. The dashed grey lines represent intimate mixtures of the two components. Once the collisional family of 2003 EL61 is excluded, no correlation is found between the fraction of water ice detected in the spectrum of KBOs and Centaurs and their visible colors.

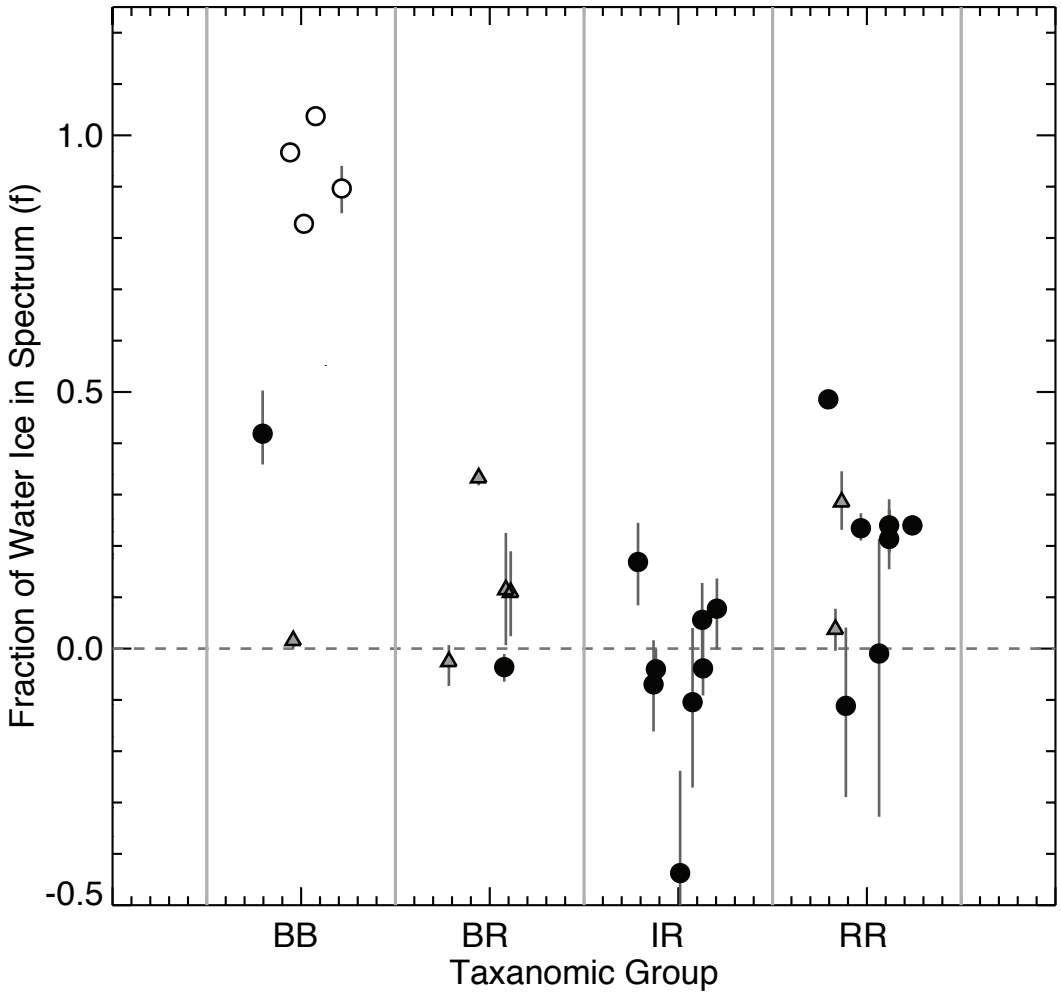

Figure 3.9: The fraction of water ice detected in the spectrum versus the taxonomic group for KBOs (black circles) and Centaurs (grey triangles). 2003 EL61 and its family are presented by white circles. The taxanomic designations are based on an analysis of the visible and NIR photometric colors and are directly from citetbar05. Each object has been offset to make them more easily distinguishable. We find that the BB (blue) group is generally well correlated with the presence of significant detections of water ice in the spectrum since this group is dominated by the 2003 EL61 collisional family members. Of the remaining groups, RB (red-blue), IR (intermediate red), and RR (red), we find no correlation with the fraction of water ice detected in the spectrum. As such these taxonomic groups do not appear to correspond to specific spectral signatures in our NIR spectra.

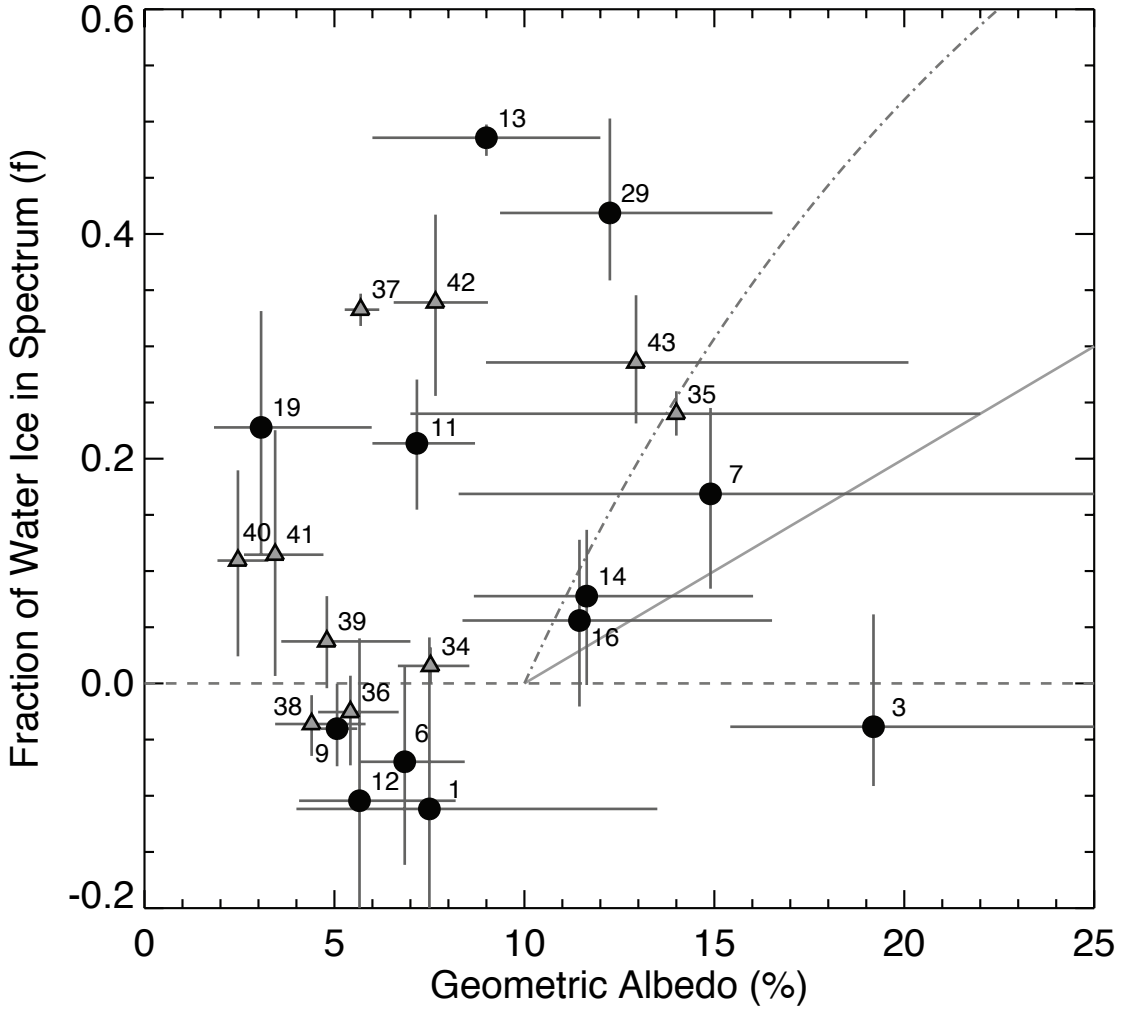

Figure 3.10: The fraction of water ice detected in the spectrum versus the albedo for KBOs (black circles) and Centaurs (grey triangles). 2003 EL61 is not shown, but has an albedo of 84^{+10}_{-20} and an f of $0.83^{+0.01}_{-0.01}$. The albedos are from Stansberry et al. (2007). Objects of interest are labeled with numbers as they appear in tables. We find no correlation in the fraction of water ice detected in the spectrum and the albedo measured for the object. The thick grey line represents the expected albedo for a given surface fraction of water ice and is determined from our two component synthetic surface model. In the model we assume water ice with at 60% albedo and a dark, featureless material with a V-band albedo of 10 % mix geographically in various ratios. The dashed line represents the distribution expected for an intimate mixture of the two components.

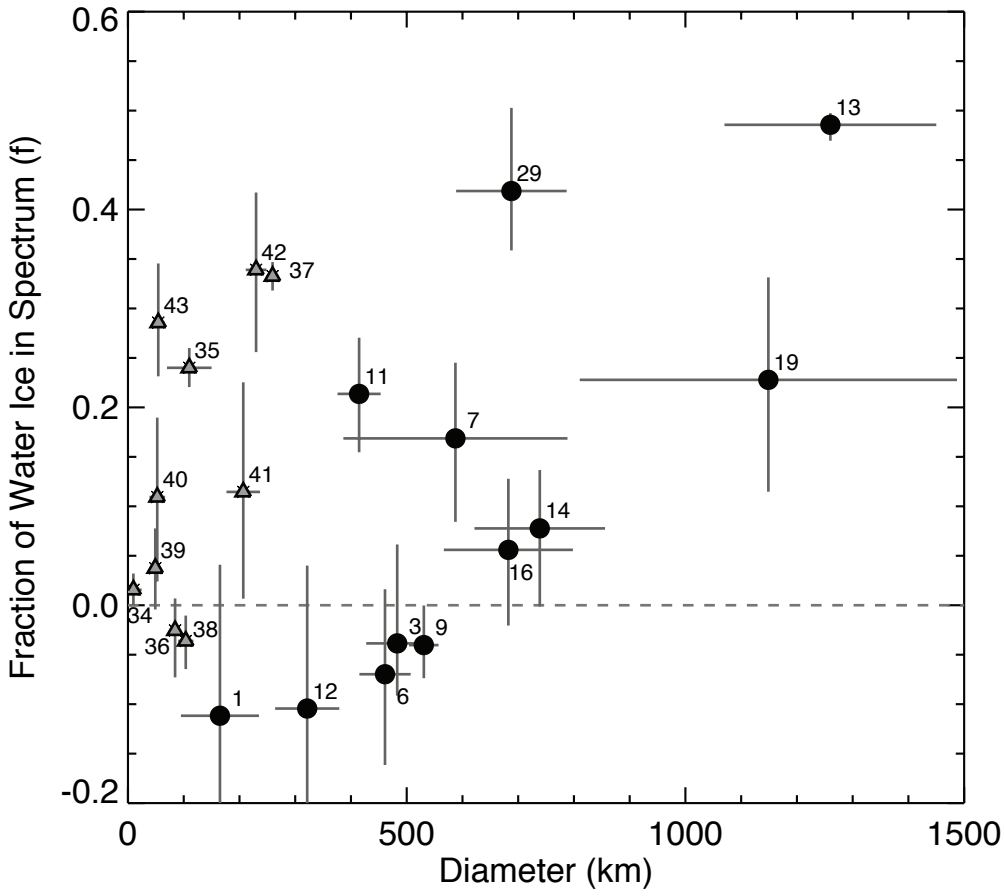

Figure 3.11: The fraction of water ice detected in the spectrum versus the diameter of KBOs (black circles) and Centaurs (grey triangles). The objects are labeled with numbers corresponding to their appearance in the tables. We find a correlation between the size and the degree of water ice detected for KBOs. A Kendall rank correlation giving a coefficient of 0.5 with a probability of obtaining this value for a random data set of 1%. A similar correlation is not seen for Centaurs.

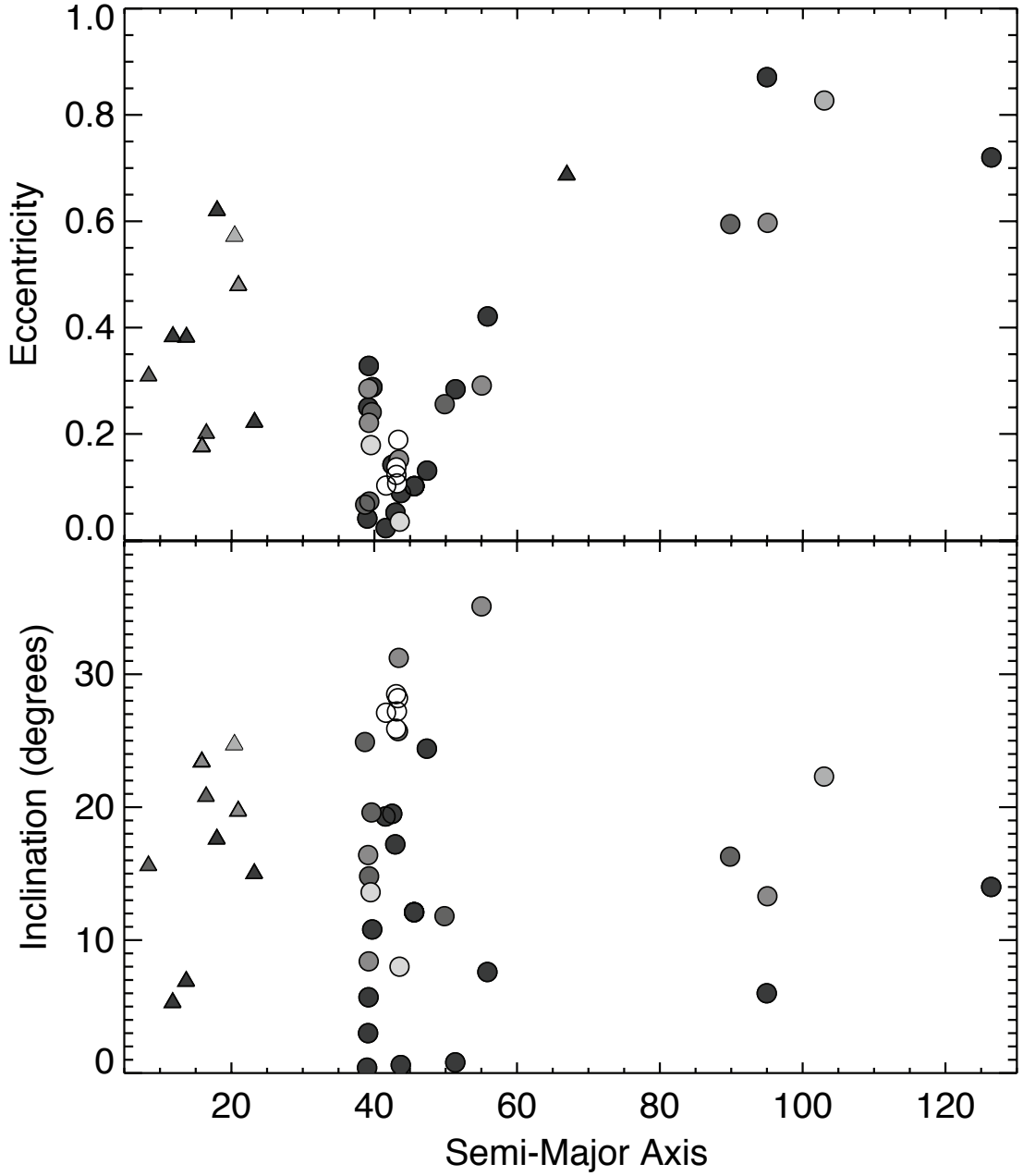

Figure 3.12: The orbital parameters of objects in our survey. KBOs are represented by circles and Centaurs by triangles. Shading represents the fraction of water ice in the spectrum, f. The white data points are objects with $f > 0.4$, medium grey have $0.4 < f > 0.2$, and dark grey have $f < 0.2$. The white objects are concentrated in orbits near 2003 EL61 and are the collisional family members. The remaining objects with moderate water ice detection are scattered throughout the trans-Neptunian region. Once the 2003 EL61 family is discarded, we find no correlation between the NIR spectral properties of the objects in our survey and their orbital parameters.

Journal of Near Infrared Camera Observations

Number	Object	UT Date	Exposure Time	Air mass	Calibration Source
		Kuiper Belt Objects			
1	15875 (1996 TP66)	2000 Jul 22	5000 s	1.27-1.02	BD +17 209
		2000 Aug 5	6200 s	1.21-1.02	BD +05 5212
		2000 Aug 6	1000 s	1.01-1.02	BD +05 5212
2	19521 Chaos (1998 WH24)	2000 Sept 15	11000 s	1.00 - 1.36	HD30701, SAO 149875
3	20000 Varuna (2000 WR106)	2001 Mar 10	6000 s	1.47-1.05	HD 42112, HD 41919
					HD 42358, HD41880
4	24835 (1995 SM55) [1]	2006 Oct 9	3000 s	1.10-1.20	HD 254985
5	26181 (1996 GQ21)	2001 Mar 10	8000 s	1.14-1.38	HD 150583, HD 148592
					HD 151786, HD 149826
		2001 May 5	4000 s	1.14-1.27	HD 133688
6	26375 (1999 DE9)	2000 Mar 10	6000 s	1.05-1.22	HD 43515, HD 40977
					HD 42112, HD 148116
7	28978 Ixion (2001 KX76)	2002 May 27	4000s	1.29-1.39	HD100803
8	33340 (1998 VG44)	2003 Nov 13	4000 s	1.00-1.03	HD 285216
9	38628 Huya (2000 EB173)	2000 Jun 18	1800 s	... [2]	SAO 11973
		2000 Jun 19	2700 s	... [2]	SAO 11973
10	42301 (2001 UR163)	2004 Nov 22	3000 s	1.02-1.08	BD +09 93
11	47171 (1999 TC36)	2000 Aug 6	5200 s	1.18 - 1.46	BD +05 5212
		2003 Nov 11	4000 s	1.11-1.16	BD +07 173
12	47932 (2000 GN171)	2001 May 6	6000 s	1.10-1.18	HD 133688
13	50000 Quaoar (2002LM60)	2003 May 10	3000 s	1.22	HD 155731
		2003 May 12	7000 s	1.23-1.41	HD 161788, HD 155731
14	55565 (2002 AW197)	2003 Nov 10	3000 s	1.02-1.04	HD 262124
		2003 Nov 11	1000 s	1.07-1.10	BD +09 2095
		2003 Nov 12	1000 s	1.14	BD +09 2095
15	55636 (2002 TX300) [1]	2003 Nov 10	2000 s	1.01-1.00	HD 461
		2004 Sep 5	5000 s	1.01-1.13	HD 4820
16	55637 (2002 UX25)	2003 Nov 10	6000 s	1.01-1.04	HD 461, BD +07 369
17	55638 (2002 VE95)	2003 Nov 11	8000 s	1.01-1.09	BD +8 615
18	66652 (1999 RZ253)	2000 Aug 5	2000 s	1.33-1.23	HD 204741
		2000 Aug 6	4000 s	1.22-1.43	HD 204741, BD +05 5212

Journal of Near Infrared Camera Observations Continued

Number	Object	UT Date	Exposure Time	Air mass	Calibration Source
19	84522 (2002 TC302)	2003 Nov 13	5000 s	1.24-1.00	HD13650
20	84922 (2003 VS2)	2005 Oct 15	4000 s	1.20-1.49	HD 281368
21	119951 (2002 KX14)	2003 May 10	3000 s	1.29-1.33	HD 143955
22	120132 (2003 FY128)	2003 May 5	3000 s	1.09-1.10	HD 113254
23	120178 (2003 OP32) [1]	2005 Oct 15	4000 s	1.11- 1.36	HD 206938
24	120348 (2004 TY364)	2005 Oct 15	5000 s	1.18-1.25	HD 15907
25	136108 (2003 EL61) [1]	2005 Apr 26	5000 s	1.01-1.19	HD 126694
26	136472 (2005 FY9)	2005 Apr 26	3000 s	1.02-1.11	HD 113338
		2005 Apr 27	6000 s	1.17-1.04	HD 100796
27	145452 (2005 RN43)	2006 Oct 7	4000 s	1.07-1.08	HD 206938
28	145453 (2005 RR43) [1]	2006 Oct 8	3000 s	1.05-1.15	G32-8
		2006 Oct 9	3000 s	1.17 -1.29	HD 34828
29	2003 AZ84	2004 Nov 22	4000 s	1.01 -1.12	HD 264528
					HD 63690
		2007 Apr 5	5000 s	1.02-1.49	BD +13 1721, HD 77708
					BD +25 1858, HD 87860
		2007 Apr 6	4000 s	1.02-1.10	HD 77708
30	2004 NT33	2005 Oct 14	3000 s	1.06-1.01	BD +12 4466
31	2004 PG115	2004 Sep 5	6000 s	1.08-1.23	SAO 144860
32	2005 QU182	2006 Oct 9	4000 s	1.23-1.39	G 32-8
33	2005 UQ513	2006 Oct 7	3000 s	1.07-1.09	BD +03 351
		2006 Oct 8	3000 s	1.04-1.11	BD +14 4758
		Centaurs			
34	2060 Chiron (1977 UB)	1998 Aug 03	500 s	1.76-1.83	SAO 159027 (A0)
35	5145 Pholus (1992 AD)	1998 Mar 08	2000 s	1.05-1.22	SAO 100913 (A3)
36	8405 Asbolus (1995 GO)	1998 Mar 07	1000 s	1.33-1.34	SAO 182160 (A2)
37	10199 Chariklo (1997 CU26)	1998 Mar 07	1000 s	1.03- 1.05	SAO 098558 (A2)
38	29981(1999 TD10)	2000 Aug 6	4000 s	1.05 - 1.08	BD +05 5212
39	31824 Elatus (1999 UG5)[2]	...	...	...	...
40	52872 Okyrhoe (1998 SG35)	2003 Nov 12	4000 s	1.04-1.08	HD 26064
41	54598 Bienor (2000 QC243)	2003 Nov 11	6000 s	1.10-1.18	SAO 146792
					HD221221

Journal of Near Infrared Camera Observations Continued

Number	Object	UT Date	Exposure Time	Air mass	Calibration Source
42	65489 Ceto (2003 FX128)	2003 May 11	1800 s	1.05-1.41	HD160805, HD 107514
		2003 May 12	3200 s	1.04-1.07	HD 113254
		2007 Apr 5	4000 s	1.25-1.65	BD +01 2956, HD 146396
					HD 159741, HD 155598
		2007 Apr 6	6000 s	1.05-1.25	HD 130875, HD 155598
43	83982 Crantor (2002 GO9)	2003 May 12	3000 s	1.07 -1.13	HD 126170
44	95626 (2002 GZ32)	2003 May 11	2600 s	1.01	HD 107514
45	127546 (2002 XU93)	2003 Nov 10	7000 s	1.03-1.17	HD 262124
		2003 Nov 11	4000 s	1.01-1.03	HD 262125

[a]2003 EL61 and its associated family members
[b]Observing log records could not be recovered

Spectral Properties

	Name	Tax. [1]	Vis Gradient [2]	NIR gradient (m) [3]	f [4]	depth [5]	χ^2_v [6]	Ices prev Detected[7]	References
				Kuiper Belt Objects					
1	15875 (1996 TP66)	RR	30.61± 4.45	$-3.76^{+0.45}_{-0.47}$	$-0.11^{+0.16}_{-0.18}$	$-0.03^{+0.04}_{-0.04}$	1.22	···	1
2	19521 Chaos (1998 WH24)	IR	23.44± 3.34	$-1.86^{+0.09}_{-0.26}$	$-0.44^{+0.06}_{-0.06}$	$-0.12^{+0.04}_{-0.02}$	1.85	···	2
3	20000 Varuna (2000 WR106)	IR	27.18± 2.95	$-1.86^{+0.17}_{-0.17}$	$-0.04^{+0.06}_{-0.06}$	$-0.01^{+0.02}_{-0.02}$	1.07	H_2O	2,3
4	24835 (1995 SM55) [8]	BB	2.41± 2.88	$4.89^{+1.50}_{-1.50}$	$0.90^{+0.04}_{-0.04}$	$0.56^{+0.06}_{-0.06}$	1.11	···	1
5	26181 (1996 GQ21)	RR	37.37± 2.85	$-1.50^{+0.18}_{-0.18}$	$0.24^{+0.06}_{-0.06}$	$0.09^{+0.02}_{-0.02}$	1.32	none	1,4
5	26181 (1996 GQ21)	RR	37.37± 2.85	$-1.50^{+0.18}_{-0.18}$	$0.24^{+0.06}_{-0.06}$	$0.09^{+0.02}_{-0.02}$	1.32	none	1,4
6	26375 (1999 DE9)	IR	20.64± 2.35	$-3.33^{+0.30}_{-0.30}$	$-0.07^{+0.08}_{-0.10}$	$-0.02^{+0.02}_{-0.02}$	1.41	H_2O	1, 5
7	28978 Ixion (2001 KX76)	IR/RR	23.44± 2.06	$-1.01^{+0.23}_{-0.24}$	$0.17^{+0.08}_{-0.08}$	$0.06^{+0.04}_{-0.04}$	1.09	possible H_2O	1, 6, 7
8	33340 (1998 VG44)	IR	20.67± 3.49	$-3.85^{+0.78}_{-0.78}$	$-0.17^{+0.32}_{-0.38}$	$-0.05^{+0.10}_{-0.10}$	1.08	···	2
9	38628 Huya (2000 EB173)	IR	24.09± 4.73	$-1.64^{+0.09}_{-0.09}$	$-0.04^{+0.04}_{-0.04}$	$-0.01^{+0.02}_{-0.02}$	2.21	possible H_2O	1,5, 8, 9
10	42301 (2001 UR163)	RR	53.03± 6.70	$0.15^{+0.65}_{-0.65}$	$-0.01^{+0.22}_{-0.32}$	$-0.00^{+0.08}_{-0.10}$	1.17	···	10
11	47171 (1999 TC36)	RR	31.80± 2.22	$-1.16^{+0.16}_{-0.16}$	$0.21^{+0.06}_{-0.06}$	$0.08^{+0.02}_{-0.02}$	1.27	H_2O	10, 11, 12
12	47932 (2000 GN171)	IR	25.55± 2.61	$0.30^{+0.22}_{-0.22}$	$-0.10^{+0.14}_{-0.16}$	$-0.03^{+0.04}_{-0.04}$	0.95	none	1, 9
13	50000 Quaoar (2002 LM60)	RR?	27.55± 0.20	$0.47^{+0.03}_{-0.04}$	$0.49^{+0.02}_{-0.02}$	$0.21^{+0.00}_{-0.00}$	2.56	H_2O	13, 14
14	55565 (2002 AW197)	IR	22.48± 7.32	$0.75^{+0.16}_{-0.16}$	$0.08^{+0.06}_{-0.08}$	$0.03^{+0.02}_{-0.02}$	1.52	H_2O	2, 15
15	55636 (2002 TX300) [8]	BB	0.00± 1.30	$-27.33^{+1.94}_{-1.94}$	$0.97^{+0.01}_{-0.01}$	$0.64^{+0.01}_{-0.00}$	1.13	H_2O	16, 17
16	55637 (2002 UX25)	IR	20.64± 2.26	$-0.20^{+0.14}_{-0.14}$	$0.06^{+0.08}_{-0.08}$	$0.02^{+0.02}_{-0.02}$	1.31	···	10
17	55638 (2002 VE95)	RR	38.81± 2.59	$0.98^{+0.07}_{-0.07}$	$0.23^{+0.02}_{-0.02}$	$0.09^{+0.02}_{-0.02}$	1.78	H_2O, CH_3OH	18
18	66652 (1999 RZ253)	RR	28.67± 3.61	$-5.24^{+0.72}_{-0.72}$	$-0.72^{+0.60}_{-0.64}$	$-0.17^{+0.14}_{-0.12}$	1.14	···	2
19	84522 (2002 TC302)	···	33.72± 2.50	$1.65^{+0.37}_{-0.37}$	$0.23^{+0.10}_{-0.12}$	$0.09^{+0.04}_{-0.04}$	1.21	···	1
20	84922 (2003 VS2)	···	24.08± 2.32	$-0.50^{+0.10}_{-0.15}$	$0.18^{+0.04}_{-0.04}$	$0.07^{+0.02}_{-0.02}$	1.41	···	10
21	119951 (2002 KX14)	···	26.42± 2.37	$-0.28^{+0.26}_{-0.26}$	$-0.67^{+0.58}_{-0.66}$	$-0.17^{+0.12}_{-0.10}$	1.12	···	10
22	120132 (2003 FY128)	···	···	$-2.61^{+0.96}_{-1.17}$	$0.18^{+0.72}_{-0.21}$	$0.07^{+0.16}_{-0.16}$	1.29	···	···
23	120178 (2003 OP32)[8]	BB?	-1.09± 2.20	$42.42^{+2.19}_{-0.74}$	$1.04^{+0.01}_{0.01}$	$0.74^{+0.00}_{0.00}$	···	19	
24	120348 (2004 TY364)	···	···	$0.99^{+0.16}_{-0.15}$	$0.10^{+0.06}_{-0.06}$	$0.04^{+0.02}_{-0.02}$	1.14	···	···
25	136108 (2003 EL61) [8]	BB	-0.17± 1.78	$-10.68^{+0.19}_{-0.22}$	$0.83^{+0.01}_{-0.01}$	$0.48^{+0.00}_{-0.00}$	2.05	H_2O	20, 21,22
26	136472 (2005 FY9)	BR	···	$-6.39^{+0.13}_{0.00}$	···	···	···	CH_4, C_2H_6	23, 24
27	145452 (2005 RN43)	···	···	$-0.24^{+0.13}_{-0.14}$	$-0.11^{+0.08}_{-0.10}$	$-0.03^{+0.02}_{-0.02}$	1.05	···	···
28	145453 (2005 RR43) [8]	···	···	$-28.64^{+1.07}_{-2.52}$	$0.97^{+0.01}_{-0.01}$	$0.65^{+0.02}_{-0.00}$	1.84	H_2O	25

Spectral Properties Continued

	Name	Tax. [1]	Vis Gradient [2]	NIR gradient (m) [3]	f [4]	depth [5]	χ^2_υ [6]	Ices prev Detected [7]	References
29	2003 AZ84	BB	2.23± 0.87	$-1.53^{+0.28}_{-0.48}$	$0.42^{+0.06}_{-0.06}$	$0.18^{+0.04}_{-0.04}$	1.20	···	13
30	2004 NT33	···	···	$1.26^{+0.38}_{-0.38}$	$0.10^{+0.05}_{-0.07}$	$0.03^{+0.01}_{-0.01}$	2.72	···	···
31	2004 PG115	···	···	$0.62^{+0.28}_{-0.28}$	$0.25^{+0.07}_{-0.07}$	$0.10^{+0.02}_{-0.01}$	1.27	···	···
32	2005 QU182 ···	···	$1.43^{+0.26}_{-0.26}$	$-0.31^{+0.14}_{-0.16}$	$-0.09^{+0.02}_{-0.02}$	1.63	···	···	
33	2005 UQ513	···	···	$0.12^{+0.20}_{-0.20}$	$0.18^{+0.07}_{-0.07}$	$0.06^{+0.01}_{-0.01}$	1.26	···	···
				Centaurs					
34	2060 Chiron (1977 UB)	BB	-0.07± 1.35	$1.35^{+0.12}_{-0.12}$	$0.02^{+0.02}_{-0.02}$	$0.01^{+0.00}_{-0.00}$	3.52	H_2O	1, 26,27,28
35	5145 Pholus (1992 AD)	RR	48.42± 2.37	$-2.20^{+0.08}_{-0.08}$	$0.24^{+0.02}_{-0.02}$	$-0.02^{+0.00}_{-0.00}$	4.94	H_2O, CH_3OH	1, 29
36	8405 Asbolus (1995 GO)	BR	13.60± 2.96	$-0.30^{+0.22}_{-0.22}$	$-0.03^{+0.03}_{-0.05}$	$-0.01^{+0.01}_{-0.01}$	1.67	none	1, 30, 31, 32
37	10199 Chariklo (1997 CU26)	BR	13.03± 1.10	$0.19^{+0.05}_{-0.05}$	$0.33^{+0.01}_{-0.01}$	$0.13^{+0.00}_{-0.00}$	3.91	H_2O	1, 33,34
38	29981 (1999 TD10)	BR	13.25± 2.27	$-0.59^{+0.09}_{-0.09}$	$-0.04^{+0.02}_{-0.02}$	$-0.01^{+0.00}_{-0.00}$	1.76	···	1
39	31824 Elatus (1999 UG5)	RR	26.01± 2.74	$1.16^{+0.37}_{-0.37}$	$0.04^{+0.04}_{-0.04}$	$0.01^{+0.01}_{-0.01}$	1.14	H_2O	1, 35
40	52872 Okyrhoe (1998 SG35)	BR	11.23± 3.84	$0.17^{+0.20}_{-0.20}$	$0.11^{+0.08}_{-0.09}$	$0.04^{+0.02}_{-0.02}$	1.32	H_2O ?	1, 11
41	54598 Bienor (2000 QC243)	BR	8.50± 3.21	$-0.20^{+0.60}_{-0.60}$	$0.11^{+0.11}_{-0.11}$	$0.04^{+0.02}_{-0.02}$	1.08	H_2O	1,11
42	65489 Ceto (2003 FX128)	···	20.64± 3.39	$-1.65^{+0.27}_{-0.33}$	$0.34^{+0.08}_{-0.08}$	$0.14^{+0.04}_{-0.04}$	1.14	···	1
43	83982 Crantor (2002 GO9)	RR	39.55± 2.89	$-1.29^{+0.41}_{-0.41}$	$0.29^{+0.06}_{-0.05}$	$0.11^{+0.01}_{-0.01}$	1.22	H_2O	1, 15
44	95626 (2002 GZ32)	···	28.23± 4.24	$-4.08^{+4.14}_{-3.83}$	$-0.37^{+0.77}_{-2.15}$	$-0.10^{+0.02}_{-0.01}$	0.95	···	···
45	127546 (2002 XU93)	···	···	$-0.30^{+1.54}_{-1.54}$	$0.08^{+0.32}_{-0.50}$	$0.03^{+0.06}_{-0.08}$	1.36	···	···

Table 3.1: References: (1) Hainaut and Delsanti (2002); (2) Barucci et al. (2005); (3) Licandro et al. (2001); (4) Doressoundiram et al. (2003); (5) Jewitt and Luu (2001); (6) Licandro et al. (2002); (7) Boehnhardt et al. (2004); (8) Brown et al. (2000); (9) de Bergh et al. (2004); (10) Tegler, et. al. in prep. Available at http://www.physics.nau.edu/∼tegler/research/survey.htm; (11) Dotto et al. (2003a); (12) Merlin et al. (2005); (13) Fornasier et al. (2004a); (14) Jewitt and Luu (2004); (15) Doressoundiram et al. (2005a); (16) Doressoundiram et al. (2005b); (17) Licandro et al. (2006a); (18) Barucci et al. (2006); (19) Rabinowitz et al. (2007); (20) Rabinowitz et al. (2006); (21) Trujillo et al. (2007); (22) Merlin et al. (2007); (23) Licandro et al. (2006c); (24) Brown et al. (2007a); (25) Pinilla-Alonso et al. (2007); (26) Luu et al. (2000); (27) Foster et al. (1999); (28) Romon-Martin et al. (2003); (29) Cruikshank et al. (1998); (30) Barucci et al. (2000); (31) Brown (2000); (32) Romon-Martin et al. (2002); (33) Brown and Koresko (1998); (34) Dotto et al. (2003b) ; (35) Bauer et al. (2002)

[a]The Taxonomic groups as defined in Barucci et al., 2005; BB - blue, BR intermediate blue red, IR- moderately red, RR- red

[b]The visible (500-800 nm) color gradient in % change in reflectance per 100 nm, calculated using the methods in Hainaut and Delsanti (2002)

[c]The NIR (1.5-2.4 μm) color gradient in % change in reflectance per 100 nm found from slope of the continuum component (m) used to fit the spectral model

[d]The fraction of water ice in the spectrum

[e]The fractional depth of the 2.0 μm to 1.7 μm spectral regions, where larger depth indicates stronger water ice spectral signatures. The depth is shown here for comparison with previous studies (e.g. Brown et al (2007)). The depth is calculated using the fitted model spectrum rather than the data to reduce the noise and has had the continuum contribution subtracted out.

[f]The reduced χ^2 value of the spectral model fit to the data

[g]Spectral features identified in the NIR spectra by other authors

[h]2003 EL61 and its associated family members

Table of Physical Parameters

Number	Name	H [1]	p_v (%) [2]	D (km)	a (AU)	Ecc	Inc (deg)	q (AU)	References
				Kuiper Belt Objects					
1	15875 (1996 TP66)	6.8	7.4^{+7}_{-3}	160^{-45}_{+45}	39.21	0.33	5.7	26.35	1
2	19521 Chaos (1998 WH24)	4.9	> 5.8	< 747	45.59	0.10	12.1	40.94	2, 3
3	20000 Varuna (2000 WR106)	3.7	16^{+10}_{-8}	500^{-100}_{+100}	42.95	0.05	17.2	40.72	1
4	24835 (1995 SM55) [3]	4.8	> 6.7	< 704	41.65	0.10	27.1	37.36	2, 3
5	26181 (1996 GQ21)	5.2	...	...	95.06	0.597	13.3	38.31	...
6	26375 (1999 DE9)	4.7	$6.85^{+1.58}_{-1.19}$	$461.0^{-45.3}_{+46.1}$	55.85	0.42	7.60	32.34	1
7	28978 Ixion (2001 KX76)	3.2	12^{+14}_{-6}	650^{-220}_{+260}	39.62	0.24	19.6	30.072	1
8	33340 (1998 VG44)	6.5	...	...	39.14	0.25	3.0	29.35	...
9	38628 Huya (2000 EB173)	4.7	$5.04^{+0.5}_{-0.41}$	$532.6^{-24.4}_{+25.1}$	39.75	0.28	15.5	28.54	1
10	42301 (2001 UR163)	4.2	...	...	51.35	0.284	0.80	36.7666	...
11	47171 (1999 TC36)	4.9	$7.18^{+1.53}_{-1.17}$	$414.6^{-38.2}_{+38.8}$	39.23	0.22	8.4	30.56	1
12	47932 (2000 GN171)	6.0	$5.68^{+2.54}_{-1.59}$	$321.05^{-54.2}_{+57.4}$	39.72	0.29	10.8	28.28	1
13	50000 Quaoar (2002 LM60)	2.6	9 ± 3	1260 ± 190	43.54	0.03	8.0	42.02	1, 4
14	55565 (2002 AW197)	3.3	$11.77^{+4.42}_{-3.00}$	$734.6^{-108.3}_{+116.4}$	47.37	0.13	24.4	41.16	1
15	55636 (2002 TX300) [3]	3.3	> 19	< 709	43.08	0.123	25.9	37.78	3, 5
1	55637 (2002 UX25)	3.6	$11.50^{+5.09}_{-3.09}$	$681.2^{-114.0}_{+115.6}$	42.52	0.142	19.5	36.48	1
17	55638 (2002 VE95)	5.3	...	...	39.15	0.285	16.4	27.9923	...
18	66652 (1999 RZ253)	5.9	29 ± 12	170 ± 39	43.72	0.09	0.60	39.83	2, 3
19	84522 (2002 TC302)	3.9	$3.1^{+2:9}_{-1:2}$	1150^{325}_{+337}	55.03	0.29	35.1	39.02	1
20	84922 (2003VS2)	4.2	...	...	39.28	0.073	14.8	36.41	...
21	119951 (2002 KX14)	4.4	...	...	39.00	0.041	0.40	37.40	...
22	120132 (2003 FY128)	5.0	...	...	49.700	0.25	11.8	37.09	...
23	120178 (2003 OP32) [3]	4.1	...	...	43.18	0.107	27.2	38.56	...
24	120348 (2004TY364)	4.5	...	...	38.7	0.067	24.9	36.11	...
25	136108 (2003 EL61) [3]	0.20	$84.^{+10}_{-20}$	1150^{-150}_{+150}	43.33	0.19	28.2	35.14	1, 6
26	136472 (2005FY9)	-0.30	$80.^{+10}_{-20}$	1500^{-200}_{+300}	45.71	0.15	29.0	38.62	1
27	145452 (2005 RN43)	3.9	...	...	41.53	0.02	19.29	40.62	...
28	145453 (2005 RR43)	4.0	...	...	43.05	0.14	28.54	37.19	...
29	2003 AZ84	3.9	$12.32^{+4.31}_{-2.91}$	$685.8^{-95.5}_{+98.8}$	39.50	0.179	13.6	32.43	1
30	2004 NT33	...	...	...	43.44	0.15	31.22	36.85	...
31	2004 PG115	...	...	...	89.83	0.59	16.28	36.42	...
32	2005 QU182	...	...	...	126.4	0.72	14.00	35.39	...
33	2005 UQ513	...	...	...	43.336	0.14	25.72	36.84	...

Table of Physical Parameters Continue

Number	Name	H [1]	p_v (%) [2]	D (km)	a (AU)	Ecc	Inc (deg)	q (AU)	References
				Centaurs					
34	2060 Chiron (1977 UB)	6.5	$7.57^{+1.03}_{-0.87}$	$233.3^{-14.4}_{+14.7}$	13.701	0.38	6.9	8.45	1
35	5145 Pholus (1992 AD)	7.0	8.0^{+7}_{-3}	140^{-40}_{+40}	20.411	0.57	24.7	8.74	1
36	8405 Asbolus (1995 GO)	9.0	$5.46^{+1.27}_{-0.86}$	$84.2^{-7.8}_{+7.8}$	18.02	0.621	17.6	6.82	1
37	10199 Chariklo (1997 CU26)	6.4	$5.73^{+0.49}_{-0.42}$	$258.6^{-10.3}_{+10.3}$	15.854	0.175	23.4	13.07	1
38	29981 (1999 TD10)	8.8	$4.40^{+1.42}_{-0.96}$	$103.7^{-13.5}_{+13.6}$	94.97	0.87	6.0	12.25	1
39	31824 Elatus (1999 UG5)	10.1	10^{+4}_{-3}	$30+^{-8}_{+8\|}$	11.769	0.38	5.3	7.27	1
40	52872 Okyrhoe (1998 SG35)	11.3	$2.49^{+0.81}_{-0.55}$	$52.1^{-6.9}_{+6.9}$	8.38	0.308	15.6	5.79	1
41	54598 Bienor (2000 QC243)	7.6	$3.44^{+1.27}_{-0.82}$	$206.7^{-30.1}_{+30.1}$	16.48	0.200	20.7	13.15	1
42	65489 Ceto (2003 FX128)	6.3	$7.67^{+1.38}_{-1.10}$	$229.7^{-18.2}_{+18.6}$	103.00	0.83	22.3	17.82	1
43	83982 Crantor (2002 GO9)	9.1	11^{+7}_{-4}	60^{-13}_{+15}	19.537	0.28	12.8	10.92	1
44	95626 (2002 GZ32)	6.8	···	···	23.196	0.223	15.0	18.06	1
45	127546 (2002 XU93)	7.9	···	···	66.950	0.687	78.0	20.95	1

Table 3.2: References: (1) Stansberry et al. (2007); (2) Altenhoff et al. (2004); (3) Grundy et al. (2005a); (4) Brown and Trujillo (2004); (5) Ortiz et al. (2004); (6) Rabinowitz et al. (2006)

[a] 1. The absolute visual magnitude as reported by the Minor Planet Center

[b] 2. The visual geometric albedo

[c] 3. 2003 EL61 and its associated family members

Chapter 4

Visible Spectral Properties of Kuiper Belt Objects

4.1 Introduction

The region beyond Neptune is occupied by a remnant population of small bodies left over from the formation of the solar system called Kuiper Belt Objects (KBOs). The smallest KBOs likely resemble comets and are a relatively pristine reservoir of primitive materials from the solar nebula. However, the largest KBOs ($\sim$ 1000 km in diameter) appear more planetary in nature and are more likely to have differentiated interiors, early geothermal activity, and tenuous atmospheres. Their early accretional and radiogenic heating altered the primitive materials from which they formed. With such a range in size, the KBO population provides a unique opportunity to study the original materials that formed the planets, the evolution of icy bodies, and the processes of planet formation.

In general, little is known about the physical and chemical properties of KBOs as most are too faint to study with spectroscopic techniques. Many of the larger KBOs have been studied with Near infrared (NIR) instruments, which are sensitive to several abundant solar system ices. These studies have revealed that a majority of KBOs can be described by a combination of essentially two end-members: a spectrally featureless component and water ice component (see Chapter 3 and Barucci et al. (2008) for overview). However, when visible color data is also considered, it is evident that the surfaces of these KBOs cannot be explicitly described by two specific end members. Thus far, photometric and spectroscopic studies suggest an inherent heterogeneity in surface composition

of KBOs. The NIR spectral characteristics, specifically the abundance of water ice in the spectrum, were found to only correlate with diameter. This suggests that the presence of water ice on the surface is possibly geophysically controlled, though no evidence for recent activity was observed. The NIR studies also identify two additional, less populated sub groups of KBOs based on their spectral properties; the methane giants and the 2003 EL61 collisional family. The methane giants have methane-dominated NIR spectra and sizes similar to Pluto. 2003 EL61 along with the members its collisional family have surfaces covered by water ice. The family members also have similar orbits to 2003 EL61 suggesting their origin as mantle fragments from a proto-2003 EL61 that were ejected during a giant impact (see Chapter 1).

While the NIR spectra are sensitive to a variety of ices, the visible spectral region (3000 to 10,000 Å) can be diagnostic of mineralogy and complex organic materials. Mineral absorptions in the blue-UV wavelength region as well as broad absorptions at 7000 Å have been identified on C-type asteroids and a number of its sub-classes. The blue-UV absorptions have been identified as absorptions from iron and titanium-bearing minerals (Burns, 1981). Its correlation with a 3μm water absorption on various C-type asteroids and its subclasses suggests the blue-UV absorption could be an indicator of phyllosilicates and other hydrated minerals (Lebofsky, 1980; Gaffey and McCord, 1978). Iron oxides in phyllosilicates and aqueously altered minerals have also been invoked to explain broad absorptions at 7000 Å observed in CM2 carbonaceous chondrites and on some outer belt asteroids (Vilas and Gaffey, 1989). Similar absorptions were reported by de Bergh et al. (2004) for the KBOs Huya and 2000 GN171 on one night of observations, but subsequent observations failed to detect the features again. A U-band survey recently published by Jewitt et al. (2007) also looked for the blue-UV absorption feature seen on asteroids but failed to detect any such absorption.

While Jewitt et al. (2007) do not see indications of the blue-UV absorptions, they do see an upturn in the reflectance at the blue wavelengths for some objects, which they argue are more likely caused by the presence of complex organic materials like tholins and kerogens. These materials are expected to be common on the surfaces of KBOs and are made by the irradiation of simple organic ices by UV radiation and cosmic rays (Khare et al., 1984; Strazzulla et al., 1991). They are

commonly invoked to explain the red spectral slope observed for most KBOs, as well as the neutral, featureless IR spectra and low albedos (Barucci et al., 2008). This material may also explain the spectral characteristics of D-type asteroids. D-type asteroids are found in the outer asteroid belt and are thought to contain of water ice, though their surfaces appear dehydrated (Lazzarin et al., 1995). Their reflectance spectra suggest that they may some similarities to KBOs in surface composition.

Finally, methane O_2, and O_3 ices have also been detected in the visible spectra of icy solar system bodies. Licandro et al. (2006c,b); Tegler et al. (2007); Brown et al. (2007a); Dumas et al. (2007); Spencer et al. (1995) have observed methane in the visible spectra of the methane giants, 2005 FY9 and Eris. Licandro et al. (2006c,b) examined the spectra to look for evidence of shifts in the methane lines that would suggest presence of N_2. O_2 and O_3 is expected to be formed in water ice surfaces that are exposed to radiation. Both species have been detected on Ganymede while O_2 is also detected on Callisto, and Europa (Spencer et al., 1995; Spencer and Calvin, 2002). Tegler et al. (2007) searched for O_2 on 2003 EL61, but did not detect it due to insufficient signal to noise.

Thus far, only a handful of visible spectra of KBOs have been published (see Barucci et al. (2008)) giving a limited view of the spectral visible character of KBOs. With few exceptions, they largely show few spectroscopic features and only a small number of these objects are observed at wavelengths shortward of 5000 Å. A U-band photometric survey of KBOs done by Jewitt et al. (2007) provides some information about the spectral characteristics in the region. Here we present a survey of visible spectra, which provides more insight into the surface characteristics in the Kuiper Belt.

To collect a large sample of KBO reflectance spectra, we obtained visible spectra using the Double Spectrograph (DBSP) on Palomar Observatory's Hale telescope. We collected spectra on 19 KBOs over a two year campaign from February 2005 to April 2007. The spectra were taken to augment our NIR survey using the Keck Telescopes (see chapter 3), and therefore many targets were observed with both instruments. The visible spectroscopy, however, was a secondary project for poor observing conditions and therefore not all KBOs observed at Keck were likewise observed at Palomar.

4.2 The Sample

Objects were selected for observing based on several criteria. Foremost, all KBOs were required to have a visual magnitude of < 21, with preference given to brighter objects. Objects were required to have less than 2 arcsecond errors in their ephemeredes as DBSP has no imaging field camera, and objects are aligned into the 2 arcsecond slit through blind offsets. This generally constrained us to observe objects that had recently been discovered in the Mike Brown's all-sky survey (Trujillo and Brown, 2003) or had multi-year observations. In several cases, we used Palomar's 60-inch telescope to observe objects in advance of DBSP observations to obtain accurate ephemeredes for the period of DBSP observations. In all, 10 nights on the 60-inch telescope were awarded for recovery observations of KBOs and data was primarily taken in support of further observations at Palomar and Keck Observatories. We also selected objects that would be observed as part of our survey using NIRC on the Keck I Telescope, so that a full spectral data set could be collected on these objects. Finally, we excluded a few objects from observation because their proximity to the galactic plane introduced a significant number of additional objects to be observable in the slit. Without the use of an imager, the potential for source confusion for these objects was high and therefore we abandoned these KBOs. See table 4.2 for a full list of observed objects.

4.3 Observations & Data Analysis

4.3.1 Observations

DBSP is the Palomar observatory's mid-resolution visual spectrograph and observes simultaneously in blue and red wavelengths by using a dichroic to send light into two separate grating systems. The light is then sent to two separate CCD cameras. We observed our targets using the facility dichroic that reaches 50% transmittance at 5500 Å. The grating angles on DBSP can be adjusted to observe different wavelength ranges. For our observations, the gratings were set to give a spectral resolution of $\lambda/\Delta\lambda \sim 3000$ between 3500 Å and 5500 Å in the blue channel and a resolution of $\lambda/\Delta\lambda \sim 1800$ between 5500 Å and 9200 Å in the red channel. The grating settings were checked

at the beginning of each observing run to ensure consistency between observations, though each run had slightly different settings due to the analog nature of the grating system.

DBSP has no field imaging camera apart from a guide system that can image the slit. Our target KBOs were generally too dim to observe in the slit images and therefore we used blind offsetting from nearby bright stars to place KBOs into the slit. To determine this offset, we first obtained nightly ephemeredes for our objects using the JPL's HORIZONS ephemeris computation service[1]. Using the ephemeris positions, nearby astrometric standard stars were selected from the USNO-B2.0[2] catalog. We restricted the stars to be dimmer than magnitude 12 to prevent the inclusion of high proper motion stars as well as prevent damage to the guide cameras. Stars dimmer than magnitude 16 were also excluded as they are too dim to see reliably in the images of the slit. To observe the KBO, first a USNO astrometric standard was placed in the slit and then the telescope was offset to the KBO position. Offsets were generally of order $\sim$ 100 arcseconds and no more than 400 acrseconds, which is well within the slewing precision of the Hale Telescope. We used the 2 arcsecond slit to allow both for errors in the slewing and in the ephemeredes. Between new target observations, several bright SAO stars in Palomar's pointing catalog were observed in the vicinity of the KBO to ensure accurate slewing. In general, we found our target KBO was in the expected position.

During observations, the telescope tracked the KBO at its rate of motion, which provided another check that the object in the slit was the intended target for KBOs near opposition. In general observations were sufficiently lengthy that background field stars would move out of the slit. Spectra were taken with 600 s integrations to prevent the OH sky lines from saturating the red camera. The telescope was returned to the astrometric standard star between integrations to check pointing. The star was also used to dither the telescope along the slit by 10-20 arcseconds between observations. During observations, the slit was maintained along the parallactic angle, where the parallactic angle is the angle perpendicular to the horizon. Differential diffraction can cause a wavelength-dependent loss of light entering into the slit, which corrupts the spectral data (Filippenko, 1982). We generally

[1]JPL's HORIZONS system is available at http://ssd.jpl.nasa.gov/?horizons

[2]The US Navel Observatory's current catalog of astrometric standards can be accesses at http://cdsarc.u-strasbg.fr/viz-bin/Cat?USNO, which includes a full description of the catalog

observed at sufficiently low airmass that the effect is small, but took care in maintaining the slit to within 15 degrees of the parallactic angle for all observations.

The KBOs are illuminated by sunlight, and therefore to create a reflectance spectrum, each KBO spectrum must be divided by a solar spectrum. As a proxy to the solar spectrum, we observed true solar analogs. Many solar analogs are too bright for the Hale telescope and we observed by stopping down the telescope to a smaller aperture size (typically 80 to 100 inches) or by defocusing the telescope. These solar analogs were checked against dimmer analogs when the telescope was not stopped down to check that vignetting and flat fielding were not problematic. For each night, we took observations of solar analogs at a variety of airmasses to correct for atmospheric extinction.

At each target location we also observed a set of arc lamps for wavelength calibration. The gratings in DBPS are prone to jitter throughout the night, especially after large slews causing the location of the spectrum to shift on the chip slightly throughout the night. We observed Fe-Ne standard lamps for the blue camera and Ar-Ne lamps for the red camera. We typically found the shifts to be no more than a few pixels throughout the night and should not impact our data significantly.

4.3.2 Data Analysis

Image processing and the extraction of spectra from the raw data were done within IDL using standard methods. We first subtracted a median bias image from the raw data images and divided the result by the median flat field image to correct for pixel to pixel variations in the CCD sensitivity. The flat fields were obtained by imaging an evenly illuminated portion of the dome. The original DBPS blue camera was plagued by a significant number of bad columns, and the camera was replaced in the summer of 2005. Data taken with the old blue camera required that the bad columns be masked in the data reduction. The spectral data has slight curvature in both the spatial and spectral domains. The curvature in spatial direction was measured using the position of the target and removed by straightening the spectrum by whole-pixel shifts. Spectral lines from the arc lamp calibration images were used to measure the remaining curvature in the spatial direction.

Corrections to the curvature in the spatial direction were centered on the target so that the region around the target is the least altered by the correcting shifts in the spectral direction.

The background sky emission was measured by finding the median sky spectrum in 20-pixel swaths located above and below the target spectrum. An average of the two sky spectra were then used to construct a master sky spectrum which is then subtracted from the image to remove the background sky emission. In general, this lead to good correction of the background sky, though telluric OH lines become stronger in the red and increase the noise in our data for the region longward of 7000 Å. The final spectrum is extracted by summing the signal from the target in the spatial direction, generally over 6 to 18 pixel swaths, depending on the seeing conditions. The spectra from the solar analogs were extracted using the same method. A reflectance spectrum was obtained by dividing the target spectrum by a solar analog spectrum taken at a similar airmass. In general, we found that the solar analogs provided a good correction to the solar analogs except at the 5890 Å Na doublet line and the 7600 Å O_2 Fraunhofer lines.

The wavelength scale was calibrated using the arc lamps taken at a similar time to observations. The spectral images of the lamps were corrected in the same way as the target data and a lamp spectrum was extracted from the same spatial location as the target. The lamp lines were identified using standard spectral line catalogs provided by Palomar Observatory and the National Optical Astronomy Observatory[3]. The pixel positions for ten spectral lines were measured for the blue camera and seven for the red camera using Gaussian fits to the lines. A second order fit to the line positions was used to calculate the wavelength at each pixel. We found that the second order correction is small, and therefore higher order fit parameters were unnecessary. The error in the wavelength calibration was found by measuring the wavelength of bright telluric Hg and OH lines and comparing them to reported values. We find that the error in the wavelength calibration is $\gtrsim 3$ Å. In general, we found the changes in the wavelength scale were very small over a given observing run, but were significantly different between observing runs due to the analog adjustments that are made to the grating angles for DBSP.

[3]The NOAO spectral library is available at http://www.noao.edu/kpno/specatlas/

The signal to noise is low in individual spectra, therefore the spectra were added together to build a final spectrum. Data that were obtained on different observing runs were interpolated to a common wavelength scale before they were added together to prevent blending of spectral features. Since the conditions were often variable during observing runs, the spectra were added using a weighted mean where the weight for each spectrum was found by calculating the inverse of the RMS of the data. The final spectra have higher resolution than most of the spectral features we expect to find in the optical, where typical absorptions are hundreds of angstroms wide. Therefore we smoothed the spectra using a boxcar smoothing scheme down to a resolution of $\sim$ 40 Å per pixel to further increase the signal to noise.

4.4 Results

The spectrum from 3500 to 9200 Å for each object in our survey is shown in figures 4.1 through 4.5. The spectra were created by normalizing the red spectrum to 1.0 at 6400 Å , which is the center of the central wavelength of the Johnson V filter commonly used for photometric studies. This normalization is frequently used in photometric studies of KBOs, allowing us to compare our spectral data with previous reported photometric properties. We find that our spectra are generally quite linear in the region between 5500 Å and 8000 Å , which is consistent with photometric studies that suggest KBO reflectances can be described by a single gradient (that is a single line) in this wavelength region. We fit a line to our spectral data between 6000 and 7700 Å , where our spectra suffer the least noise, and find that the slope is generally in good agreement with previously published values (see table 3.6 for published gradients). We find the difference in our slopes and reported spectral gradients to be less than a few percent, with differences likely arising from the use of solar analogs at slightly different airmass than observations as we do not adjust the solar analog spectra with an airmass correction. The fitted line is extrapolated to the wavelength region of our blue data and its mean value is used to scale the blue spectrum to fit with the red data. In this manner, we get a continuous spectrum from 3500 to 9200 Å. The exception are the methane objects in our survey, Eris and 2005 FY9, which required that the spectral gradient be fit at regions where methane does

not have absorptions.

The data have been divided into panels by their NIR spectral properties. Figure 4.1 shows the spectra for Eris and 2005 FY9 and are discussed in more detail in §4.4.1. The spectra of 2003 EL61 and its family members are in Figure 4.2 and discussed in §4.4.2. Figure 4.3 shows the spectra of KBOs for which water ice was detected in NIR spectra at least the 3-σ level. Finally, figures 4.4 and 4.5 show the visible spectra of objects which have no spectral signatures of water ice in the NIR. These objects generally show much stronger red spectral slopes compared to their icier brethren.

While we find that a single slope generally describes the spectra well from 4500 Å to 8000 Å , we find that shortward of 4500 Å many of the objects in our survey show a distinct flattening or up-turn in the spectral slope similar to that observed by Jewitt et al. (2007). To examine this change in the spectral slope for our KBOs more closely, we divided each blue spectrum by the gradient fit to the red data. The resulting blue spectra are shown in Figures 4.6 through 4.9, which are organized by their NIR spectral properties. Changes in the spectral gradient shortward of $\sim$ 4500 Å have been associated with both hydrated minerals and complex organic materials. For comparison to our KBO spectra, representative spectra for G, C, and D type asteroids from Tholen and Barucci (1989) are shown as well as a complex carbon rich material from Cloutis (1989). The spectra of these objects have essentially single gradients from 4500 to 8000 Å like our KBOs and have been scaled in a similar fashion to highlight their change in spectral gradient shortward of 4500 Å. The C and G type asteroids are shown as archetypical of a blue absorber that has been observed on some asteroids and is generally identified with Fe or Ti bearing hydrated minerals (Burns, 1981). A strong blue absorber detected on G-type asteroids is particularly associated with aqueously altered minerals such as phyllosilicates. Conversely, the typical D-type asteroid spectrum as well as a silicate-tar mixture are shown to illustrate the spectral "up-turn" or concave-up spectral feature seen in some, but not all, materials rich in complex organic matter.

Though the region shortward of 4500 Å is increasingly noisy due to the fall off of sunlight at blue wavelengths, we find that none of the objects in our survey show any strong blue absorption indicating the presence of hydrated minerals like those observed on G-type asteroids. The signal-

to-noise though is sufficiently poor that absorptions similar to C-type asteroids cannot be ruled out for most objects. For modestly icy to non-icy KBOs, we find that their blue spectra are essentially flat or show an up-turn in reflectance to varying degree, more suggestive of carbon-rich materials than hydrated minerals. However, we do not attempt to fit precise spectral models to these KBOs. Studies of the likely materials show a variety of general shapes that depend on the exact chemistry of the samples (e.g. see Cloutis et al. (1994). Without the presence of distinct spectral features in the blue, there are too many unknown parameters to make complex spectral modeling particularly informative. Rather, we find that the overall blue spectral characteristics are highly suggestive of the presence of organic materials.

In addition to looking for changes in the spectral slope at blue wavelengths, we examine the spectra for broad absorptions at ∼7000 Å associated with aqueously altered minerals that have been observed on some meteorites and asteroids (Vilas and Gaffey, 1989). The absorptions seen on these objects are typically $\lesssim 10\%$ of the continuum and therefore are difficult to detect on faint KBOs, though such absorptions at 10-15% have been reported for Huya and 2000 GN171 by de Bergh et al. (2005). Since the absorptions are weak, we only examined the highest signal to noise spectra of non-icy objects to look for similar features. Figure 4.12 shows the red spectra for 2003 VS2, 2002 AW197, 2004 NT33, and 2000 GN171 with the spectral gradient removed. The spectrum of the CM2 chondrite Nogoya from Vilas and Gaffey (1989) is also shown for comparison. We find no evidence for absorptions at ∼7000 Å , though we do observe the turn-down in reflectance at ∼ 9000 Å which is generally observed on KBOs relating to the flattening of the spectral reflectance through the infrared. For all these objects though, an absorption of a few percent would not be observed. For 2000 GN171, the noise is higher, but we argue that we do not see similar features to seen by de Bergh et al. (2005) on their first night of observations and our spectrum is more consistent with their second night's data.

The overall spectral characteristics of the non-icy objects in our survey suggest that the irradiated, organic-rich materials are the dominant spectral contributor on most KBOs. This surface material remains poorly understood. Modeling of the visible gradient and NIR spectral character-

istics suggests that this material is heterogeneous in nature, perhaps reflecting differing chemistries or alteration histories. The materials appear to have a variety of visible spectral gradients, but essentially flat NIR spectra. In an effort to understand this material better, we have examined the blue up-turn and compared it to the gradient measured in the red data for those objects in which the organic material appears to be the dominant spectral contributor. The degree of up-turn was quantified by fitting a line to the data shortward of 4500 Å once the visual spectral gradient from the red data was removed. Using this method, we find that only one KBO, 2002 TX300, had a positive blue gradient (indicated a blue absorber), but this object has poor atmospheric extinction correction due to problems with its solar analog observations. Figure 4.11 shows a comparison of the blue gradient as a function of the visual gradient for non-icy objects and we find no significant correlation between the degree of up-turn and the visual spectral gradient.

We specifically examined 2003 EL61, which is sufficiently bright to have good signal-to-noise even in the blue for evidence of phyllosilicates which were reported by Trujillo et al. (2007) as possible components of the NIR spectrum. Spectral fitting to the phyllosilicates proposed by Trujillo et al. (2007) are discussed in more detail in §4.4.2. We also examine the spectra of the methane giants in our survey in §4.4.1 to determine if our data shows shifts that are reported by other authors.

4.4.1 Methane Giants

The largest KBOs, those similar in size to Pluto, have all been found to retain their methane on their surfaces (e.g. Schaller and Brown (2007a)) and their NIR spectra are dominated by the methane absorption bands. However, methane has a weaker bands in the visible that have been observed on several of these Pluto-sized KBO. In our survey, we find that both 2005 FY9 and Eris show strong spectral signatures of methane at 7600 Å and 8900 Å (see figure 4.1). The spectrum of 2005 FY9 has sufficient signal to noise to clearly detect additional absorptions at 6200 Å, 7900 Å, 8400 Å, and 8700 Å. All the absorption features in the red channel for both objects can be identified as methane. We modeled both spectra using a pure methane model from (Grundy et al., 2002) and find that a grain size of $1.9^{+3.0}_{-1.4}$ mm is required to fit the spectrum of Eris. This grain size is consistent

Lab Spectrum (Grundy et al., 2002)	Eris (Licandro et al., 2006b)	Eris (this work)	2005 FY9 (Licandro et al., 2006c)	2005 FY9 (this work)	Pluto (Grundy and Fink
7299	7296	···	7296	7296 ± 4	7290
8897	8881	···	8891	8892 ± 2.3	8885

Table 4.1: The measured shifts for the methane-giants Eris and 2005 FY9

with what has been observed by Dumas et al. (2007), though slightly smaller than that reported by Tegler et al. (2007); Licandro et al. (2006b). For 2005 FY9, I find that the spectrum is better fit by a larger grain size of $4.5^{+4.5}_{-3.0}$ mm. This is about half the size of the grain size reported by Brown et al. (2007a) using the J through K spectrum. However, Brown et al. (2007a) find that 2005 FY9 has a red component in the optical spectrum. If a second red component is added and the visible spectrum of 2005 FY9 is color corrected, then the 2005 FY9 model can accommodate a larger grain size similar to Brown et al. (2007a).

Shifts in the position of the methane bands have previously been detected for Pluto and Eris (Douté et al., 1999; Licandro et al., 2006b). Laboratory studies indicate that the shifts are likely induced by a small amount of methane dissolved in a nitrogen ice matrix (Quirico and Schmitt, 1997). Observations of the shift can be used to indirectly detect the nitrogen ice since it is difficult to detect Nitrogen's extremely weak, narrow, absorption band in the NIR. Detecting the differences in shifts at various wavelengths can also provide information about compositional gradients on the surfaces of the KBOs as different bands probe different depths in the ice (Licandro et al., 2006b). We find for 2005 FY9 that we do not detect any significant shift away from the laboratory spectra of pure methane for the 7300 Å line and our shift is within 2-σ of the 8900 Å line. Our measurements are similar to those by Licandro et al. (2006c) and are reported in table 4.1. Our observations support the lack of detectable N_2 2005 FY9's NIR spectrum, as predicted by models from Schaller and Brown (2007a). We attempted to measure the shifts in the data for Eris as well where N_2 is expected to be found, but the signal to noise in our visible spectrum is considerably lower than 2005 FY9's. Unfortunately, we found that our measurements were unreliable for Eris and are not reported.

No spectral features were observed in the blue channel for either object, though narrow absorp-

tions of $\sim 10\%$ are not observable. We do note an upturn in 2005 FY9's spectrum at wavelengths shortward of 4500 Å which may be a result of the higher order hydrocarbons and carbonaceous material on this object. Ethane has also been observed in the NIR spectrum of 2005 FY9 and higher order hydrocarbons are also expected (Brown et al., 2007a) , which may be responsible for the up-turn. A similar up-turn is not observed in the spectrum of Eris.

4.4.2 2003 EL61 and the Collisional Family

Through our NIR survey with the Keck telescopes, we identified a subset of unusual KBOs with very strong water ice spectra. These surfaces were unexpected because these objects are likely too small to differentiate or form icy surfaces from cryovolcanism. In addition to the spectral features, these objects were also found to have orbits very similar to 2003 EL61's (Brown et al., 2007b). It was proposed that the KBOs were fragments of 2003 EL61 that were ejected during the giant collision that spun-up 2003 EL61 to its current 4 hour rotational period and formed its small moons. The strong water ice signatures on 2003 EL61 and the fragments suggest that they originated from an icy mantle on a differentiated proto-2003 EL61.

Since the 2003 EL61 collision is likely ancient (Ragozzine and Brown, 2007), but unlike other KBOs, the family members do not appear to have formed radiation crusts. It has been suggested that the fragments are "carbon-depleted", possibly having lost their volatile carbon inventory during differentiation or the subsequent collision to explain the lack of organic material on these objects (Brown et al., 2007b; Pinilla-Alonso et al., 2007). However surface models using pure water ice have produced poor fits to the NIR spectra. A second NIR blue component has been reported to increase the fit for nearly all the fragments (See Chapter 3, Licandro et al. (2006a); Trujillo et al. (2007); Pinilla-Alonso et al. (2007)), allowing for the possibility that the surfaces of the fragments and 2003 EL61 are not pure water ice. The secondary blue component was modeled in detail for 2003 EL61 by Trujillo et al. (2007), who proposed a number of candidates but found the best improvement of their spectral models resulted from including either hydrated tholin, phyllosilicates or HCN. However, the signal-to-noise in their NIR spectrum was insufficient to determine which of these species could be

responsible for the "blue component". Hydrated tholins were rejected due to the mismatch in their red visible colors and 2003 EL61's neutral color. Phyllosilicates were proposed because they tend to be more neutral in the visible, and could form during differentiation or the giant impact. Trujillo et al. (2007) found that linear models with ∼80% water ice and ∼20% kaolinite or montmorillinite significantly improved the model fit over models with just water ice. With the addition of optical spectra, we now consider whether this abundance of phyllosilicates can plausibly exist on the surface.

To model the phyllosilicate component, we used kaolinite and montmorillinite spectra are from the spectral library of Clark et al. (2007) that cover a wavelength range from 2700 Å to 29760 Å with a $\lambda/\Delta\lambda \sim 80$. For the purpose of spectral modeling, we interpolated the spectrum to the same wavelengths and resolution as the 2003 EL61 data. Spectral models were created by combining one of the mineral spectra with a neutral continuum component that represents a water ice spectrum in the visible. The models were created by geographical (i.e. linear) mixing the two components and allowing their abundances to vary. Since the albedo of the water ice component is not known and depends on the microphysics of the surface, it was allowed to vary. We normalized our 2003 EL61 spectrum to its visual albedo of 70% (Rabinowitz et al., 2006) and fit our spectral model to the data using a standard linear least-squares method available in IDL. We find that the spectra do not support the inclusion of either of the phyllosilicates, especially at the level required by the NIR data. The best fit models giving an ice albedo of 70% (similar to fresh snow) and a surface abundance of 2% ± 0.5% for either phyllosilicate.

While phyllosilicates and tholins can be ruled out based on our optical data, we cannot exclude HCN as a candidate for the "blue component" since it is spectrally featureless in the optical (Dumas et al., 2001). However, we argue that this material is unlikely to be present at the level of 30% as suggested by Trujillo et al. (2007) since radiation will transform HCN into more complex carbon species on timescales short compared to the age of the family (Gerakines et al., 2004). As such, we argue that it is an unlikely constituent on the surface of 2003 EL61, at least at the level required to account for the "blue component". Instead, we suggest that the blue component may be caused by wavelength-dependent scattering, possibly due to small impurities and imperfections in the ice

matrix (for example see Price and Bergström (1997b)).

4.5 Discussion

The survey presented here provides the first broad view of the visible spectral properties of KBOs, with all the spectral classes represented. With the exception of the methane giants, we find most our visible spectra are linear through much of the visible wavelength region, with no substantial ($\gtrsim 10\%$) broad absorptions observed. The pervasive up-turn observed in the reflectance at wavelengths $<$ 4500 Å and the down-turn at wavelength $>$ 9000 Å argues that materials abundant in complex organics are a dominant spectral contributor in the visible region for non-icy KBOs and 2005 FY9. However, the variety of observed spectral gradients and the various degrees of up-turn/down-turn suggests that this material may be quite heterogeneous across the KBO population.

We do not find any evidence for hydrated minerals on any of our KBOs nor any other mineralogical features such as those found on asteroids are detected. This corroborates the findings of Jewitt et al. (2007), who find similar results using photometric data. In the case of 2003 EL61, we can rule out the presence of phyllosilicates that were proposed as a possible surface component based on its blue NIR spectrum. As a whole, our survey suggests that any mineralogical signatures on the surfaces of KBOs are overwhelmed by presence of organic materials.

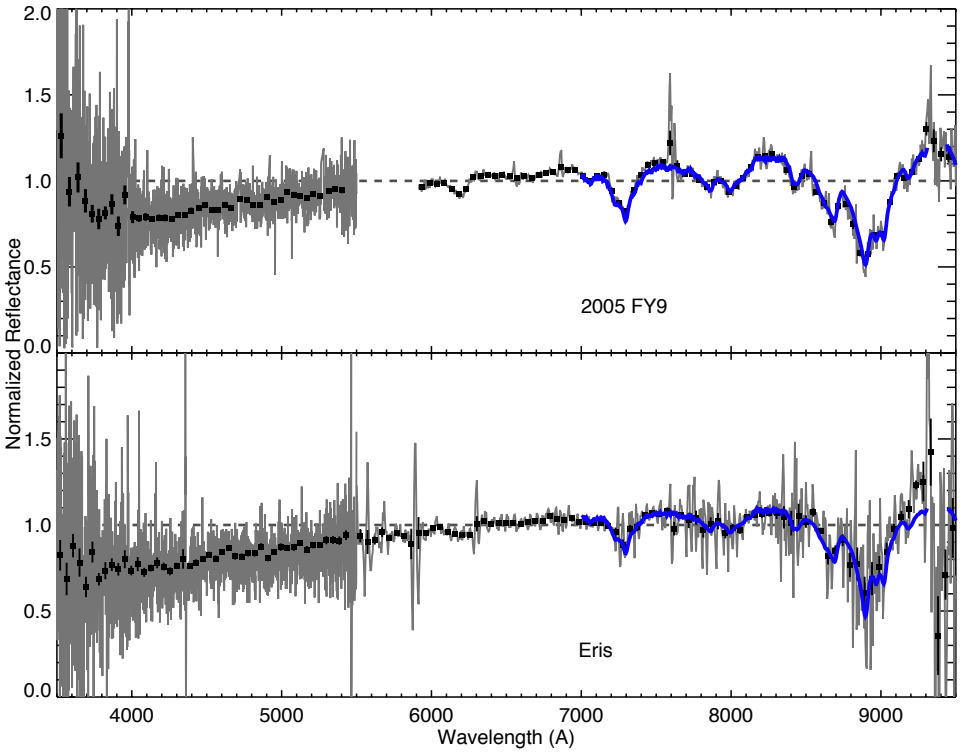

Figure 4.1: The visible reflectance spectra of the methane giants 2005 FY9 and Eris from 3500 to 9200 Å. The high resolution data is plotted in grey while a lower resolution, smoothed spectrum is plotted with black squares. The formal 1-σ error bars from smoothing are also shown. The higher noise at 5890 Å and 7600 Å are due to poor correction of the Na doublet line and the O_2 Fraunhofer lines. The spectra are a composite from blue and red spectra taken with separate cameras on DBSP. The red spectrum is scaled to 1.0 at 6400 Å. A line fit to the red data is used to scale the blue data to match the red data. The thick blue line shows the best fit of a methane spectral model to data from 6800 to 9200 Å. We find that the Eris spectrum is best fit using an ice grain size of $1.9^{+3.0}_{-1.4}$ mm and 2005 FY9 is fit with a grain size of $4.5^{+4.5}_{-3.0}$ mm. Grain sizes as large as 1 cm can be accommodated by 2005 FY9 if an additional red component is included, which is similar to the grain size measured for its NIR spectrum. We find that the spectral lines on 2005 FY9 show little shift compared to laboratory spectrum, suggesting that N_2 is not as a significant component on the surface as it is on Pluto. The signal to noise was insufficient on Eris to make similar measurements. The up-turn in 2005 FY9 is further evidence of organic materials on this body.

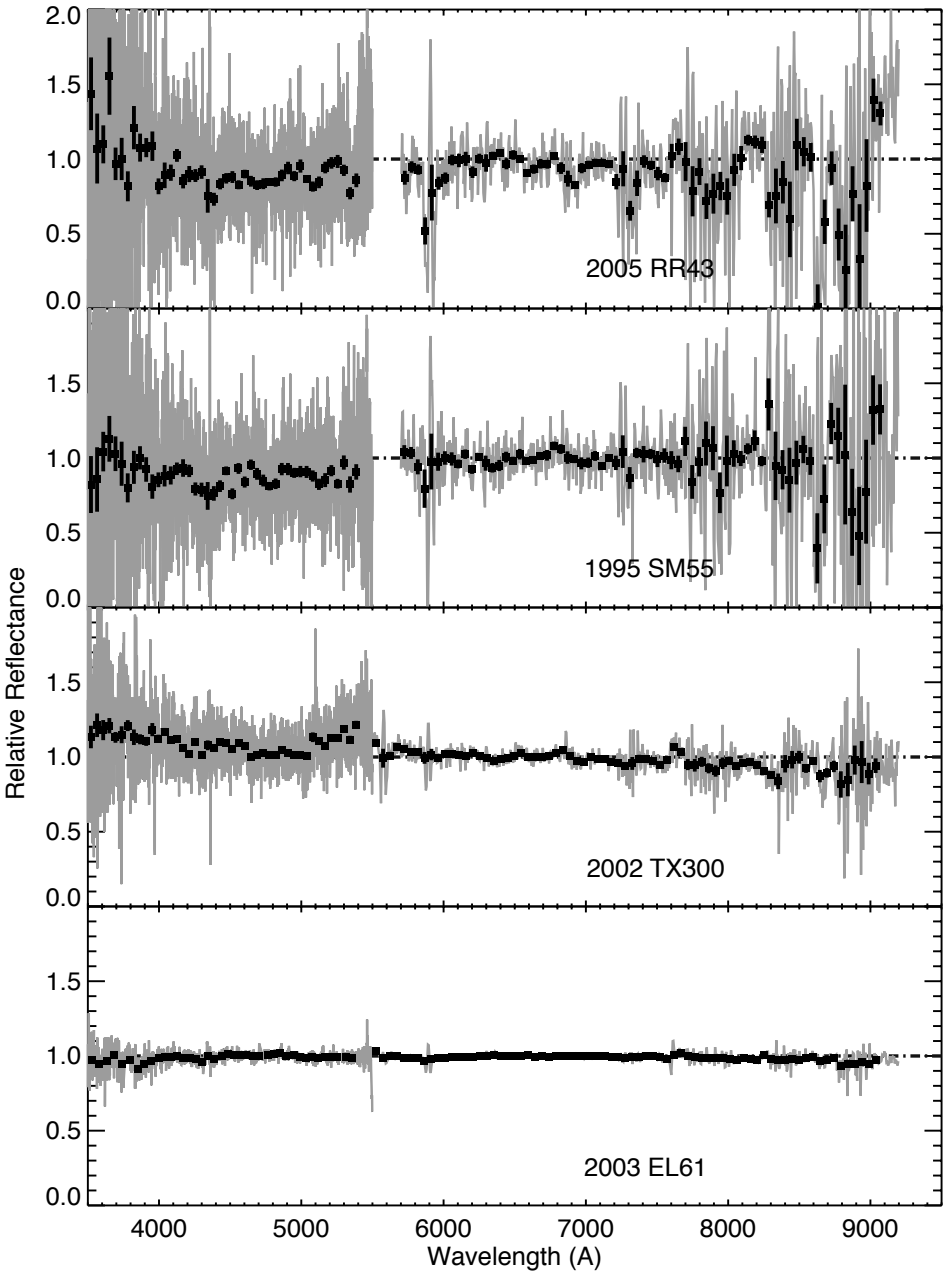

Figure 4.2: The visible reflectance spectra from 3500 to 9200 Å of 2003 EL61 and three of its collisional family members. The high resolution data is plotted in grey while a lower resolution, smoothed spectrum is plotted with black squares. The formal 1-σ error bars from smoothing are also shown. The higher noise at 5890 Å and 7600 Å are due to poor correction of the Na doublet line and the O_2 Fraunhofer lines. The spectra are a composite from blue and red spectra taken with separate cameras on DBSP. The red spectrum is scaled to 1.0 at 6400 Å. A line fit to the red data is used to scale the blue data to match the red data. The spectra of 2006 EL61 and family members are relatively neutral reflecting the high water ice content on their surfaces.

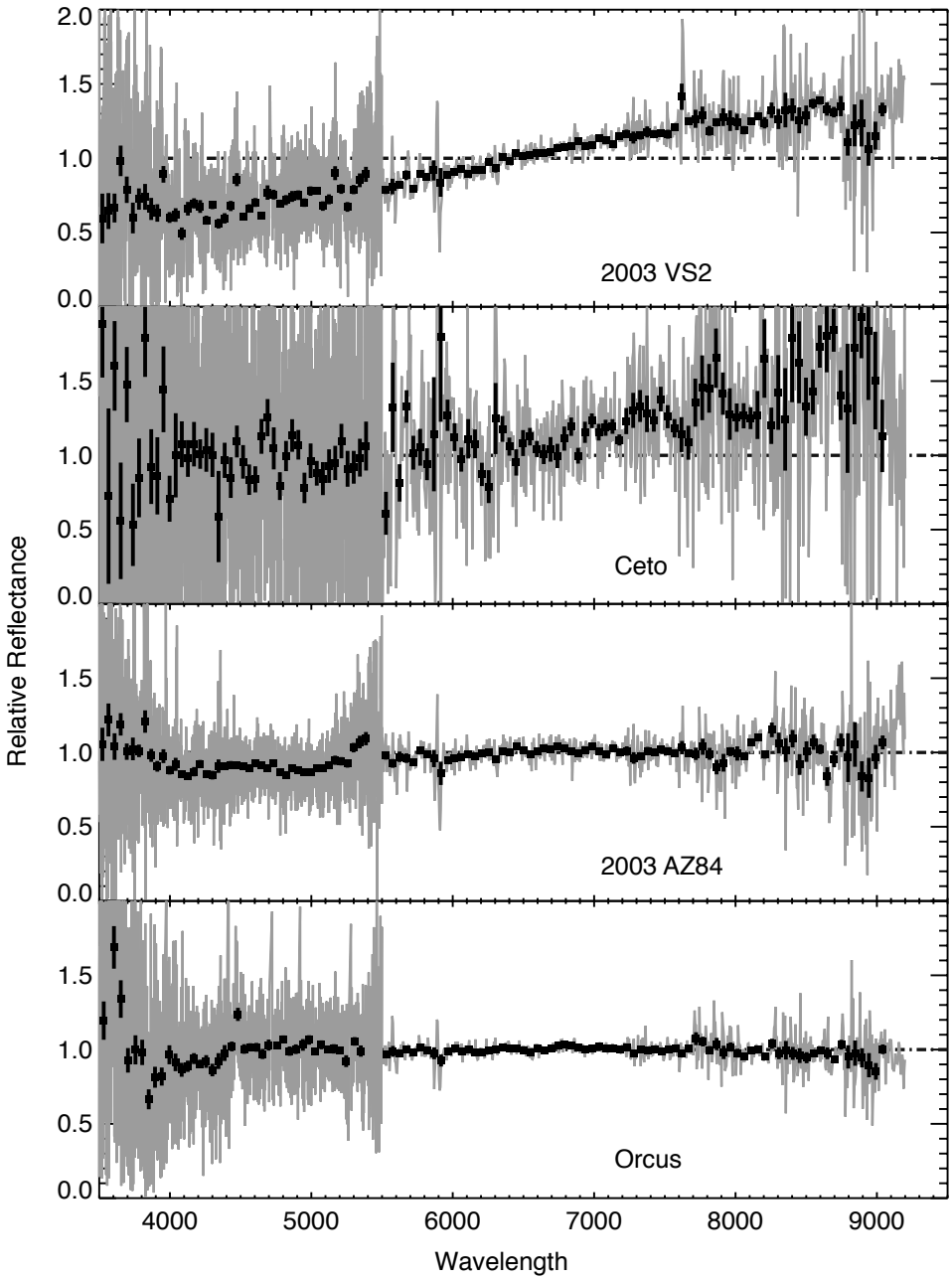

Figure 4.3: The visible reflectance spectra from 3500 to 9200 Å of KBOs with moderate detections of water ice. The high resolution data is plotted in grey while a lower resolution, smoothed spectrum is plotted with black squares. The formal 1-σ error bars from smoothing are also shown. The higher noise at 5890 Å and 7600 Å are due to poor correction of the Na doublet line and the O_2 Fraunhofer lines. The spectra are a composite from blue and red spectra taken with separate cameras on DBSP. The red spectrum is scaled to 1.0 at 6400 Å. A line fit to the red data is used to scale the blue data to match the red data. The spectra are plotted in increasing fraction of water ice on their surfaces with Orcus having the highest surface coverage. The gradient of the spectral slope in our data is similar to those reported in photometric studies. Both Ceto and 2003 AZ84 have similar NIR spectra with modest detections of water ice, but very different spectral slopes. The difference is slope suggest that the secondary surface component that creates the red slope is different between the two bodies.

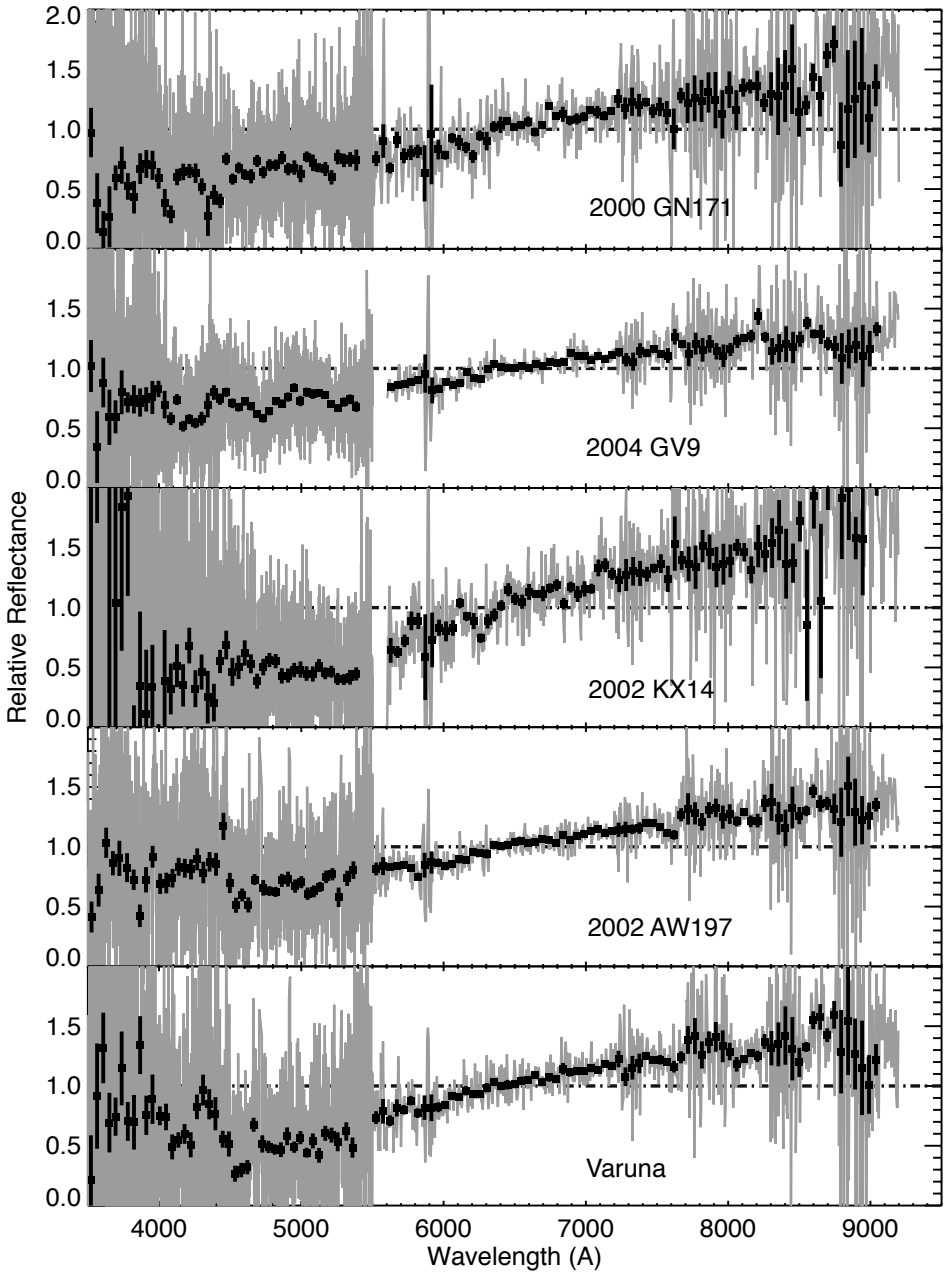

Figure 4.4: The visible reflectance spectra from 3500 to 9200 Å of KBOs with no detections of water ice on their surface. The high resolution data is plotted in grey while a lower resolution, smoothed spectrum is plotted with black squares. The formal 1-σ error bars from smoothing are also shown. The higher noise at 5890 Å and 7600 Å are due to poor correction of the Na doublet line and the O_2 Fraunhofer lines. The spectra are a composite from blue and red spectra taken with separate cameras on DBSP. The red spectrum is scaled to 1.0 at 6400 Å. A line fit to the red data is used to scale the blue data to match the red data.The gradient of the spectral slope in our data is similar to those reported in photometric studies. We find many of these objects have a flattening of spectral slope at wavelengths shortward 4500 Å, which is consistent with observed spectra of some compounds rich in complex organic materials.

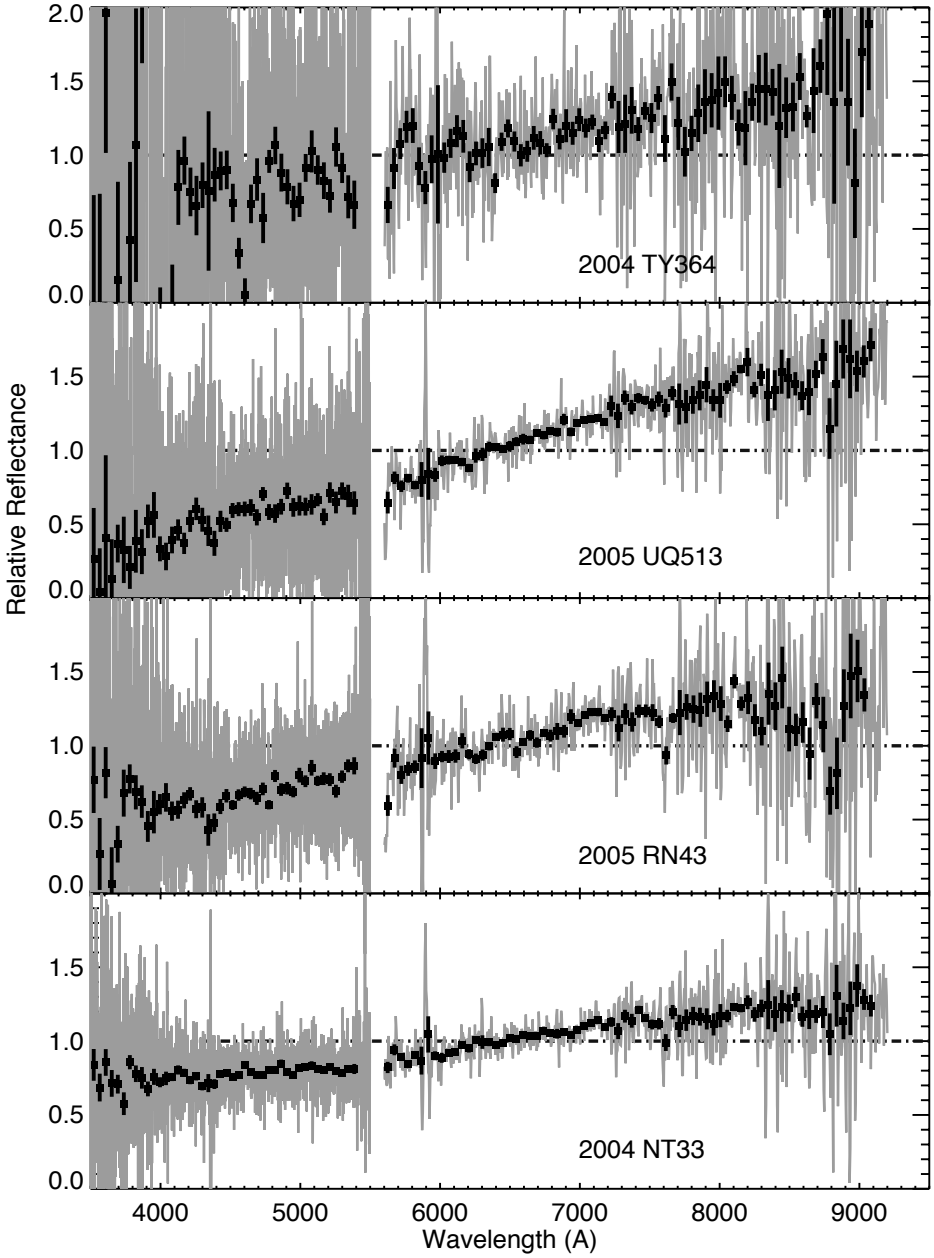

Figure 4.5: The visible reflectance spectra from 3500 to 9200 Å of KBOs with no detections of water ice on their surface. The high resolution data is plotted in grey while a lower resolution, smoothed spectrum is plotted with black squares. The formal 1-σ error bars from smoothing are also shown. The higher noise at 5890 Å and 7600 Å are due to poor correction of the Na doublet line and the O_2 Fraunhofer lines. The spectra are a composite from blue and red spectra taken with separate cameras on DBSP. The red spectrum is scaled to 1.0 at 6400 Å. A line fit to the red data is used to scale the blue data to match the red data. The gradient of the spectral slope in our data is similar to those reported in photometric studies. We find many of these objects have a flattening of spectral slope at wavelengths shortward 4500 Å, which is consistent with observed spectra of some compounds rich in complex organic materials.

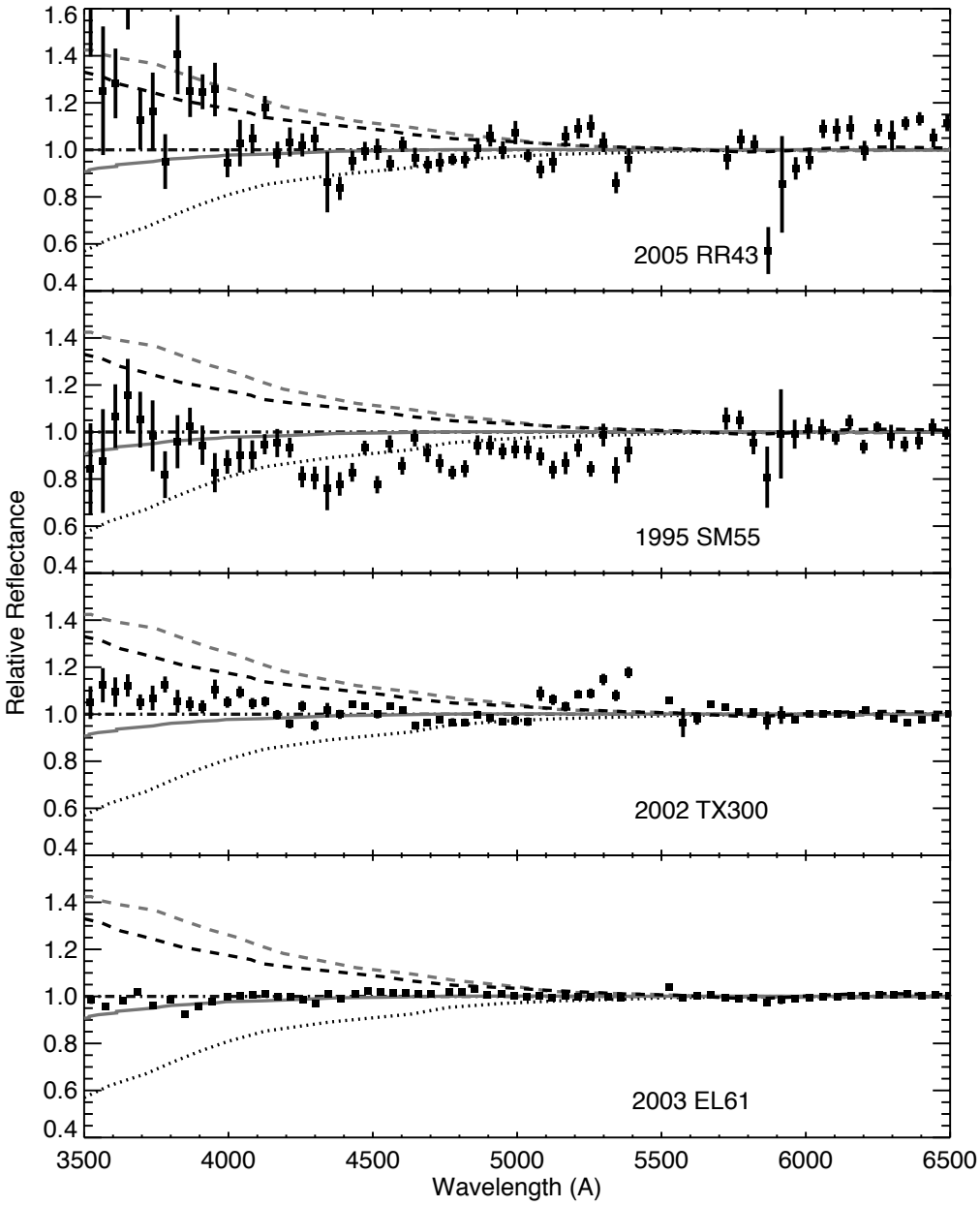

Figure 4.6: The blue spectra of 2003 EL61 and its family. These objects have strong water ice signatures in the NIR spectra. Their visible gradient has been removed to clarify the change in spectral gradient observed at 4500 Å. The data has been smoothed to a resolution of $\lambda/\Delta\lambda \sim 160$ to increase the signal-to-noise. The variations in reflectance seen on 2002 TX300 may be caused by poor correction of the solar spectrum, and the best solar analog data had a higher airmass than 2002 TX300 during observations. The spectra are expected to be relatively flat from the high fraction of water ice that must be present on their surfaces. Phyllosilicates were reported to increase the fit the NIR spectrum of 2003 EL61 from just water ice alone. We find no evidence for significant levels of phyllosilicates on 2003 EL61 or its family members. More detailed spectral modeling is shown in figure 4.10. For comparison purposes, we have included a spectrum of a silicate-tar mixture (dashed light grey line) from Cloutis et al. (1994) and a archetypical spectrum carbon-rich D-type asteroid from Tholen and Barucci (1989). Also shown are typical spectra of C-type and G-type asteroids from Tholen and Barucci (1989) which have down-turning spectra at 4500Ådue to hydrated minerals.

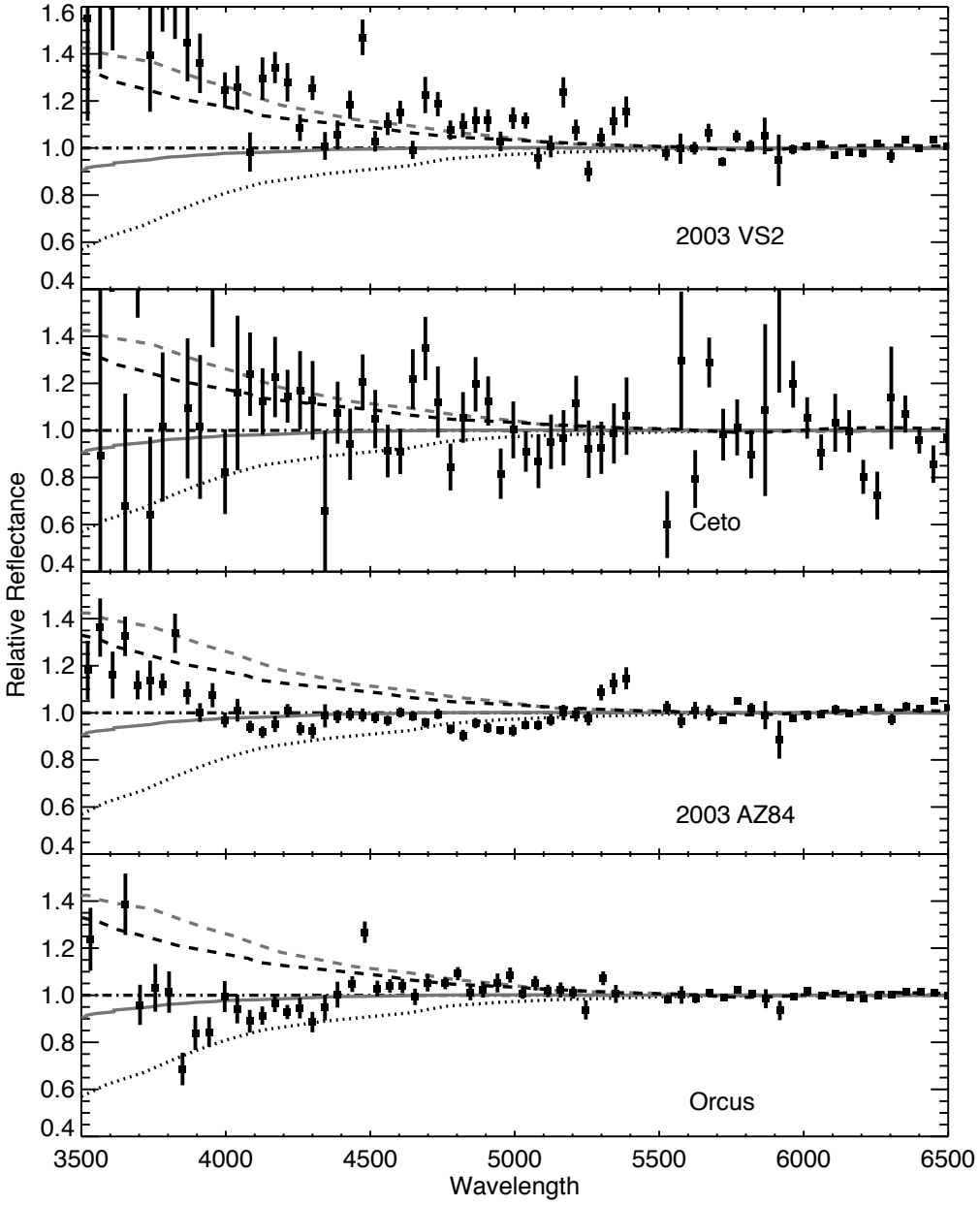

Figure 4.7: The blue spectrum of moderately icy KBOs. These objects have neutral NIR spectra with some detectable water ice signatures, though they aren't as strong as those observed on the 2003 EL61 family. Their visible gradient has been removed to clarify the change in spectral gradient observed at 4500 Å. The data has been smoothed to a resolution of $\lambda/\Delta\lambda \sim 160$ to increase the signal-to-noise. The KBOs generally show slight to strong up-turns in their reflectance which is observed in some materials containing complex organics. For comparison purposes, we have included a spectrum of a silicate-tar mixture (dashed light grey line) from Cloutis et al. (1994) and a archetypical spectrum carbon-rich D-type asteroid from Tholen and Barucci (1989). Also shown are typical spectra of C-type and G-type asteroids from Tholen and Barucci (1989) which have down-turning spectra at 4500Ådue to hydrated minerals. Aqueously altered minerals have been proposed to explain spectral features on some KBOs, though we do not find any KBOs in our sample with down-turning slopes.

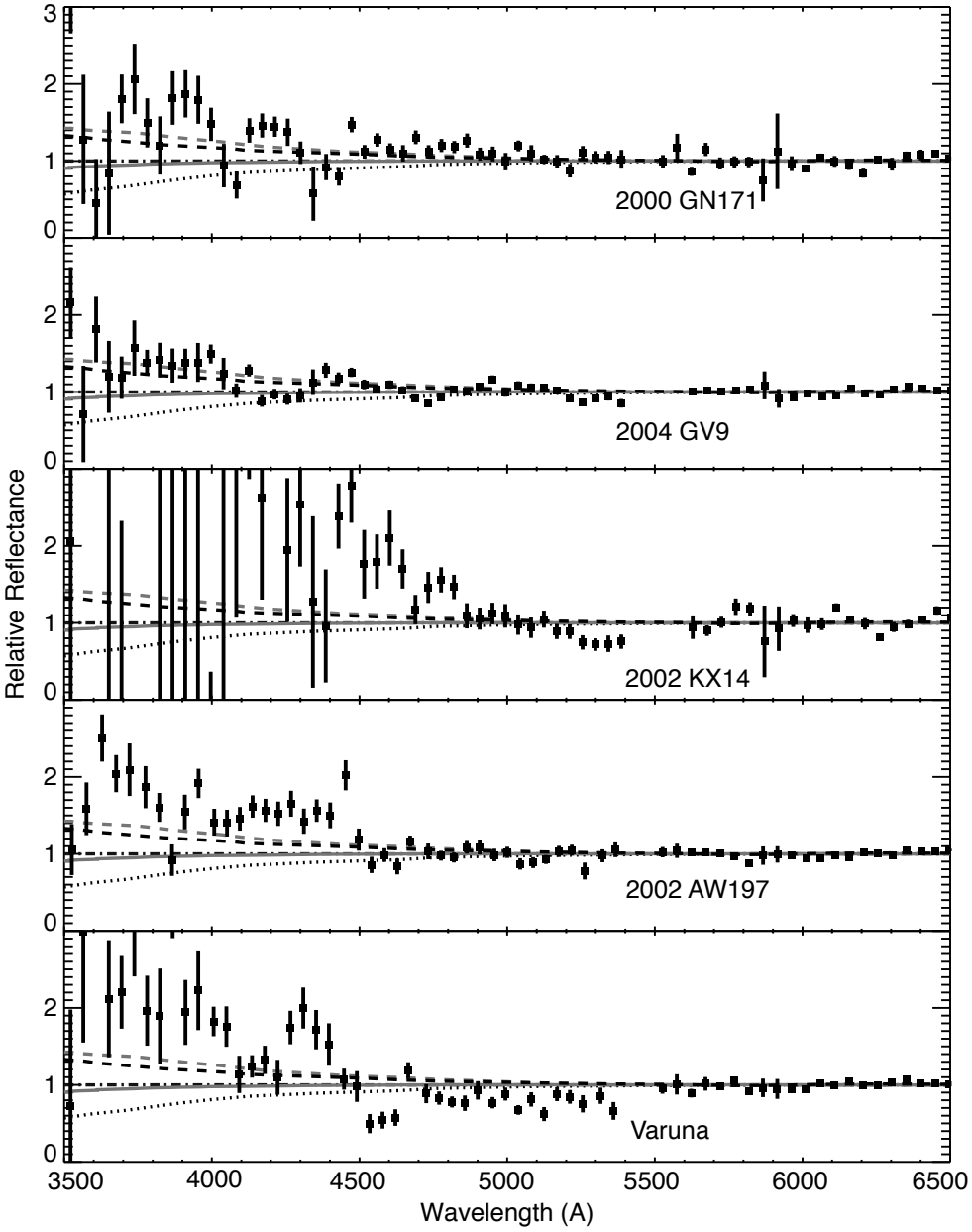

Figure 4.8: The blue spectrum of non-icy KBOs. These objects have neutral NIR spectra with no detectable water ice signatures. Their visible gradient has been removed to clarify the change in spectral gradient observed at 4500 Å. The data has been smoothed to a resolution of $\lambda/\Delta\lambda \sim 160$ to increase the signal-to-noise. The variations in reflectance seen on 2004 GV9 may be caused by poor correction of the solar spectrum, though different solar analogs still produced a similar upturn in its spectrum. The blue camera suffered some electronic problems on the night that Varuna was observed and therefore this data should also be considered with some caution. The KBOs generally show slight to strong up-turns in their reflectance which is observed in some materials containing complex organics. For comparison purposes, we have included a spectrum of a silicate-tar mixture (dashed light grey line) from Cloutis et al. (1994) and a archetypical spectrum carbon-rich D-type asteroid from Tholen and Barucci (1989). Also shown are typical spectra of C-type and G-type asteroids from Tholen and Barucci (1989) which have down-turning spectra at 4500Ådue to hydrated minerals. Aqueously altered minerals have been proposed to explain spectral features on some KBOs, though we do not find any KBOs in our sample with down-turning slopes.

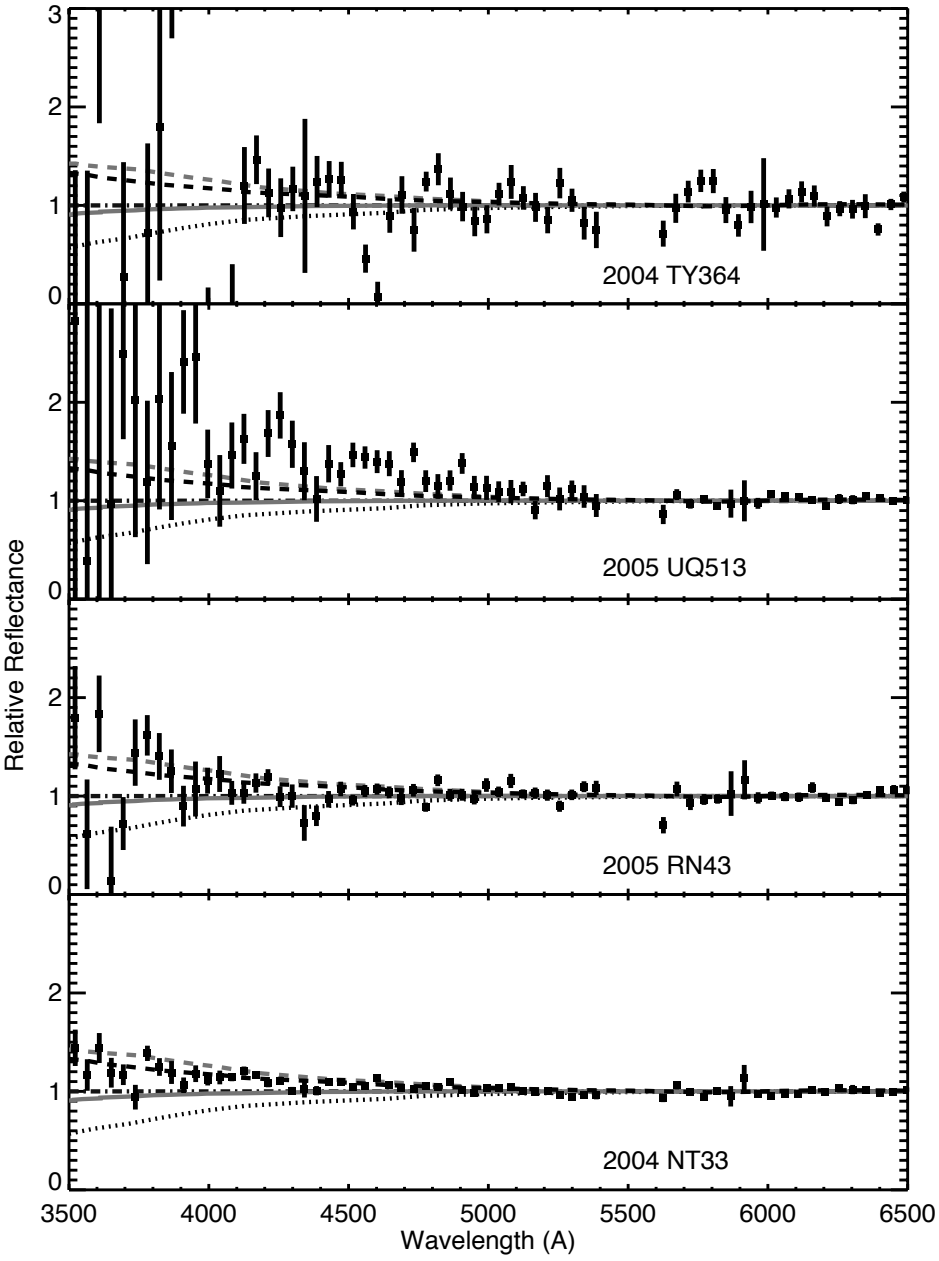

Figure 4.9: The blue spectrum of non-icy KBOs. These objects have neutral NIR spectra with no detectable water ice signatures. Their visible gradient has been removed to clarify the change in spectral gradient observed at 4500 Å. The data has been smoothed to a resolution of $\lambda/\Delta\lambda \sim 160$ to increase the signal-to-noise. The KBOs generally show slight to strong up-turns in their reflectance which is observed in some materials containing complex organics. For comparison purposes, we have included a spectrum of a silicate-tar mixture (dashed light grey line) from Cloutis et al. (1994) and a archetypical spectrum carbon-rich D-type asteroid from Tholen and Barucci (1989). Also shown are typical spectra of C-type and G-type asteroids from Tholen and Barucci (1989) which have down-turning spectra at 4500Ådue to hydrated minerals. Aqueously altered minerals have been proposed to explain spectral features on some KBOs, though we do not find any KBOs in our sample with down-turning slopes.

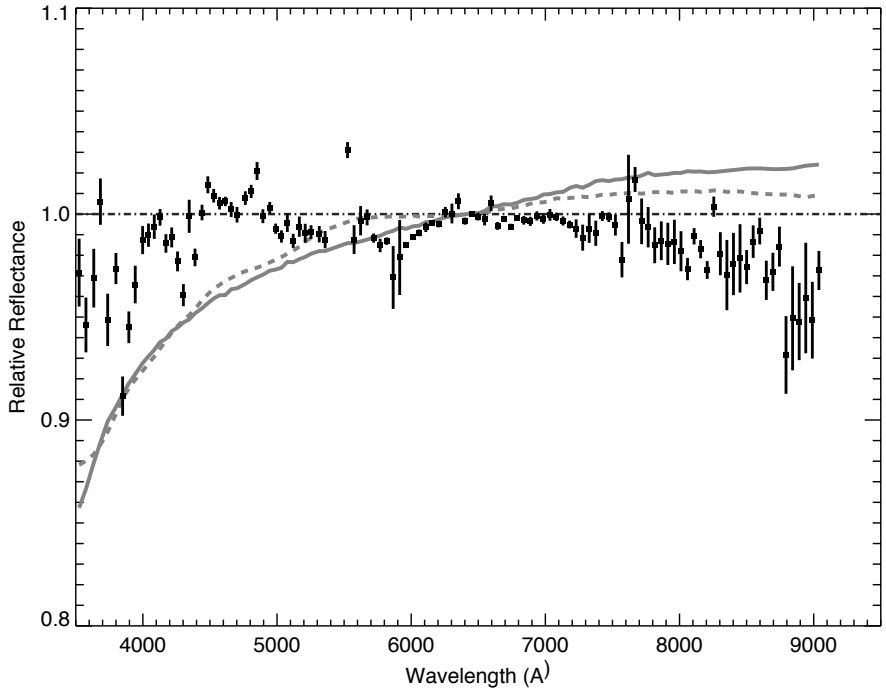

Figure 4.10: The visible spectrum of 2003 EL61 and two surface models of a water ice and phyllosilicate mixture. The spectrum of 2003 EL61 has been smoothed to a resolution of $\lambda/\Delta\lambda \sim 160$ to increase the signal-to-noise. The grey solid line shows the model a geographic mixture of 80% water ice and 20% montmorilinite. The dashed line shows the model for 80% water ice and 20% kaolinite. Both species were reported to increase the goodness of fit for spectral models of 2003 EL61's NIR spectrum (Trujillo et al., 2007). Our spectral models of visible spectrum of 2003 EL61 find that only $\sim$2% of either mineral can been present on the surface in a geographic mixture, and therefore are unlikely to be the material responsible for the blue component seen in the NIR spectrum of 2003 EL61. Based on our modeling, we find that the blue slopes observed in the NIR on 2003 EL61 are not likely caused by phyllosilicates.

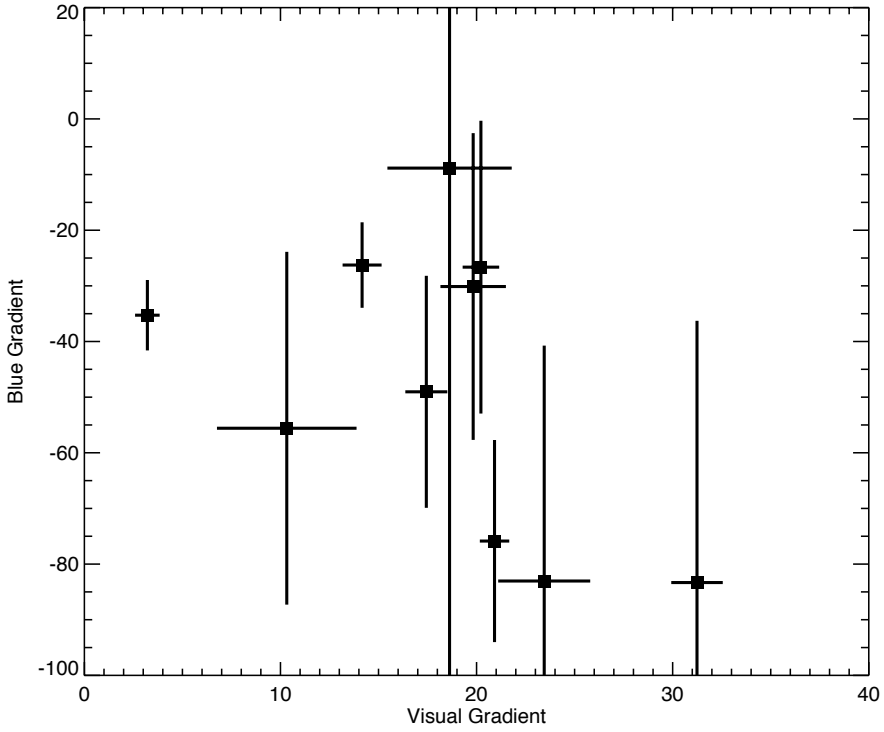

Figure 4.11: The observed blue gradient as a function of the observed visible gradient for non-icy KBOs in our sample. The visible gradient is calculated by normalizing our reflectance spectra to 1.0 at 6400 Å and fitting a line to the spectra. Our measured gradient is similar to values reported from photometric studies when data is available. The blue gradient is found by fitting a line to the data shortward of 4500 Å after the visible gradient is removed. A negative value for the blue gradient indicates an up-turn or a concave up departure in the slope of the spectrum. Such up-turns have been observed in the spectra of some organic-rich compounds. We do not observe any suggestion of the presence of aqueously altered minerals, which could be seen as a positive blue gradient our data. We also find no significant correlation between the blue and visible gradients, though the noise is high in the measurements of the blue gradient. No correlation between these parameters may suggest that the organic-rich component is heterogeneous in character in our KBO sample.

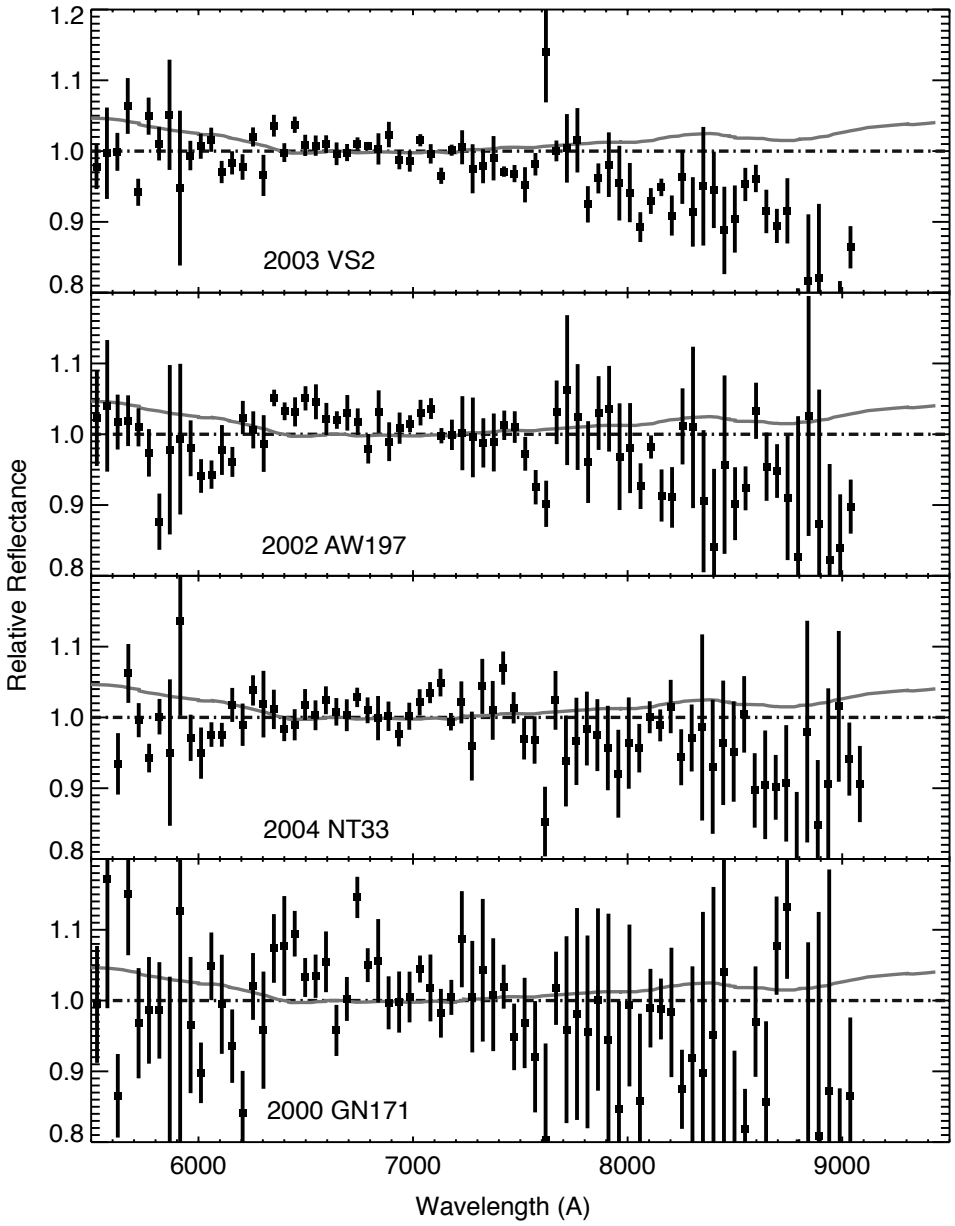

Figure 4.12: The 5500 to 9200 Å reflectance spectra of four non-icy KBOs with their spectral gradient removed. The data represent a smoothed average of the original data with formal 1-sigma error bars shown. The higher noise at 5890 Å and 7600 Å are due to poor correction of the Na doublet line and the O_2 Fraunhofer lines. The thick grey line is a spectrum of the CM2 chondrite Nogoya from Vilas and Gaffey (1989) that has been scaled the same way as the data. The slight absorption from 6500 to 8500 Å on Nogoya are attribsuted to aqueously altered iron-bearing minerals. None of our objects have broad absorptions at the level of $\sim 10\%$ that have been previously been reported on Huya and 2000 GN171 centered at ~ 7000 Å (de Bergh et al., 2004), though weaker absorptions are possible. Our spectrum of 2000 GN171 is more consistent with the flat spectrum obtained by de Bergh et al. (2004) in follow-up observations of this object. A down-turn in the reflectance is observed on these four KBOs and others in our survey, which is expected since many KBOs have much more neutral NIR spectra.

Object	UT Date	Red Exp. Time	Blue Exp Time	Air mass	Calibration Source
20000 Varuna (2000 WR106)	2005 Feb 2	4200	3000	1.01 - 1.03	HD 73708
24835 (1995 SM55)	2006 Oct 19	4800	4800	1.02 -1.07	HD 28099
47932 (2000 GN171)	2007 Apr 19	4800	4200	1.50 - 1.78	SA 107988
55565 (2002 AW197)	2005 Feb 2	6600	6600	1.11 - 1.27	HD 72708
	2005 Feb 3	3000	3000	1.11 - 1.15	HD 73708
55636 (2002 TX300)	2005 Oct 7	4800	4200	1.01 - 1.07	HD 222427
65489 Ceto (2003 FX128)	2007 Apr 19	4800	3000	1.21 - 1.50	SA 107988
84922 (2003 VS2)	2005 Feb 3	3000	3000	1.10 - 1.23	HD 28099
	2005 Feb 4	3000	3000	1.07 - 1.17	HD 28099
	2005 Dec 2	1200	1200	1.06-1.07	HD 20630
90568 (2004 GV9)	2006 Apr 25	4800	4800	1.97 - 2.01	HD 114710
90482 Orcus (2004 DW)	2005 Feb 4	7200	7200	1.26 - 1.60	BD042739
119951 (2002 KX14)	2006 Apr 25	4800	4200	1.71 -1.85	HD 114710
120348 (2004 TY364)	2005 Nov 30	3000	3000	1.44 -1.46	HD 217014
136108 (2003 EL61)	2005 Feb 3	6000	6000	1.04 -1.21	HD 124019
	2005 Mar 7	4200	2400	1.05-1.33	SA 107-998
	2006 Mar 30	3000	3000	1.05-1.07	HD 114710
	2007 Apr 19	4800	4800	1.22-1.25	SA 102-1081
136199 Eris (2003 UB313)	2005 Oct 8	3000	3000	1.46 -1.62	SA 98-978
136472 (2005 FY9	2005 Apr 12	1800	1800	1.04-1.06	SA 102-1081
145452 (2005 RN43)	2006 Oct 19	3000	3000	1.32 -1.44	SAO 82827
145453 (2005 RR43)	2006 Oct 18	5400	4800	1.20-1.33	HD165898, Hyades 142
	2006 Oct 19	4200	3600	1.25-1.82	SAO 86827
2003 AZ84	2005 Feb 4	4800	NA	1.07 -1.09	HD 73708
	2005 Dec 2	6000	6000	1.06 -1.09	HD 86728
2004 NT33	2005 Oct 19	5400	5400	1.07 - 1.14	SAO 82827
2005 UQ513	2006 Oct 19	4800	4800	1.01 - 1.09	SAO 82827

Table 4.2: Journal of Double Spectrograph Observations

That's the good thing about life- old pain is always replaced by new pain.

-- Nellie McKay

Bibliography

W. J. Altenhoff, F. Bertoldi, and K. M. Menten. Size estimates of some optically bright KBOs. *Astronomy and Astrophysics*, 415:771–775, February 2004. doi: 10.1051/0004-6361:20035603.

E. Asphaug, C. B. Agnor, and Q. Williams. Hit-and-run planetary collisions. *Nature*, 439:155–160, January 2006. doi: 10.1038/nature04311.

K. M. Barkume, M. E. Brown, and E. L. Schaller. Water Ice on the Satellite of Kuiper Belt Object 2003 EL61. *Astrophysical Journal Letters*, 640:L87–L89, March 2006. doi: 10.1086/503159.

M. A. Barucci, C. de Bergh, J.-G. Cuby, A. Le Bras, B. Schmitt, and J. Romon. Infrared spectroscopy of the Centaur 8405 Asbolus: first observations at ESO-VLT. *Astronomy and Astrophysics*, 357: L53–L56, May 2000.

M. A. Barucci, I. N. Belskaya, M. Fulchignoni, and M. Birlan. Taxonomy of Centaurs and Trans-Neptunian Objects. *Astronomical Journal*, 130:1291–1298, September 2005. doi: 10.1086/431957.

M. A. Barucci, F. Merlin, E. Dotto, A. Doressoundiram, and C. de Bergh. TNO surface ices. Observations of the TNO 55638 (2002 VE_{95}. *Astronomy and Astrophysics*, 455:725–730, August 2006. doi: 10.1051/0004-6361:20064951.

M. A. Barucci, H. Boehnhardt, D. Cruikshank, and A. Morbidelli, editors. *The Solar System Beyond Neptune*. University of Arizona Press, 2008.

J. M. Bauer, K. J. Meech, Y. R. Fernández, T. L. Farnham, and T. L. Roush. Observations of the Centaur 1999 UG_5: Evidence of a Unique Outer Solar System Surface. *Publications of the ASP*, 114:1309–1321, December 2002.

G. M. Bernstein, D. E. Trilling, R. L. Allen, M. E. Brown, M. Holman, and R. Malhotra. The Size Distribution of Trans-Neptunian Bodies. *Astronomical Journal*, 128:1364–1390, September 2004. doi: 10.1086/422919.

P. R. Bevington. *Data reduction and error analysis for the physical sciences*. McGraw-Hill, 1969.

H. Boehnhardt, S. Bagnulo, K. Muinonen, M. A. Barucci, L. Kolokolova, E. Dotto, and G. P. Tozzi. Surface characterization of 28978 Ixion (2001 KX_{76}). *Astronomy and Astrophysics*, 415:L21–L25,

February 2004. doi: 10.1051/0004-6361:20040005.

M. E. Brown. Near-Infrared Spectroscopy of Centaurs and Irregular Satellites. *Astronomical Journal*, 119:977–983, February 2000. doi: 10.1086/301202.

M. E. Brown. The Inclination Distribution of the Kuiper Belt. *Astronomical Journal*, 121:2804–2814, May 2001. doi: 10.1086/320391.

M. E. Brown and W. M. Calvin. Evidence for Crystalline Water and Ammonia Ices on Pluto's Satellite Charon. *Science*, 287:107–109, January 2000.

M. E. Brown and C. C. Koresko. Detection of Water Ice on the Centaur 1997 CU 26. *Astrophysical Journal, Letters*, 505:L65+, September 1998. doi: 10.1086/311593.

M. E. Brown and C. A. Trujillo. Direct Measurement of the Size of the Large Kuiper Belt Object (50000) Quaoar. *Astronomical Journal*, 127:2413–2417, April 2004. doi: 10.1086/382513.

M. E. Brown, G. A. Blake, and J. E. Kessler. Near-Infrared Spectroscopy of the Bright Kuiper Belt Object 2000 EB173. *Astrophysical Journal, Letters*, 543:L163–L165, November 2000. doi: 10.1086/317277.

M. E. Brown, A. H. Bouchez, D. Rabinowitz, R. Sari, C. A. Trujillo, M. van Dam, R. Campbell, J. Chin, S. Hartman, E. Johansson, R. Lafon, D. Le Mignant, P. Stomski, D. Summers, and P. Wizinowich. Keck Observatory Laser Guide Star Adaptive Optics Discovery and Characterization of a Satellite to the Large Kuiper Belt Object 2003 EL_{61}. *Astrophysical Journal, Letters*, 632:L45–L48, October 2005a. doi: 10.1086/497641.

M. E. Brown, C. A. Trujillo, and D. L. Rabinowitz. Discovery of a Planetary-sized Object in the Scattered Kuiper Belt. *Astrophysical Journal, Letters*, 635:L97–L100, December 2005b. doi: 10.1086/499336.

M. E. Brown, M. A. van Dam, A. H. Bouchez, D. Le Mignant, R. D. Campbell, J. C. Y. Chin, A. Conrad, S. K. Hartman, E. M. Johansson, R. E. Lafon, D. L. Rabinowitz, P. J. Stomski, Jr., D. M. Summers, C. A. Trujillo, and P. L. Wizinowich. Satellites of the Largest Kuiper Belt Objects. *Astrophysical Journal, Letters*, 639:L43–L46, March 2006. doi: 10.1086/501524.

M. E. Brown, K. M. Barkume, G. A. Blake, E. L. Schaller, D. L. Rabinowitz, H. G. Roe, and C. A. Trujillo. Methane and Ethane on the Bright Kuiper Belt Object 2005 FY9. *Astronomical Journal*, 133:284–289, January 2007a. doi: 10.1086/509734.

M. E. Brown, K. M. Barkume, D. Ragozzine, and E. L. Schaller. A collisional family of icy objects in the Kuiper belt. *Nature*, 446:294–296, March 2007b. doi: 10.1038/nature05619.

R. H. Brown, D. P. Cruikshank, and Y. Pendleton. Water Ice on Kuiper Belt Object 1996 TO_{66}.

Astrophysical Journal, Letters, 519:L101–L104, July 1999. doi: 10.1086/312098.

R. G. Burns. Intervalence Transitions in Mixed-Valence Minerals of Iron and Titanium. *Annual Review of Earth and Planetary Sciences*, 9:345–+, 1981. doi: 10.1146/annurev.ea.09.050181.002021.

R. M. Canup. A Giant Impact Origin of Pluto-Charon. *Science*, 307:546–550, January 2005. doi: 10.1126/science.1106818.

R. M. Canup and E. Asphaug. Origin of the Moon in a giant impact near the end of the Earth's formation. *Nature*, 412:708–712, August 2001.

Y.-J. Choi, M. Cohen, R. Merk, and D. Prialnik. Long-Term Evolution of Objects in the Kuiper Belt Zone-Effects of Insolation and Radiogenic Heating. *Icarus*, 160:300–312, December 2002. doi: 10.1006/icar.2002.6976.

R. N. Clark, R. H. Brown, R. Jaumann, D. P. Cruikshank, R. M. Nelson, B. J. Buratti, T. B. McCord, J. Lunine, K. H. Baines, G. Bellucci, J.-P. Bibring, F. Capaccioni, P. Cerroni, A. Coradini, V. Formisano, Y. Langevin, D. L. Matson, V. Mennella, P. D. Nicholson, B. Sicardy, C. Sotin, T. M. Hoefen, J. M. Curchin, G. Hansen, K. Hibbits, and K.-D. Matz. Compositional maps of Saturn's moon Phoebe from imaging spectroscopy. *Nature*, 435:66–69, May 2005. doi: 10.1038/nature03558.

R. N. Clark, G. A. Swayze, R. Wise, E. Livo, T. Hoefen, Kokaly R., and S. J. Sutley. USGS digital spectral library splib06a, 2007.

E. A. Cloutis. Spectral reflectance properties of hydrocarbons - Remote-sensing implications. *Science*, 245:165–168, July 1989.

E. A. Cloutis, M. J. Gaffey, and T. F. Moslow. Spectral reflectance properties of carbon-bearing materials. *Icarus*, 107:276–287, February 1994. doi: 10.1006/icar.1994.1023.

J. C. Cook, S. J. Desch, T. L. Roush, C. A. Trujillo, and T. R. Geballe. Near-Infrared Spectroscopy of Charon: Possible Evidence for Cryovolcanism on Kuiper Belt Objects. *Astrophysical Journal*, 663:1406–1419, July 2007. doi: 10.1086/518222.

D. P. Cruikshank, C. B. Pilcher, and D. Morrison. Pluto - Evidence for methane frost. *Science*, 194: 835–837, November 1976.

D. P. Cruikshank, T. L. Roush, M. J. Bartholomew, T. R. Geballe, Y. J. Pendleton, S. M. White, J. F. Bell, J. K. Davies, T. C. Owen, C. de Bergh, D. J. Tholen, M. P. Bernstein, R. H. Brown, K. A. Tryka, and C. M. Dalle Ore. The Composition of Centaur 5145 Pholus. *Icarus*, 135:389–407, October 1998. doi: 10.1006/icar.1998.5997.

D. P. Cruikshank, T. C. Owen, C. D. Ore, T. R. Geballe, T. L. Roush, C. de Bergh, S. A. Sandford,

F. Poulet, G. K. Benedix, and J. P. Emery. A spectroscopic study of the surfaces of Saturn's large satellites: H_2O ice, tholins, and minor constituents. *Icarus*, 175:268–283, May 2005. doi: 10.1016/j.icarus.2004.09.003.

C. de Bergh, H. Boehnhardt, M. A. Barucci, M. Lazzarin, S. Fornasier, J. Romon-Martin, G. P. Tozzi, A. Doressoundiram, and E. Dotto. Aqueous altered silicates at the surface of two Plutinos? *Astronomy and Astrophysics*, 416:791–798, March 2004. doi: 10.1051/0004-6361:20031727.

C. de Bergh, A. Delsanti, G. P. Tozzi, E. Dotto, A. Doressoundiram, and M. A. Barucci. The surface of the transneptunian object 90482 Orcus. *Astronomy and Astrophysics*, 437:1115–1120, July 2005. doi: 10.1051/0004-6361:20042533.

A. Delsanti, O. Hainaut, E. Jourdeuil, K. J. Meech, H. Boehnhardt, and L. Barrera. Simultaneous visible-near IR photometric study of Kuiper Belt Object surfaces with the ESO/Very Large Telescopes. *Astronomy and Astrophysics*, 417:1145–1158, April 2004. doi: 10.1051/0004-6361:20034182.

A. Doressoundiram, G. P. Tozzi, M. A. Barucci, H. Boehnhardt, S. Fornasier, and J. Romon. ESO Large Programme on Trans-Neptunian Objects and Centaurs: Spectroscopic Investigation of Centaur 2001 BL_{41} and TNOs (26181) 1996 GQ_{21} and (26375) 1999 DE_9. *Astronomical Journal*, 125: 2721–2727, May 2003. doi: 10.1086/374632.

A. Doressoundiram, M. A. Barucci, G. P. Tozzi, F. Poulet, H. Boehnhardt, C. de Bergh, and N. Peixinho. Spectral characteristics and modeling of the trans-neptunian object (55565) 2002 AW_{197} and the Centaurs (55576) 2002 GB_{10} and (83982) 2002 GO_9: ESO Large Program on TNOs and Centaurs. *Planetary Space Science*, 53:1501–1509, December 2005a. doi: 10.1016/j.pss.2004.11.007.

A. Doressoundiram, N. Peixinho, C. Doucet, O. Mousis, M. A. Barucci, J. M. Petit, and C. Veillet. The Meudon Multicolor Survey (2MS) of Centaurs and trans-neptunian objects: extended dataset and status on the correlations reported. *Icarus*, 174:90–104, March 2005b. doi: 10.1016/j.icarus.2004.09.009.

E. Dotto, M. A. Barucci, H. Boehnhardt, J. Romon, A. Doressoundiram, N. Peixinho, C. de Bergh, and M. Lazzarin. Searching for water ice on 47171 1999 TC36, 1998 SG35, and 2000 QC243: ESO large program on TNOs and centaurs*. *Icarus*, 162:408–414, April 2003a. doi: 10.1016/S0019-1035(03)00023-X.

E. Dotto, M. A. Barucci, C. Leyrat, J. Romon, C. de Bergh, and J. Licandro. Unveiling the nature of 10199 Chariklo: near-infrared observations and modeling. *Icarus*, 164:122–126, July 2003b. doi: 10.1016/S0019-1035(03)00103-9.

S. Douté, B. Schmitt, E. Quirico, T. C. Owen, D. P. Cruikshank, C. de Bergh, T. R. Geballe, and T. L. Roush. Evidence for Methane Segregation at the Surface of Pluto. *Icarus*, 142:421–444, December 1999. doi: 10.1006/icar.1999.6226.

C. Dumas, R. J. Terrile, R. H. Brown, G. Schneider, and B. A. Smith. Hubble Space Telescope NICMOS Spectroscopy of Charon's Leading and Trailing Hemispheres. *Astronomical Journal*, 121:1163–1170, February 2001. doi: 10.1086/318747.

C. Dumas, F. Merlin, M. A. Barucci, C. de Bergh, O. Hainault, A. Guilbert, P. Vernazza, and A. Doressoundiram. Surface composition of the largest dwarf planet 136199 Eris (2003 UB313). *Astronomy and Astrophysics*, 471:331–334, August 2007. doi: 10.1051/0004-6361:20066665.

M. J. Duncan and H. F. Levison. A scattered comet disk and the origin of Jupiter family comets. *Science*, 276:1670–1672, 1997.

K. E. Edgeworth. The evolution of our planetary system. *Journal of the British Astronomical Association*, 53:181–188, 1943.

J. A. Fernandez and W.-H. Ip. Some dynamical aspects of the accretion of Uranus and Neptune - The exchange of orbital angular momentum with planetesimals. *Icarus*, 58:109–120, April 1984. doi: 10.1016/0019-1035(84)90101-5.

A. V. Filippenko. The importance of atmospheric differential refraction in spectrophotometry. *Publications of the ASP*, 94:715–721, August 1982.

S. Fornasier, A. Doressoundiram, G. P. Tozzi, M. A. Barucci, H. Boehnhardt, C. de Bergh, A. Delsanti, J. Davies, and E. Dotto. ESO Large Program on physical studies of Trans-Neptunian objects and Centaurs: Final results of the visible spectrophotometric observations. *Astronomy and Astrophysics*, 421:353–363, July 2004a. doi: 10.1051/0004-6361:20041221.

S. Fornasier, E. Dotto, M. A. Barucci, and C. Barbieri. Water ice on the surface of the large TNO 2004 DW. *Astronomy and Astrophysics*, 422:L43–L46, July 2004b. doi: 10.1051/0004-6361:20048004.

M. J. Foster, S. F. Green, N. McBride, and J. K. Davies. NOTE: Detection of Water Ice on 2060 Chiron. *Icarus*, 141:408–410, October 1999. doi: 10.1006/icar.1999.6180.

M. J. Gaffey and T. B. McCord. Asteroid surface materials - Mineralogical characterizations from reflectance spectra. *Space Science Reviews*, 21:555–628, March 1978.

P. A. Gerakines, M. H. Moore, and R. L. Hudson. Ultraviolet photolysis and proton irradiation of astrophysical ice analogs containing hydrogen cyanide. *Icarus*, 170:202–213, July 2004. doi: 10.1016/j.icarus.2004.02.005.

P. Goldreich, Y. Lithwick, and R. Sari. Formation of Kuiper-belt binaries by dynamical friction and three-body encounters. *Nature*, 420:643–646, December 2002.

R. Gomes, H. F. Levison, K. Tsiganis, and A. Morbidelli. Origin of the cataclysmic Late Heavy Bombardment period of the terrestrial planets. *Nature*, 435:466–469, May 2005. doi: 10.1038/nature03676.

R. S. Gomes. The origin of the Kuiper Belt high-inclination population. *Icarus*, 161:404–418, February 2003. doi: 10.1016/S0019-1035(02)00056-8.

W. M. Grundy and U. Fink. Synoptic CCD Spectrophotometry of Pluto Over the Past 15 Years. *Icarus*, 124:329–343, November 1996. doi: 10.1006/icar.1996.0208.

W. M. Grundy and B. Schmitt. The temperature-dependent near-infrared absorption spectrum of hexagonal H_2O ice. *Journal of Geophysics Research*, 103:25809–25822, November 1998. doi: 10.1029/98JE00738.

W. M. Grundy, B. Schmitt, and E. Quirico. The Temperature-Dependent Spectrum of Methane Ice I between 0.7 and 5 μm and Opportunities for Near-Infrared Remote Thermometry. *Icarus*, 155: 486–496, February 2002. doi: 10.1006/icar.2001.6726.

W. M. Grundy, M. W. Buie, and J. R. Spencer. Near-Infrared Spectrum of Low-Inclination Classical Kuiper Belt Object (79360) 1997 CS_{29}. *Astronomical Journal*, 130:1299–1301, September 2005a. doi: 10.1086/431958.

W. M. Grundy, K. S. Noll, and D. C. Stephens. Diverse albedos of small trans-neptunian objects. *Icarus*, 176:184–191, July 2005b. doi: 10.1016/j.icarus.2005.01.007.

W. M. Grundy, L. A. Young, J. R. Spencer, R. E. Johnson, E. F. Young, and M. W. Buie. Distributions of H_2O and CO_2 ices on Ariel, Umbriel, Titania, and Oberon from IRTF/SpeX observations. *Icarus*, 184:543–555, October 2006. doi: 10.1016/j.icarus.2006.04.016.

O. R. Hainaut and A. C. Delsanti. Colors of Minor Bodies in the Outer Solar System. A statistical analysis. *Astronomy and Astrophysics*, 389:641–664, July 2002. doi: 10.1051/0004-6361:20020431.

G. B. Hansen and T. B. McCord. Amorphous and crystalline ice on the Galilean satellites: A balance between thermal and radiolytic processes. *Journal of Geophysical Research (Planets)*, 109:1012–+, January 2004. doi: 10.1029/2003JE002149.

B. Hapke. Bidirectional reflectance spectroscopy. 1. Theory. *Journal of Geophysics Research*, 86: 4571–4586, June 1981.

B. Hapke. *Theory of reflectance and emittance spectroscopy*. Cambridge University Press, 1993.

J. Hardorp. The sun among the stars. III - Energy distributions of 16 northern G-type stars and

the solar flux calibration. *Astronomy and Astrophysics*, 91:221–232, November 1980.

W. K. Hartmann, D. P. Cruikshank, and J. Degewij. Remote comets and related bodies - VJHK colorimetry and surface materials. *Icarus*, 52:377–408, December 1982. doi: 10.1016/0019-1035(82)90002-1.

W. B. Hubbard, D. M. Hunten, S. W. Dieters, K. M. Hill, and R. D. Watson. Occultation evidence for an atmosphere on Pluto. *Nature*, 336:452–454, December 1988. doi: 10.1038/336452a0.

D. Jewitt and K. J. Meech. Cometary grain scattering versus wavelength, or 'What color is comet dust'? *Astrophysical Journal*, 310:937–952, November 1986. doi: 10.1086/164745.

D. Jewitt, N. Peixinho, and H. H. Hsieh. U-Band Photometry of Kuiper Belt Objects. *Astronomical Journal*, 134:2046–2053, November 2007. doi: 10.1086/522787.

D. C. Jewitt and J. Luu. Crystalline water ice on the Kuiper belt object (50000) Quaoar. *Nature*, 432:731–733, December 2004. doi: 10.1038/nature03111.

D. C. Jewitt and J. X. Luu. Colors and Spectra of Kuiper Belt Objects. *Astronomical Journal*, 122: 2099–2114, October 2001. doi: 10.1086/323304.

R. E. Johnson. Irradiation effects in a comet's outer layers. *Journal of Geophysical Review*, 96: 17553–+, September 1991.

B. N. Khare, C. Sagan, E. T. Arakawa, F. Suits, T. A. Callcott, and M. W. Williams. Optical constants of organic tholins produced in a simulated Titanian atmosphere - From soft X-ray to microwave frequencies. *Icarus*, 60:127–137, October 1984. doi: 10.1016/0019-1035(84)90142-8.

B. N. Khare, W. R. Thompson, L. Cheng, C. Chyba, C. Sagan, E. T. Arakawa, C. Meisse, and P. S. Tuminello. Production and optical constraints of ice tholin from charged particle irradiation of (1:6) C2H6/H2O at 77 K. *Icarus*, 103:290–300, June 1993. doi: 10.1006/icar.1993.1071.

A. Kouchi and T. Kuroda. Amorphization of cubic ice by ultraviolet irradiation. *Nature*, 344:134–+, March 1990. doi: 10.1038/344134a0.

G. P. Kuiper. O the Origin of the Solar System. In J. A. Hynek, editor, *Proceedings of a topical symposium, commemorating the 50th anniversary of the Yerkes Observatory and half a century of progress in astrophysics, New York: McGraw-Hill, 1951, edited by Hynek, J.A., p.357*, pages 357–+, 1951.

M. Lazzarin, C. Barbieri, and M. A. Barucci. Visible Spectroscopy of Dark, Primitive Asteroids. *Astronomical Journal*, 110:3058, December 1995. doi: 10.1086/117747.

L. A. Lebofsky. Infrared reflectance spectra of asteroids - A search for water of hydration. *Astronomical Journal*, 85:573–585, May 1980. doi: 10.1086/112714.

H. F. Levison and A. Morbidelli. Models of the collisional damping scenario for ice-giant planets and Kuiper belt formation. *Icarus*, 189:196–212, July 2007. doi: 10.1016/j.icarus.2007.01.004.

J. Licandro, E. Oliva, and M. Di Martino. NICS-TNG infrared spectroscopy of trans-neptunian objects 2000 EB173 and 2000 WR106. *Astronomy and Astrophysics*, 373:L29–L32, July 2001. doi: 10.1051/0004-6361:20010758.

J. Licandro, F. Ghinassi, and L. Testi. Infrared spectroscopy of the largest known trans-Neptunian object 2001 KX_{75}. *Astronomy and Astrophysics*, 388:L9–L12, June 2002. doi: 10.1051/0004-6361:20020533.

J. Licandro, L. di Fabrizio, N. Pinilla-Alonso, J. de León, and E. Oliva. Trans-neptunian object (55636) 2002 TX_{300}, a fresh icy surface in the outer solar system. *Astronomy and Astrophysics*, 457:329–333, October 2006a. doi: 10.1051/0004-6361:20064906.

J. Licandro, W. M. Grundy, N. Pinilla-Alonso, and P. Leisy. Visible spectroscopy of 2003 UB313: evidence for N2 ice on the surface of the largest TNO? *Astronomy and Astrophysics*, 458:L5–L8, October 2006b. doi: 10.1051/0004-6361:20066028.

J. Licandro, N. Pinilla-Alonso, M. Pedani, E. Oliva, G. P. Tozzi, and W. M. Grundy. The methane ice rich surface of large TNO 2005 FY_9: a Pluto-twin in the trans-neptunian belt? *Astronomy and Astrophysics*, 445:L35–L38, January 2006c. doi: 10.1051/0004-6361:200500219.

J. Luu and D. Jewitt. Color Diversity Among the Centaurs and Kuiper Belt Objects. *Astronomical Journal*, 112:2310–+, November 1996a. doi: 10.1086/118184.

J. X. Luu and D. C. Jewitt. Reflection Spectrum of the Kuiper Belt Object 1993 SC. *Astronomical Journal*, 111:499–+, January 1996b. doi: 10.1086/117801.

J. X. Luu and D. C. Jewitt. Optical and Infrared Reflectance Spectrum of Kuiper Belt Object 1996 TL 66. *Astrophysical Journal, Letters*, 494:L117+, February 1998. doi: 10.1086/311172.

J. X. Luu, D. C. Jewitt, and C. Trujillo. Water Ice in 2060 Chiron and Its Implications for Centaurs and Kuiper Belt Objects. *Astrophysical Journal, Letters*, 531:L151–L154, March 2000. doi: 10.1086/312536.

P. S. Lykawka and T. Mukai. A Distant Massive Planet Beyond Pluto and Origin of Kuiper Belt Architecture. In *AAS/Division for Planetary Sciences Meeting Abstracts*, volume 39 of *AAS/Division for Planetary Sciences Meeting Abstracts*, page 64.08, October 2007.

R. Malhotra. The Origin of Pluto's Peculiar Orbit. *Nature*, 365:819, October 1993. doi: 10.1038/365819a0.

K. Matthews and B. T. Soifer. The near infrared camera on the W.M. Keck telescope. *Experimental*

Astronomy, 3:77–84, 1994.

W. B. McKinnon. On convection in ice I shells of outer Solar System bodies, with detailed application to Callisto. *Icarus*, 183:435–450, August 2006. doi: 10.1016/j.icarus.2006.03.004.

W. B. McKinnon. On the origin of the Pluto-Charon binary. *Astrophysical Journal, Letters*, 344: L41–L44, September 1989. doi: 10.1086/185526.

R. Merk and D. Prialnik. Combined modeling of thermal evolution and accretion of trans-neptunian objects-Occurrence of high temperatures and liquid water. *Icarus*, 183:283–295, August 2006. doi: 10.1016/j.icarus.2006.02.011.

F. Merlin, M. A. Barucci, E. Dotto, C. de Bergh, and G. Lo Curto. Search for surface variations on TNO 47171 and Centaur 32532. *Astronomy and Astrophysics*, 444:977–982, December 2005. doi: 10.1051/0004-6361:20053642.

F. Merlin, A. Guilbert, C. Dumas, M. A. Barucci, C. de Bergh, and P. Vernazza. Properties of the icy surface of the TNO 136108 (2003 EL{61}). *Astronomy and Astrophysics*, 466:1185–1188, May 2007. doi: 10.1051/0004-6361:20066866.

M. H. Moore, B. Donn, R. Khanna, and M. F. A'Hearn. Studies of proton-irradiated cometary-type ice mixtures. *Icarus*, 54:388–405, June 1983. doi: 10.1016/0019-1035(83)90236-1.

A. Morbidelli, H. F. Levison, K. Tsiganis, and R. Gomes. Chaotic capture of Jupiter's Trojan asteroids in the early Solar System. *Nature*, 435:462–465, May 2005. doi: 10.1038/nature03540.

A. Morbidelli, H. F. Levison, and R. Gomes. The Dynamical Structure of the Kuiper Belt and its Primordial Origin. *ArXiv Astrophysics e-prints*, March 2007.

J. L. Ortiz, A. Sota, R. Moreno, E. Lellouch, N. Biver, A. Doressoundiram, P. Rousselot, P. J. Gutiérrez, I. Márquez, R. M. González Delgado, and V. Casanova. A study of Trans-Neptunian object 55636 (2002 TX_{300}). *Astronomy and Astrophysics*, 420:383–388, June 2004. doi: 10.1051/0004-6361:20034507.

M. Pan and R. Sari. Shaping the Kuiper belt size distribution by shattering large but strengthless bodies. *Icarus*, 173:342–348, February 2005. doi: 10.1016/j.icarus.2004.09.004.

N. Pinilla-Alonso, J. Licandro, R. Gil-Hutton, and R. Brunetto. The water ice rich surface of (145453) 2005 RR_{43}: a case for a carbon-depleted population of TNOs? *Astronomy and Astrophysics*, 468: L25–L28, June 2007. doi: 10.1051/0004-6361:20077294.

P. B. Price and L. Bergström. Optical properties of deep ice at the South Pole: scattering. *Applied Optics*, 36:4181–4194, June 1997a.

P. B. Price and L. Bergström. Optical properties of deep ice at the South Pole: scattering. *Applied*

Optics, 36:4181–4194, June 1997b.

E. Quirico and B. Schmitt. Near-Infrared Spectroscopy of Simple Hydrocarbons and Carbon Oxides Diluted in Solid N_2 and as Pure Ices: Implications for Triton and Pluto. *Icarus*, 127:354–378, June 1997. doi: 10.1006/icar.1996.5663.

D. L. Rabinowitz, K. Barkume, M. E. Brown, H. Roe, M. Schwartz, S. Tourtellotte, and C. Trujillo. Photometric Observations Constraining the Size, Shape, and Albedo of 2003 EL61, a Rapidly Rotating, Pluto-sized Object in the Kuiper Belt. *Astrophysical Journal*, 639:1238–1251, March 2006. doi: 10.1086/499575.

D. L. Rabinowitz, B. E. Schaefer, and S. W. Tourtellotte. The Diverse Solar Phase Curves of Distant Icy Bodies. I. Photometric Observations of 18 Trans-Neptunian Objects, 7 Centaurs, and Nereid. *Astronomical Journal*, 133:26–43, January 2007. doi: 10.1086/508931.

D. Ragozzine and M. E. Brown. Candidate Members and Age Estimate of the Family of Kuiper Belt Object 2003 EL61. *Astronomical Journal*, 134:2160–2167, December 2007. doi: 10.1086/522334.

J. Romon-Martin, M. A. Barucci, C. de Bergh, A. Doressoundiram, N. Peixinho, and F. Poulet. Observations of Centaur 8405 Asbolus: Searching for Water Ice. *Icarus*, 160:59–65, November 2002. doi: 10.1006/icar.2002.6959.

J. Romon-Martin, C. Delahodde, M. A. Barucci, C. de Bergh, and N. Peixinho. Photometric and spectroscopic observations of (2060) Chiron at the ESO Very Large Telescope. *Astronomy and Astrophysics*, 400:369–373, March 2003. doi: 10.1051/0004-6361:20021890.

C. Sagan and B. N. Khare. Tholins - Organic chemistry of interstellar grains and gas. *Nature*, 277: 102–107, January 1979.

E. L. Schaller and M. E. Brown. Volatile Loss and Retention on Kuiper Belt Objects. *Astrophysical Journal, Letters*, 659:L61–L64, April 2007a. doi: 10.1086/516709.

E. L. Schaller and M. E. Brown. Detection of Methane on Kuiper Belt Object (50000) Quaoar. *Astrophysical Journal, Letters*, 670:L49–L51, November 2007b. doi: 10.1086/524140.

J. R. Spencer and W. M. Calvin. Condensed O_2 on Europa and Callisto. *Astronomical Journal*, 124:3400–3403, December 2002. doi: 10.1086/344307.

J. R. Spencer, W. M. Calvin, and M. J. Person. CCD Spectra of the Galilean Satellites: Molecular Oxygen on Ganymede. *Journal of Geophysics Research*, 100:19049–19056, September 1995. doi: 10.1029/95JE01503.

J. Stansberry, W. Grundy, M. Brown, D. Cruikshank, J. Spencer, D. Trilling, and J.-L. Margot. Physical Properties of Kuiper Belt and Centaur Objects: Constraints from Spitzer Space Tele-

scope. *ArXiv Astrophysics e-prints*, February 2007.

D. C. Stephens and K. S. Noll. The High Fraction of Binaries in the Cold Classical Kuiper Belt. In *Bulletin of the American Astronomical Society*, volume 37 of *Bulletin of the American Astronomical Society*, pages 747–+, August 2005.

D. J. Stevenson. Volatile loss from accreting icy protoplanets. In *Lunar and Planetary Institute Conference Abstracts*, volume 24 of *Lunar and Planetary Inst. Technical Report*, pages 1355–1356, March 1993.

D. J. Stevenson, A. W. Harris, and J. I. Lunine. *Origins of satellites*, pages 39–88. IAU Colloq. 77: Some Background about Satellites, 1986.

G. Strazzulla, G. Leto, G. A. Baratta, and F. Spinella. Ion irradiation experiments relevant to cometary physics. *Journal of Geophysics Research*, 96:17547–+, September 1991.

S. C. Tegler and W. Romanishin. Extremely red Kuiper-belt objects in near-circular orbits beyond 40 AU. *Nature*, 407:979–981, October 2000.

S. C. Tegler, W. M. Grundy, W. Romanishin, G. J. Consolmagno, K. Mogren, and F. Vilas. Optical Spectroscopy of the Large Kuiper Belt Objects 136472 (2005 FY9) and 136108 (2003 EL61). *Astronomical Journal*, 133:526–530, February 2007. doi: 10.1086/510134.

D. J. Tholen and M. A. Barucci. Asteroid taxonomy. In R. P. Binzel, T. Gehrels, and M. S. Matthews, editors, *Asteroids II*, pages 298–315, 1989.

C. A. Trujillo and M. E. Brown. The Caltech Wide Area Sky Survey. *Earth Moon and Planets*, 92: 99–112, June 2003. doi: 10.1023/B:MOON.0000031929.19729.a1.

C. A. Trujillo, M. E. Brown, D. L. Rabinowitz, and T. R. Geballe. Near-Infrared Surface Properties of the Two Intrinsically Brightest Minor Planets: (90377) Sedna and (90482) Orcus. *Astrophysical Journal*, 627:1057–1065, July 2005. doi: 10.1086/430337.

C. A. Trujillo, M. E. Brown, K. M. Barkume, E. L. Schaller, and D. L. Rabinowitz. The Surface of 2003 EL_{61} in the Near-Infrared. *Astrophysical Journal*, 655:1172–1178, February 2007. doi: 10.1086/509861.

K. Tsiganis, R. Gomes, A. Morbidelli, and H. F. Levison. Origin of the orbital architecture of the giant planets of the Solar System. *Nature*, 435:459–461, May 2005. doi: 10.1038/nature03539.

F. Vilas and M. J. Gaffey. Phyllosilicate absorption features in main-belt and outer-belt asteroid reflectance spectra. *Science*, 246:790–792, November 1989.